Optimisation of System and Sensor Selection for Safety and Reliability of Autonomous Vehicle



Haicang Li

Faculty of Engineering

University of Nottingham

A thesis submitted for the degree of

Doctor of Philosophy

October 2022

I would like to dedicate this thesis to my grandparents and parents.

Acknowledgements

Firstly, I would like to express my sincere appreciation to my supervisor Dr. Rajesh Tiwari for his guidance, inspiration, motivation and professional supports. He has been my supervisor since the final project of my Master degree. During the past years, no matter in Newcastle or Nottingham, he was one of my strongest backing all the time. His academic comments and careful editing contributes to he production of this thesis enormously.

I would also thank my supervisor Dr. Gabriele Gradoni deeply for his encouragement and valuable suggestions since I transferred from Newcastle University to the University of Nottingham. He was always nice and patient to me. His supports for both academic and daily life sides motivated me to move forward.

I would appreciate Prof. Patrick Wheeler and Dr. Steve Greedy sincerely, who have given me great help when I was applying to transfer to University of Nottingham. I cannot continue my research and Ph.D in Nottingham without their supports.

Jiachen Yin, who is not only my colleague but also my friend, gave me unconditional supports during past years. It is my pleasure to know him and be his friend. Many thanks for all your concern and assistance.

I would thank Siyue Liu for her patience, encouragement and spiritual supports during past three years. We supported each other for trying our best to go through the tough period, which is an unforgettable memory.

My friends, Yang Xian, Shuoyang Li, Handong Li, Scott Stainton, Ishita Gulati, Zeyu Fu, Yang Sun, Yulong Chen, Hao Chen, Jiawei Yan have all extended their support in a special way. I really enjoyed the friendship with them, which helps me fight against loneliness and depression.

I would like to acknowledge GMVNSL and ESA (European Space Agency) for providing me working opportunity and permitting me use the data of IMPACARS (Integrity Monitoring and Prediction Concept for Autonomous Car Resilience and Safety), which supports my Ph.D research significantly.

Finally, I would express my deep love to my family. My parents are the source of my energy and courage every single second in my life. Although I barely got chance to go back home since I studied in UK, you love is with me no matter where I am. Love you all.

Abstract

In the modern traffic system, road traffic accidents and congestion have been the most critical problems which have caused a large number of deaths and economic damage. ITS (intelligent traffic system) based on vehicular communications is one of the effective approaches to avoid vehicle collisions and increase the efficiency of traffic. GPS (global positioning system) is one of the widely used navigation systems for vehicles in ITS. However, the performance of GPS can be affected remarkably by various factors. As a result of this, it is necessary to evaluate the reliability of GPS observation to increase the safety of road users. Furthermore, for the challenging environment such as GPS-denied environment, multisensor navigation is expected to be used to improve the robustness and continuity of the positioning system. Additionally, selecting sensors to be fused according to their reliability is an effective method to mitigate the negative influence of sensors caused by challenging traffic environments.

In this thesis, a spatio-temporal roundabout and crossroad ITM algorithm has been developed, defining the confidence circle based on the reliability of GPS observation. The simulation results illustrate that the proposed ITM protocol improves safety level and traffic efficiency significantly. Secondly, a GPS/IMU integration positioning system is proposed, which uses ICC (intraclass correlation coefficient) as a reliability factor to mitigate positioning errors of GPS. The experiments results show that positioning errors are reduced by applying ICC. And further improvement of positioning is achieved by integrating IMU measurements and optimised GPS measurements. Finally, a three-sensor-based multisensor navigation system is designed, which utilises reliability evaluation to detect and select optional fusion modes. As the field trial results show, the robustness and accuracy of positioning under challenging traffic environments can be improved significantly by applying the proposed multisensor navigation system.

Contents

List of Figures viii

List of Tables xi

List of Abbreviations xii

1 Introduction 1

1.1 Introduction . . . 1

1.2 Recent Scientific Findings in ITS, Safety and Reliability of Autonomous Vehicle . . . 6

1.3 Objectives and Contribution to Knowledge . . . 9

1.4 Thesis Outline . . . 10

1.5 Publications Related to the Thesis . . . 12

2 Background and Overview 13

2.1 Autonomous Vehicle . . . 13

2.2 Communications for Autonomous Vehicles . . . 16

2.2.1 Safety Messages within Vehicular Network . . . 16

2.2.2 Vehicular Networks . . . 17

2.3 GNSS Error Sources and RINEX Files . . . 18

2.3.1 Sources of Errors of GNSS . . . 18

2.3.1.1 Multipath Effect . . . 18

2.3.1.2 Satellite and Receiver Clock offsets . . . 18

2.3.1.3 Signal Blocking/Fading and Satellite Geometry . . . 19

2.3.1.4 Tropospheric Delay . . . 19

2.3.1.5 Ionospheric Delay . . . 21

2.3.2 RINEX files . . . 21

2.4 Frames of Reference and Transformations . . . 24

2.4.1 Frames of reference 24
2.4.2 Transformations between Reference Frames 25
2.4.2.1 Transform from ECEF to WGS 84 26
2.4.2.2 Transformation between ENU and ECEF 26
2.4.2.3 Transformation between ENU and Body Frame . . . 27
2.4.2.4 Transformation between ECEF and ECI 28
2.5 LiDAR Mechanization 28
2.6 Summary 31

3 Safe and Reliable Spatio-temporal Model for Roundabouts and Road Intersections using Vehicular Communication System 33
3.1 Motivation and Problem States 33
3.2 Application of GPS Reliability on Vehicular Communication 36
3.2.1 Reliability of GPS Observation 36
3.2.2 Accuracy Measurement 39
3.3 Intelligent Traffic Management for Roundabout and Road Intersection 40
3.3.1 Roundabout and Road Intersection Model 40
3.3.2 Protocol of Basic Safety Message 41
3.3.3 Spatio-temporal Algorithm 43
3.4 Simulation Setup and Results Analysis 45
3.5 Summary 50

4 GPS Positioning Optimisation and Multisensor Fusion for Autonomous Vehicle in Urban Environment 52
4.1 Intraclass Correlation Coefficient application 53
4.1.1 Conceptions and Computation of ICC 53
4.1.2 Selection of ICC forms for GPS positioning 55
4.2 Reliability Factor Applied Positioning Optimisation of Multisensor system for Autonomous vehicle 58
4.2.1 Algorithm for ICC Applied positioning Optimisation 59
4.2.2 Data Fusion for Optimised GPS Measurements and IMU Measurements 60
4.2.2.1 Euler Angle Attitude Mechanization 61
4.2.2.2 Loosely Coupled Integration of GPS and IMU 62

4.3 Experiment Scenario and Equipment Setup 64
4.3.1 Experimental Equipment Setup 64
4.3.2 Experiment Scenario 65
4.4 Results Analysis 66
4.5 Summary 71

5 Multisensor Selection and Fusion for Autonomous Vehicle in Sensor-degraded Environment 73

5.1 Challenging Environment Navigation Switching Algorithm for Autonomous Vehicles 75
5.1.1 Algorithm for mode selecting and switching 76
5.2 Data Preprocess for LiDAR and IMU 76
5.2.1 Line Tracking and Mapping for LiDAR 76
5.2.2 IMU Mechanization 79
5.2.3 INS error models 80
5.2.3.1 Position Error Model 81
5.2.3.2 Velocity Error Model 82
5.2.3.3 Attitude Error Model 83
5.3 Data Fusion for GNSS/IMU and LiDAR/IMU 84
5.4 Field Trial Setup and Testing Scenario 86
5.4.1 Experiment Equipment 86
5.4.2 Field Trial Equipment Setup 88
5.4.3 Field Trial scenario 89
5.5 Results, Analysis and Discussion 90
5.6 Summary 94

6 Conclusion and Future Research 96

6.1 Conclusion 97
6.2 Future Work 99

References 100

List of Figures

1.1 Number of road traffic deaths: 2000-2016 [1] 1
1.2 Distribution of deaths by road user type by WHO Region [1] 2
1.3 Vehicular communication network [2] 4
1.4 The application of LiDAR confirmation switching algorithm [3] 8

2.1 SAE-defined automation levels, system capability and required integrity [4] 13
2.2 Basic safety message structure [4] 16
2.3 Multipath effect on satellite signal [5] 19
2.4 Area of uncertainty due to good and bad satellite geometry [6] 20
2.5 Layers of Earth's atmosphere [7] 20
2.6 An example of Navigation data file 22
2.7 An example of Observation data file 23
2.8 Comparison between ECEF, WGS 84 and local frame 25
2.9 Body frame 26
2.10 Transformation between ECI and ECEF 29
2.11 LiDAR positioning mechanization 30
2.12 Coordination conversion 31

3.1 The locations of road traffic accidents occurred in chosen scenario near Newcastle University during last 10 years, indicate severity: slight (yellow), serious (red), fatal (black) [8] 35
3.2 Estimated positions and the confidence circle of vehicle 39
3.3 An example of divided traffic scenario 41
3.4 Content of basic safety message 42
3.5 An example of occupied segments in each step 43

3.6 Pseudocode of trajectory reservation algorithm applied in the central controller . . . 44
3.7 Simulation scenario for proposed ITM scheme [9] . . . 46
3.8 Number of cars processed during simulation period . . . 47
3.9 Total stop time of cars when driving across the simulation scenario . 47
3.10 Average velocity of cars when driving across the simulation scenario . 48
3.11 Number of vehicle accidents during simulation . . . 49
3.12 Number of simulations with accidents (out of 10) . . . 49

4.1 The flow chart of ICC form selection [10] . . . 56
4.2 Data processing diagram for the ICC applied positioning optimisation System . . . 58
4.3 Algorithm for ICC based GPS positioning optimisation . . . 60
4.4 USRP X310, showing the front and rear panels of USRP [11] . . . 65
4.5 MTi-G [12] . . . 65
4.6 The experiment scenario for electronic trolley, reference trajectory of trolley (red) . . . 65
4.7 ICC detection of odd measurements for G02 . . . 66
4.8 Error comparison between original positioning and ICC selected positioning . . . 68
4.9 Comparison of Mean and standard derivation of errors . . . 69
4.10 Trolley trajectories comparison between original positioning (red), ICC selected positioning (blue) and reference (green) . . . 69
4.11 Error comparison between GPS only positioning and GPS/IMU fusion positioning . . . 70
4.12 Trolley trajectories comparison between GPS only positioning (blue), GPS/IMU fusion positioning (yellow) and reference (green) . . . 71

5.1 The block diagram of data processing . . . 75
5.2 Mode selecting and switching algorithm . . . 77
5.3 PolaRX 5S front and rear panel [13] . . . 86
5.4 Velodyne VLP-16 LiDAR . . . 87
5.5 NovAtel SPAN UIMU-LCI [14] . . . 88
5.6 The equipped testing van . . . 88
5.7 Experiment equipment mounting . . . 89

5.8 Scenario of field trial 89
5.9 Positioning errors comparison between sensors 91
5.10 ICC comparison between different modes 91
5.11 Positioning errors comparison between fusion modes 92
5.12 Trajectory comparison between proposed algorithm (green), reference (yellow) and odd estimation (red) on Google Earth 93
5.13 Algorithm for emergency aiding 94

List of Tables

1.1 Direct and indirect costs of congestion for UK drivers in 2017 [15] . . 3
1.2 GPS position accuracy comparison [16] 6

2.1 Summary of automation levels [17] 14
2.2 Available channels for DSRC 17

4.1 Definitions of different types of reliability [10] 53
4.2 Formulas for different types of ICC 54
4.3 An example for ICC application 54
4.4 Summary of the Kalman filter algorithm 62

List of Abbreviations

ADS	Automated Driving System
ASCII	American Standard Code for Information Interchange
AVI	Automatic vehicle Identification
BER	Bit Error Rate
BSM	Basic Safety Message
CC	Central Controller
CNR	carrier-to-noise Ratio
CRC	Cyclic Redundancy Check
CTM	Conventional Traffic Management
DCM	Direct Cosine Matrix
DDT	Dynamic Driving Test
DOP	Dilution of Precision
DRMS	Distance Root Mean Square
DSRC	Dedicated Short range Communication
ECEF	Earth-centred Earth-fixed Coordinate System
ECI	Earth-centred Inertial coordinate System
EEBL	Emergency Electronic Brake Lights
ER	External Reliability
ENU	East, North and Up coordinate system
GPS	Global Positioning System
GNSS	Global Navigation Satellite System
HDOP	Horizontal Dilution of Precision
HMI	Human Machine interface
ICC	Intraclass Correlation Coefficient
IEEE	Institute of Electrical and Electronic Engineering
IMU	Inertial Measurement unit

INS	Inertial Navigation System
ITM	Intelligent Traffic Management
ITMCC	Intelligent Traffic Management with Confidence Circle
ITS	Intelligent Traffic System
LiDAR	Light Detection and Ranging
LOS	Line-of-sight
MDB	Marginally Detectable Blunder
NLOS	Non-line-of-sight
OBU	On Board Unit
OEDR	Object Event Detection and Response
PNT	Position, Navigation and Timing
PR	Pseudorange
PVM	Probe Vehicle message
RAM	Roadside Alert Message
RF	Reliability Factor
RINEX	Receiver independent Exchange Format
SAE	Society of Automotive Engineers
USRP	Universal Software Radio Peripheral
V2I	Vehicle-to-Infrastructure
V2V	Vehicle-to-Vehicle
V2X	Vehicle-to-Anything
WAVE	Wireless Access in Vehicular Environments
WGS 84	World Geodetic System 1984

Chapter 1

Introduction

1.1 Introduction

Traffic safety is the top priority concerned in traffic management. According to the annual report of road casualties in Great Britain published by the department for transport, vehicle accidents continue to be the major contributor to casualties of all severities [18]. Statistics related to road traffic safety have been presented by the

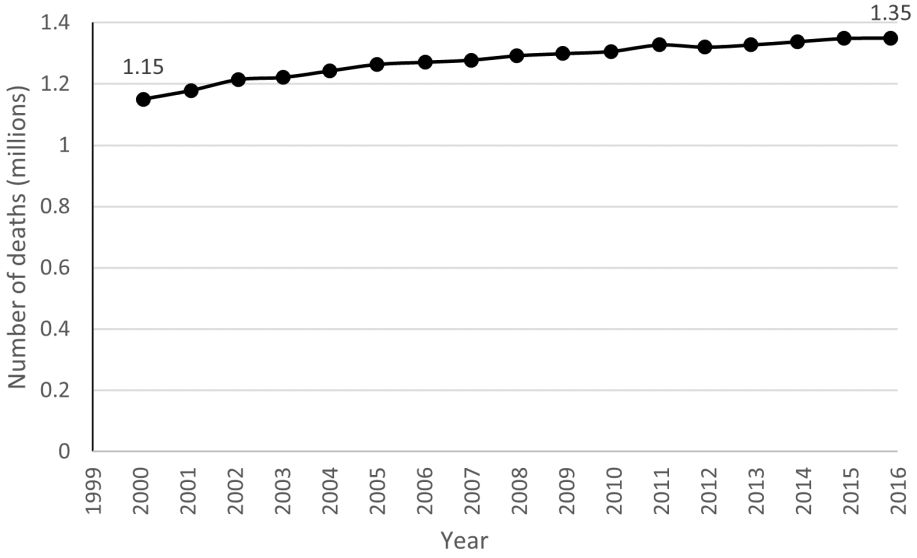


Figure 1.1: Number of road traffic deaths: 2000-2016 [1]

WHO (world health organization) global status report on road safety. Figure 1.1 presents the number of road traffic deaths from the beginning of the 21st Century to 2018. It is easy to see that the deaths caused by road traffic accidents are keeping increasing. Globally, driver/passengers of 4 wheeled vehicles account for the largest occupation of road user types in traffic deaths, which is illustrated in Figure 1.2.

Based on this data, it is necessary and significant to pay more attention to technologies related to vehicle collision avoidance. The application of these technologies and schemes can reduce the deaths, economic damages losses and other negative results caused by vehicle accidents.

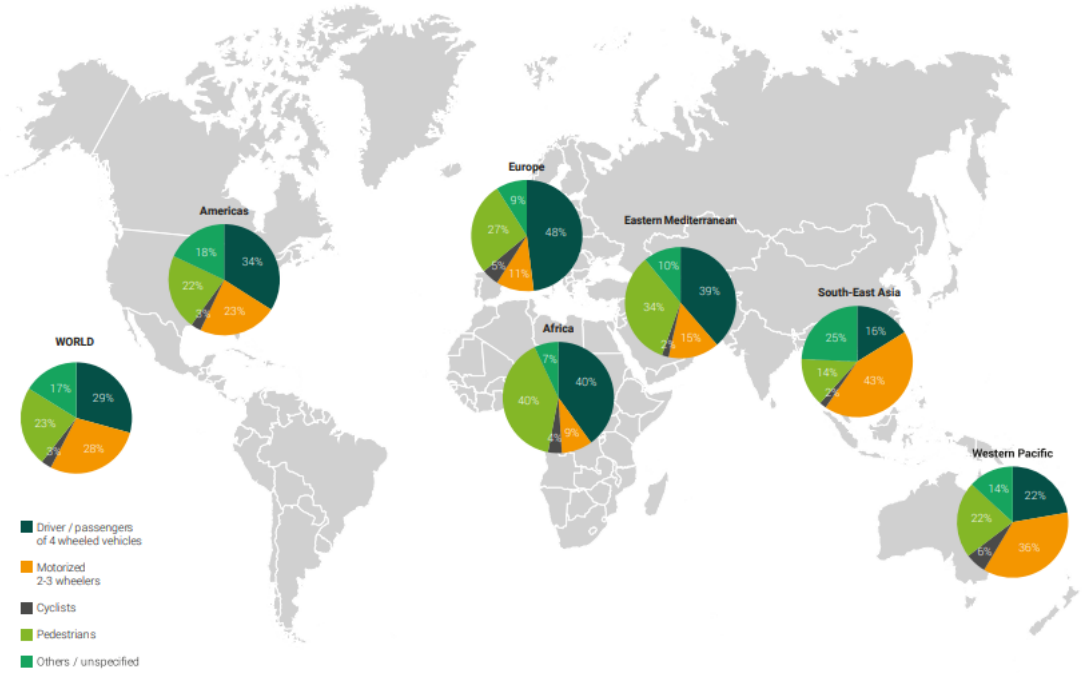


Figure 1.2: Distribution of deaths by road user type by WHO Region [1]

On the other hand, with the dramatically increasing number of total vehicles in the world, traffic jam has also been one of the most critical problems for the modern traffic system. The department of transport predicts that the traffic levels will grow up to 55% by the end of 2040 which will contribute to up to 85% of congestion levels growth at the same time [19]. It has been estimated that traffic congestion costs approximately £37.7 billion per year in the UK, which means each driver cost £1168.23 per year on average [19]. The direct and indirect costs of congestion for UK drivers are listed in Table 1.1. What is more, approximately 31 hours per year are wasted during rush hour for drivers in England and Wales [20]. Traffic jam could lead to not only huge economic cost and time wasting but also human safety problems. The congestion can contribute to higher risk of crashes by the propagation of 'shock wave' which is a phenomenon where majority of vehicles brake in traffic stream [21]. To be noticed, COVID-19 pandemic provides a significant impact on all traffic statistics after 2020, so the data for vehicle accidents and traffic congestion focus on years before 2020 more.

Intelligent traffic system (ITS) based on autonomous vehicles and vehicular com-

Table 1.1: Direct and indirect costs of congestion for UK drivers in 2017 [15]

Cost of congestion	Amount
Average direct cost per driver/car	£1046.66
Average indirect cost per driver/car	£121.57
Average total cost	£1168.23
Number of cars in the UK	32,302,800
Total cost for the UK	£37,737,255,732.50

munication have become one of the most potential research areas to deal with the problems caused by accidents and traffic jam. According to the reports and scientific studies in [22] [1] [18] [23] [24], the main cause of road accidents is linked to human error (approximately 85.2%) such as failing to observe properly and misjudging the distance. Vehicle-to-vehicle (V2V) communication provides an implementation of mutual acknowledgement between vehicles within the network which is the concept of 'connected vehicles' [25]. Based on the wireless access in vehicular environments (WAVE) protocol, basic information of vehicles including position, velocity, and acceleration can be shared within the vehicular network which could reduce the number of accidents. And with the further implementation of vehicle-to-infrastructure (V2I) communication and vehicle-to-anything (V2X) communications, the basic safety messages can be shared and processed within the whole vehicular network. By utilizing the shared information of each user within the vehicular network, an intelligent traffic system can be built up, which could lead to macroscopic control or assistance for the traffic system. Figure 1.3 shows a concise structure picture of vehicular network based ITS, where 'C2C' and 'C2I' denotes car-to-car and car-to-infrastructure communication, respectively. Based on the benefits of ITS, the traffic safety level and traffic efficiency should be improved significantly.

One of the key elements of an intelligent traffic system is the precise positioning of vehicles. The most popular and common positioning system for vehicles is the global positioning system (GPS) which is the first satellite-based navigation system [26]. There are 31 launched and operational satellites in space, which support GPS to be one of the most completed satellite positioning system. With the signal transmitted from at least 4 satellites, the position of the GPS receiver can be derived [27]. As a results of this, positioning based on GPS will be affected when not sufficient satellites are visible. The accuracy and precision of GPS positioning can also be degraded by multiple other factors such as the Doppler effect, multipath effect, ionospheric irregularities and signal block/fading caused by tall buildings, tree canopies and

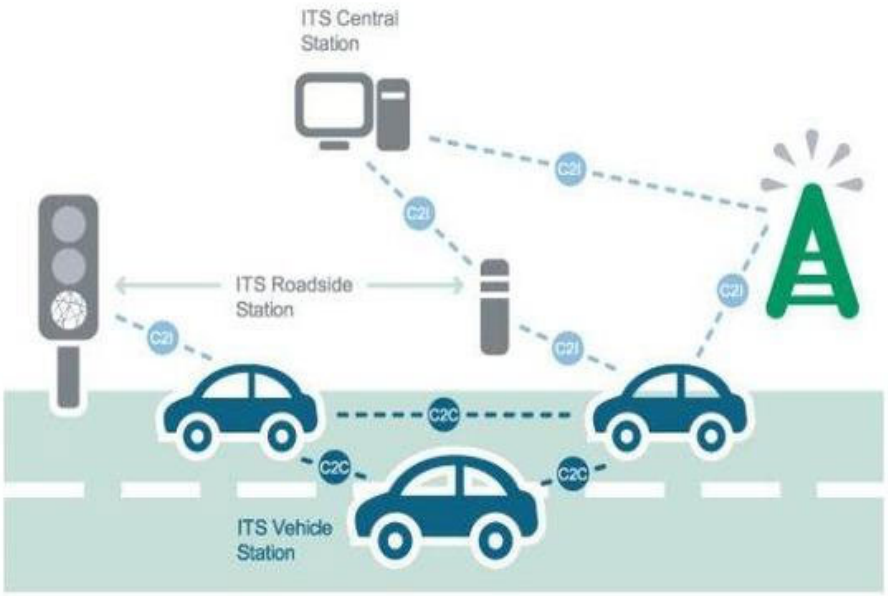


Figure 1.3: Vehicular communication network [2]

tunnels [28]. GNSS (global navigation satellite system) provides a solution for not enough visible satellites of GPS, by integrating measurements of multiple satellite navigation system besides GPS, for example, GALILEO from Europe, GLONASS from Russia and BEIDOU from China [29]. In order to avoid vehicle accidents caused by unreliable measurements of GPS within intelligent traffic system, the real time reliability of GPS measurements for each vehicle should be computed and shared within the network. In ITS protocol, the possibility of collisions could be reduced by concerning GPS reliability before determining the trajectories for each autonomous vehicle.

Multisensor data fusion is another solution to deal with GPS unreliability under challenging environments, which can also provide more precise and accurate positioning information for vehicles. Integrating sensors based on different measure concepts is able to improve the robustness and consistency of navigation system under various traffic scenarios. Several sensors which are commonly used in multisensor positioning system includes:

- GPS or GNSS

  GPS or GNSS can provide PNT (positioning, navigation and timing) information for vehicles based on visible satellites' measurements. Strong and sustainable GPS signal could be acquired under numerous scenarios, while the signal

could be weak under the challenging environments such as dense urban area. Besides estimating three-dimension positions of receivers, GPS and GNSS can also provide time synchronization support to the multisensor system.

- IMU and INS

  Inertial measurement unit (IMU) normally consists of accelerators and gyroscopes which provide measurements of angular velocity and specific force in 3-D, respectively. IMU measurements are based on the dead reckoning principle which means current positions are estimated by utilizing the determined position of the last time step [30]. Without receiving signals outside the sensor, IMU would not be affected by the environment. However, the errors for positioning of IMU are accumulated, which means it cannot provide accurate position estimation alone for a long time. INS (inertial navigation system) is a navigation system including IMU, computer (processor) or other sensors (such as GPS and compass) [31]. It can produce full position and attitude solutions by using IMU measurements.

- LiDAR

  LiDAR (light detection and ranging or laser imaging, detection and ranging) is a sensor which scans the surrounding environment using the laser. It returns the measurements for ranges and angles between surrounding obstacles and itself [32]. The LiDAR measurements can be used to derive positions, velocities and attitudes for vehicles.

Due to the different features of all these sensors, the best performance scenario for each sensor is not the same. Furthermore, measurements of sensors can be influenced by various effects and unexpected factors. It will bring extra errors if unreliable sensor measurements are fused for positioning. As a result of these, it is significant to evaluate and select sensors according to the reliability of them before data fusion, which can pick more reliable sensor combinations for fusion.

1.2 Recent Scientific Findings in ITS, Safety and Reliability of Autonomous Vehicle

In order to reduce the effects caused by traffic congestion and improve the safety level of traffic systems, a lot of ITS protocols have been developed by researchers around the world. [33] proposed an ITS intersection protocol using the vehicular network. The intersection area is divided into squares with number, so the trajectories of each vehicle can be expressed by numbers and be shared within the vehicular network. After receiving and detecting the trajectory numbers of others, vehicles will adjust velocity and acceleration to avoid collisions. However, the positioning information of vehicles in this protocol is provided by GPS only and GPS signals are assumed to be perfect, which means if GPS is unavailable or unreliable, accidents may occur due to incorrect position information shared within the network. A safe distance is added in front of vehicles for GPS inaccuracy in the updated protocol proposed by [16]. The safe distance is determined based on the GPS accuracy which is listed in Table 1.2

Table 1.2: GPS position accuracy comparison [16]

GPS Device Type	**Position Accuracy in meters**
SA-deactivated	± 10 m
Differential GPS	± 3-5 m
Wide Area Augmentation System	± 1-3 m

Nonetheless, the details of how to derive safe distance are not provided. And if the size of the safety buffer is fixed to all vehicles and determined based on the general accuracy of GPS, which does not concern different quality levels of different equipment and various factors that affect the GPS signal, the efficiency of traffic can be affected dramatically. Researchers in [9] and [34] developed intelligent traffic management using V2I infrastructure. The protocols are based on discrete time and divided traffic scenarios. Driving trajectories of vehicles are transmitted from vehicle to infrastructure for analysis. The main idea to avoid vehicle accidents is to avoid more than one vehicle occupying the same place at the same time. According to the simulation results shown in [9] and [34], by applying these protocols, vehicle collisions can be prevented and traffic throughput can be increased. As for hybrid scenarios which contain autonomous and manual vehicles, [35] uses computer vision image analysis to detect other vehicles and traffic lights, while [36] deals with this

problem by occupying all possible trajectories of vehicles without V2V equipment. Two groups of researchers explained the intersection safety service model using GPS, V2V and HMI (human machine interface) [37] [38]. Warning messages will be sent to drivers after detecting potential collisions by calculating and comparing the arrival times of vehicles. However, all these protocols trust the positioning sensors 100%, which means the reliability of sensors is not a concerned and reliability related information for each vehicle is not shared with other users. Complex traffic scenarios could bring significant effects on positioning sensors, for example, tall buildings can block, fade and contribute to multipath effects on GPS signals.

There are various factors which are used to evaluate reliability. As it is explained in [39], the MDB (marginally detectable blunder) is defined as the internal reliability of GPS observation. MDB means the smallest blunder that can be detected by the system and the external reliability is defined to represent the effects caused by undetected blunders [39]. Heidi Kuusniemi and his team determined a GPS reliability monitoring scheme based on these theories under poor GPS signal environments including urban area and indoor environments [40]. Research in [41] defined the reliability of GPS as the ability to provide the information corresponding to the reality. Assume σ to be the standard deviation between measured and given positions, then the reliability can be expressed by the ratio for the number of observations within 3σ against all available observations. The number of visible satellites and HDOP (horizontal dilution of precision) are also considered as two parameters to evaluate the reliability of satellites positioning system.

Even GPS is one of the most common and popular navigation systems, the signal can be denied, blocked or degraded dramatically under challenging environments such as tunnels and dense urban areas. Integrating other sensors with GPS to build up a multisensor navigation system is an effective approach to solve the problem. The fusion of GPS and inertial navigation system (or inertial measurement unit) has been implemented in [42], [43] and [44]. Inertial measurements can provide constant estimation when the GPS signal lost tracking and multiple sensors are able to be fused by different kinds of Kalman filter to provide more accurate positioning information. Other than IMU, more sensors are utilized as aiding schemes, for example, [45] and [46] applied an odometer and digital compass, respectively. Odometers and digital compasses can provide the speed and direction of vehicles. However, they cannot provide positioning information independently. LiDAR is used to assist

GPS and IMU for more accurate and precise navigation in [47] and [48]. LiDAR can provide measurements to derive position, velocity and attitude of vehicles, which is more supportive than odometer or compass. These two algorithms fused measurements from different sensors without evaluating the reliability of them first, which may contribute to large errors if sensors are not reliable. The application environment of LiDAR and GPS is a little different. Usually, GPS performs better in open areas while LiDAR can collect more data when more obstacles are in the surrounding environment. In order to detect unavailable sensors and switch between suitable fusion combinations of sensors, [49] and [3] proposed detection and switching algorithms. However, the detecting and switching algorithm can be applied to

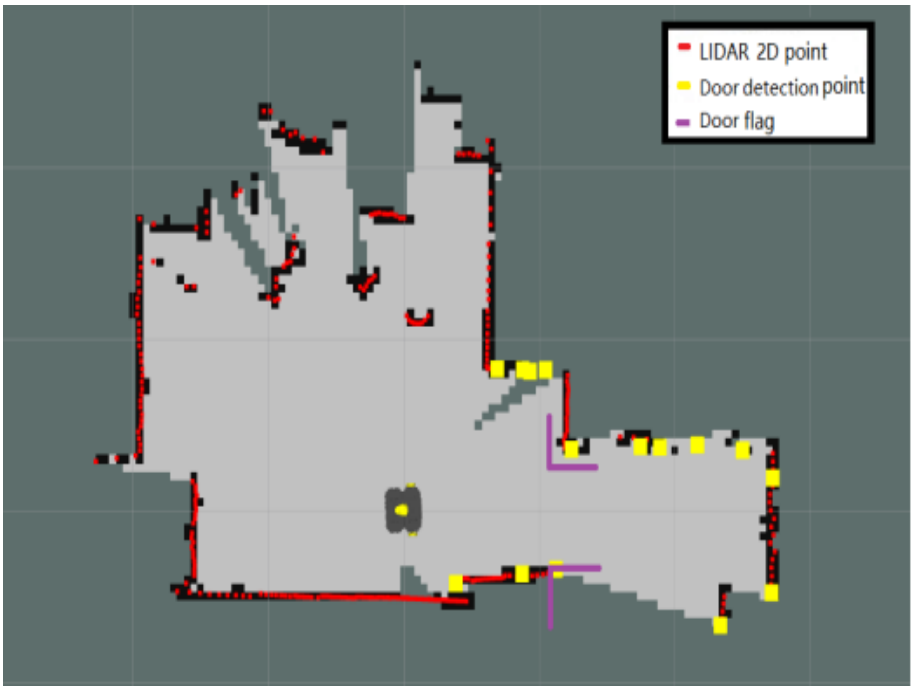


Figure 1.4: The application of LiDAR confirmation switching algorithm [3]

specific scenarios only, such as underground garages and indoor scenarios with gate and ramp. As Figure 1.4 shows, switching algorithm proposed in [3] utilized LiDAR to detect garage gate to confirm switch between sensors. [49] decides switching by monitoring the strength of GPS signal. Only one sensor are evaluated or used to confirm switching flag in these algorithm, which means the availability and reliability of other sensors are not concerned. As the result of this, these detecting and switching algorithm can not be used for the system with more other sensors under other complex traffic scenarios.

1.3 Objectives and Contribution to Knowledge

Based on the introduction aforementioned and literature review, more accurate specific positioning is necessary for ITS and autonomous vehicles, in order to support vehicles operate precisely and safely under complex surroundings within vehicular network. Positions accuracy can affect the ITS and autonomous vehicles significantly because critical decisions such as trajectory and velocity are made based on vehicles' positions and known positions of other vehicles. The reliability of satellites measurements and other sensors can contribute to positioning optimisation and higher precision. According to these, there are three main objectives for this research work, which are listed with sub-objectives of them:
(1) Develop a GPS reliability applied intelligent traffic management model for roundabout and road intersections to increase traffic safety level and traffic efficiency.

- Utilize the reliability of GPS observation to evaluate GPS measurements and determine the confidence circle of the vehicle. Inject reliability related information in basic safety messages by using the alternative space defined by IEEE 802.11p standard.

- In order to increase the safety and efficiency of traffic, develop a spatio-temporal intelligent traffic management algorithm using vehicular communication system for safety message sharing.

- Implement simulation for scenario consisting of roundabout and road intersection to compare the safety level and traffic efficiency between conventional traffic light management, proposed ITM without confidence circle and proposed ITM with confidence circle.

(2) Develop a multisensor based positioning optimisation model which fuse IMU measurements and intraclass correlation coefficient (ICC) processed GPS measurements.

- Use ICC as a reliability factor to process GPS raw measurements to increase accuracy and precision of GPS positioning.

- Implement loosely coupled integration of IMU positioning and optimised GPS positioning to estimate the positions of users with higher accuracy.

- Design and implement a trolley test under challenging environments which includes IMU and GPS receiver to evaluate the proposed positioning optimisation algorithm.

(3) Develop a multisensor navigation system which includes GNSS, IMU and LiDAR. A reliability factor based selecting and switching mode should be designed to support multisensor system to select fusion combinations under various challenging scenarios.

- Develop a selecting and switching algorithm which can pick fusion mode with better performance for each time step.
- In order to provide more reliable PNT information of the vehicle, implement data fusion for measurements of GNSS, IMU and LiDAR according to the decision of selecting mode.
- The proposed multisensor navigation system should be validated and evaluated by simulation/field testing representing real traffic environment.

The primary and secondary objectives listed above are implemented and presented in this thesis. The contribution to knowledge for this research work is:

- Define the confidence circle of vehicles according to satellites observation reliability and develop an ITS management algorithm using vehicular network to improve safety level and efficiency of traffic.
- Apply ICC to GPS satellite measurements for more precise positioning and positioning optimisation of GPS/IMU navigation system.
- Apply ICC as reliability factor to GNSS/IMU/LiDAR measurements and develop a selecting and switching module for multisensors navigation system to obtain more accurate and reliable positioning information of vehicles under challenging environment.

1.4 Thesis Outline

This thesis is organized into seven chapters.

Chapter 1 analyzes the problem state of modern traffic systems and introduces the background of the intelligent traffic systems, vehicular networks and multisensor navigation system. The motivation for developing reliable ITS management and

multisensor integration is also explained in this chapter. Literature review which investigates and describes the existing research achievements in the intelligent traffic system, GPS precise positioning and multisensor data fusion is presented. The advantages and disadvantages are compared and analysed for inspiration for research in literature review section. The objectives and contribution to knowledge of this project are presented as well.

Chapter 2 presents background knowledge about autonomous vehicles, V2X communiation, GPS positioning and sensor combination approaches. The specifications of different coordinate frames and the transformation between them are presented in detail. The concepts of LiDAR mechanization are also explained in Chapter 2.

Chapter 3 presents a safe and reliable spatio-temporal model for roundabouts and crossroads using a vehicular communication system. The application of GPS observation reliability and design of the confidence circle have been explained. The proposed ITS management algorithm is simulated based on an open source vehicular network traffic simulator.

Chapter 4 proposes an ICC applied positioning optimisation algorithm. The procedure of processing GPS measurements according to the evaluation of reliability is described. The kalman filter data fusion for IMU and GPS is explained. The trolley test setup and experiment results are presented and analysed at the end of this chapter.

Chapter 5 describes a multisensor navigation system which includes a reliability based selecting and switching algorithm. Besides explaining the fusion modes switching scheme, the pre-processing of sensor data is also presented such as the IMU mechanization and LiDAR feature extraction. After presenting the data fusion procedure, the details of the field trial are provided as well. The results of experiments and unexpected issues are analysed.

Chapter 6 restates the main outcomes of thesis work, and concludes the key points and contributions of the research presented in this thesis. The significance of the work and expected future work are also provided in this chapter.

1.5 Publications Related to the Thesis

1. **H. Li** and R. Tiwari. "Safe and Reliable Spatio-temporal Model for Roundabouts and Road Intersections using Vehicular Communication System", *16th International Conference on Intelligent Transportation Systems Telecommunications (ITST), 2018, pp. 1-7, doi: 10.1109/ITST.2018.8566865.*

2. **H. Li**, J. Yin, R. Tiwari, G. Gradoni, S. Greedy and P. Wheeler. "GPS Positioning Optimisation and Multisensor Fusion for Autonomous Vehicles in Challenging Environments", *2023 European Navigation Conference (ENC)*, Accepted

3. **H. Li**, J. Yin, R. Tiwari, G. Gradoni, S. Greedy and P. Wheeler. "Optimisation of System and Multisensor Selection for Autonomous Vehicles in Challenging Environments", Prepared in IET Intelligent Transport System journal format, to be submitted in July 2023

Chapter 2

Background and Overview

The automation levels of autonomous vehicles are presented and explained in this chapter. To utilize basic safety message and vehicular communications, the messages definitions and vehicular network standard are reviewed. The main sources of errors in GNSS/GPS positioning and data exchanging format are also described for positioning optimisation and raw data processing. As for multisensor navigation system, the background knowledge of reference frames and LiDAR mechanization are presented.

2.1 Autonomous Vehicle

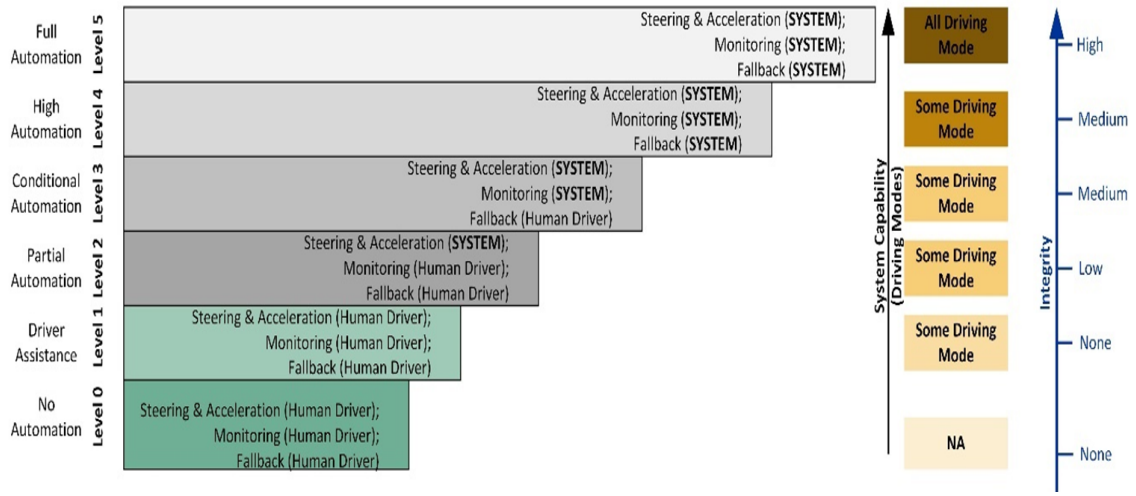


Figure 2.1: SAE-defined automation levels, system capability and required integrity [4]

The automation levels of vehicles have been defined by the SAE (Society of Automotive Engineers). When vehicles are operating in a dynamic environment,

there are 6 levels of automation in where level 0 denotes no automation and level 5 denotes full automation [17]. The vehicular automation levels, system capability and required integrity according to SAE J3016 standard are shown in Figure 2.1. The differences depend on whether human or system control steering and acceleration of vehicles, which are illustrated. Level 4 and level 5 are defined as high automation and full automation, respectively. Vehicles in level 4 and level 5 are autonomous operated, which means they do not need any human interaction for controlling and the operation will not fall back to the human driver when deviance occurs. Compared with level 5, the only limitation of level 4 is the application scenario. Autonomous vehicles in level 4 can only be operated in a specific scenario such as campus and shipping yards, while level 5 autonomous vehicles are not limited by driving locations [4].

Table 2.1: Summary of automation levels [17]

Level	Name/Description	Sustained lateral and longitudinal vehicle motion control	OEDR	DDT fall-back
0	No Driving Automation	Driver	Driver	Driver
1	Driver Assistance	Driver and System	Driver	Driver
2	Partial Driving Automation	System	Driver	Driver
3	Conditional Driving Automation	System	System	Driver
4	High Driving Automation	System	System	System
5	Full Driving Automation	System	System	System

The comparison between automation levels is summarised in Table 2.1. OEDR denotes object event detection and response, and DDT represents a dynamic driving test. A dynamic driving test consists of two subjects which are sustained lateral and longitudinal vehicle motion control and OEDR [50]. According to SAE standard, full sustained lateral and longitudinal vehicle motion control and unconditional performance of OEDR by ADS (automated driving system) are required for level 5 vehicles [17]. As a result of these, the integrity grade for level 5 is required to be much higher than levels 2 to 4. Automation levels 2 to 5 are described in detail:

- Level 2 automation

  Level 2 automation is defined as partial driving automation, which means that

vehicles at level 2 automation get limited OEDR. The operation system of the vehicle is not able to recognise and respond to specific events. These can only be completed when the driver of the vehicles takes control of the system. The automated driving system can implement sustained lateral and longitudinal motion control tasks and will disengage immediately after receiving the request from the drivers.

- Level 3 automation

  Level 3 automation is defined as conditional driving automation, which means the driver must take control of the vehicle under some conditions. The specific conditions include but are not limited to: ADS sends a request for disengagement, ADS starts a procedure of fall-back while the risks are evaluated as a minimum, ADS fails to process the procedure it was trying to carry out [17]. The driver must be prepared to operate the vehicle when ADS issue an alert to them. The alert should be triggered by ADS with sufficient time for drivers to take charge properly.

- Level 4 automation

  Level 4 automation is defined as high driving automation, which means autonomous vehicles at level 4 do not need any supervision or response from drivers when ADS is operating. The difference between level 4 and level 3 automation is that level 4 ADS can operate the fall-back procedure without interacting with drivers. At this automation level, drivers become passengers when the automated driving system is operating. ADS at level 4 is capable of taking charge of the whole journey in specific scenarios, for example, a closed loop on the university campus.

- Level 5 automation

  Level 5 automation is defined as full driving automation, which represents that the automated driving system at level 5 gets the full capability to carry out the whole DDT and DDT fall-back procedures. There is no application scenario limitation for level 5 autonomous vehicles. The ADS can be classified as level 5 automation only when it is capable to operate independently for all traffic environments, especially complex challenging environments.

2.2 Communications for Autonomous Vehicles

The communication standards and protocols of vehicular networks have been defined by SAE [51].

2.2.1 Safety Messages within Vehicular Network

Three kinds of messages sharing within the vehicular network are defined by SAE J2735 standard, which includes BSM (Basic Safety Messages), RAM (Roadside Alert Messages) and PVM (Probe Vehicle Messages) [51].

```
BasicSafetyMessageVerbose ::= SEQUENCE {
   -- Part I, sent at all times
   msgID       DSRCmsgID,              -- App ID value, 1 byte

   msgCnt      MsgCount,               -- 1 byte
   id          TemporaryID,            -- 4 bytes
   secMark     DSecond,                -- 2 bytes
   -- pos      PositionLocal3D,
   lat         Latitude,               -- 4 bytes
   long        Longitude,              -- 4 bytes
   elev        Elevation,              -- 2 bytes
   accuracy    PositionalAccuracy,     -- 4 bytes

   -- motion   Motion,
   speed       TransmissionAndSpeed,   -- 2 bytes
   heading     Heading,                -- 2 bytes
   angle       SteeringWheelAngle,     -- 1 bytes
   accelSet    AccelerationSet4Way,    -- 7 bytes

   -- control  Control,
   brakes      BrakeSystemStatus,      -- 2 bytes

   -- basic    VehicleBasic,
   size        VehicleSize,            -- 3 bytes

   -- Part II, sent as required
   -- Part II,
   safetyExt   VehicleSafetyExtension OPTIONAL,
   status      VehicleStatus          OPTIONAL,
   ... -- # LOCAL_CONTENT
   }
```

Figure 2.2: Basic safety message structure [4]

The contents of these three messages are described as:

- Basic Safety Messages

  BSM are primarily illustrated by the application EEBL (Emergency Electronic Brake Lights), which are used to track neighbouring vehicles and make related decisions. Figure 2.2 shows the construction of the basic safety message and the size for each category. There are two parts in BSM including a compulsory

part and an optional part. The compulsory part contains information which needs to be sent all the time such as message ID, time tag, 3-D positions of vehicle, motion information and control information [52]. An optional part will be sent as required where trajectory, sensor data, and reliability information can be injected.

- Roadside Alert Messages

  RAM are utilised for various traffic information-sharing applications, especially when informing emergency alert to nearby vehicles. RAM are usually sent from roadside safety infrastructures and public on-board safety units to users. When emergent situations occur such as traffic congestion, road traffic accidents and emergency vehicles passing through, RAM will be broadcast to nearby users. RAM can also be used to transmit control information between central control infrastructure and vehicles.

- Probe Vehicle Messages

  PVM are usually used for sharing information about traffic conditions, weather and road surface conditions. On-board sensors and equipment can collect relevant data of the surrounding environment, which can be shared with other vehicles, roadside infrastructures and central controllers.

2.2.2 Vehicular Networks

According to the SAE J2735 protocol and IEEE 802.11p standard, information within vehicular is shared over network DSRC (Dedicated Short-range Communication). There is a dedicated frequency band for DSRC, which is located at 5.9 GHZ with 75 MHz bandwidth. Compared with cellular network communications and satellite communications, the communication range of DSRC is much shorter, which is less than one kilometer. As Table 2.2 shows, The DSRC band is divided into 7 channels with different power and function. where CCH and SCH denotes

Table 2.2: Available channels for DSRC

Channel	**172**	**174**	**176**	**178**	**180**	**182**	**184**
Channel type	SCH	SCH	SCH	CCH	SCH	SCH	SCH
Power (dBm)	33	33	33	44.8	23	23	40
Frequency (GHz)	5.86	5.87	5.88	5.89	5.90	5.91	5.92

control channel and service channel, respectively. The control channel gets highest power and carries out transmitting safety information. Each vehicle will utilize channel 172 to share basic safety messages (BSM) with 10-20 Hz frequency. Channel 184 can support long-distance V2I (vehicle to infrastructure) communication. The emergency information will be transmitted with high priority in channel 184 [53].

2.3 GNSS Error Sources and RINEX Files

2.3.1 Sources of Errors of GNSS

For satellite navigation system, at least 4 satellites are required to estimate the position of receivers, 3 of which are positioning accuracy related and the other one satellite is time synchronization related [54]. As it mentioned, because GNSS/GPS is a LOS (line of sight) based navigation service, numerous factors can bring negative effects on the positioning measurements of them [55]. Some of them are listed and described below.

2.3.1.1 Multipath Effect

Multipath effect occurs when GNSS/GPS signal is reflected by obstacles such as skyscrapers and tree canopy between satellites and receivers. As it is shown in Figure 2.3, besides the direct line-of-sight signal transmitted by satellites, receiver can also receive non-line-of-sight signals which are reflected by obstacles. Reflected signals are received with effects caused by time delay and channel fading, which can contribute to degradation of positioning and communication performance. The errors caused by multipath effect can be up to 10 meters and can also lead to sensitivity reduction of receivers, if multipath mitigation is not applied [56].

2.3.1.2 Satellite and Receiver Clock offsets

The clock bias caused by satellite and receiver clock offsets are one of the main sources of errors. The positions of receivers are derived based on distance which is computed from time and speed of light. That means even minor clock offsets can lead to major errors in position estimation. The receiver clock bias is usually larger than satellite clock bias due to higher precision of satellite clock and the additional clock term in navigation message for satellite clock correction [57]. One of the effective

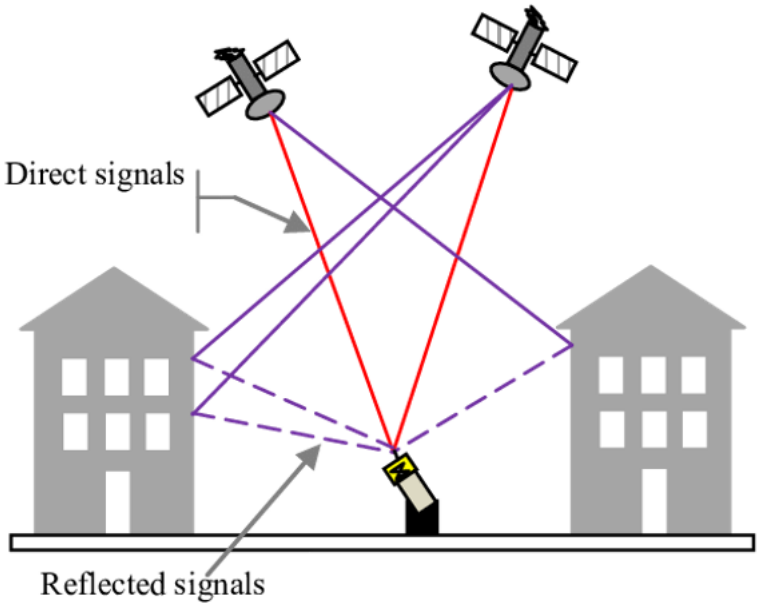


Figure 2.3: Multipath effect on satellite signal [5]

approaches to mitigate satellite and receiver clock offsets is to consider them as estimated elements in the positioning algorithm such as least square method and kalman filter method.

2.3.1.3 Signal Blocking/Fading and Satellite Geometry

The signal strength of GNSS/GPS can be influence by barriers such as the wall of buildings dramatically. The performance of receivers under challenging environment such as tunnel and indoor scenarios will be degraded significantly due to weak signal. Extreme weak signal caused by blocking and fading can lead to failure for locking satellites and dramatic inaccuracy for positioning. What is more, bad satellite geometry can also increase the errors of navigation. As Figure 2.4 illustrates, according to the navigation concepts of GNSS, bad satellites geometry can introduce higher uncertainty and larger range errors, which is also known as dilution of precision (DOP) [55]. Higher value of DOP indicates poorer satellites geometry and less precision of positioning, in contrast, lower DOP value represents better satellites geometry, more precision and less errors.

2.3.1.4 Tropospheric Delay

Figure 2.5 shows the layers of Earth's atmosphere. it is easy to see that troposphere is the lowest layer over the surface of the Earth, which extends to around 12 km.

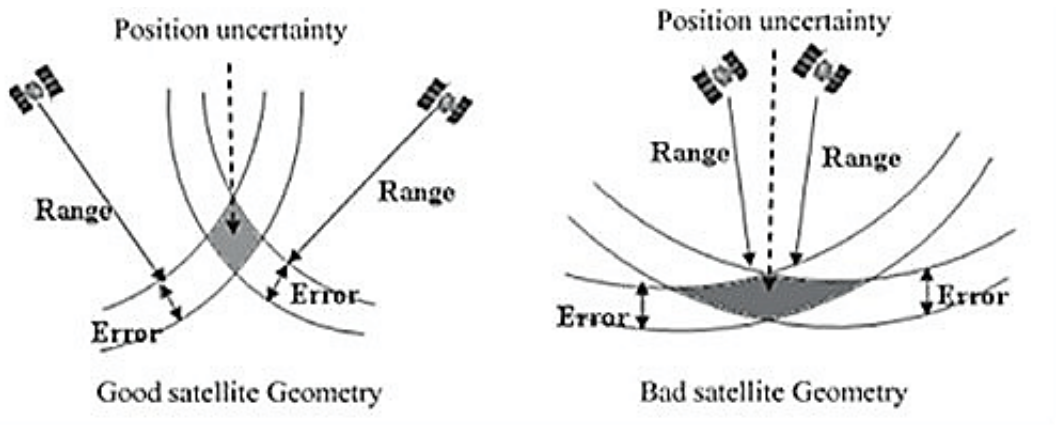


Figure 2.4: Area of uncertainty due to good and bad satellite geometry [6]

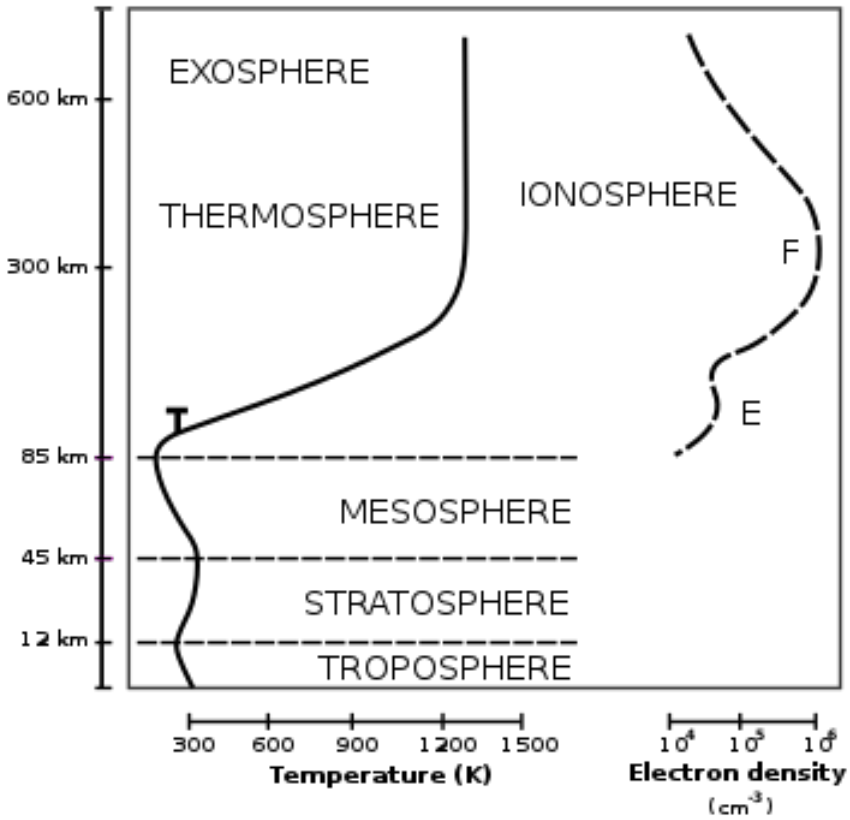


Figure 2.5: Layers of Earth's atmosphere [7]

Due to the non-dispersive property of troposphere for GPS frequencies, it can contribute to significant delay for pseudorange and carrier phase measurements. The tropospheric delay can be calculated based on the elevation angle by [58]:

$$t_d = \frac{2.47}{sinE + 0.0121} \quad meters \tag{2.1}$$

where E denotes the elevation angle.

2.3.1.5 Ionospheric Delay

According to the layers distribution in Figure 2.5, ionosphere locates between 80 km to more than 600 km over the surface of the Earth. The delay introduced by ionosphere is from affecting signal propagation group velocity. Although there is ionosphere delay terms in the navigation file for ionospheric delay mitigation, ionosphere can still introduce delay at L1 frequency band of GPS when the receiver can receive signal from dual frequency bands. The time delay caused by ionosphere can be expressed as [59]:

$$t_i = \frac{f_2^2}{f_1^2 - f_2^2}\delta(t) \tag{2.2}$$

where f_1 and f_2 denotes the carrier frequencies of L1 and L2 bands. $\delta(t)$ represents the time delay between these two frequencies.

2.3.2 RINEX files

Receiver independent exchange format (RINEX) is a data exchange format which is widely used for satellite navigation system data [60]. It was first developed for the easy exchange of GPS data and with the version update, more and more satellite navigation systems are involved such as GLONASS, GALILEO, BEIDOU, QZSS and IRNSS. By utilizing RENIX files, it is convenient to post-process the received raw data from satellites for research and further investigation.

There are three types of ASCII files for the RENIX version 3 series including observation data file, navigation message file and meteorological data file. Every type of RINEX file is consist of a header section and a data section [60]. There are three basic quantities in satellites observable including time, phase and range.

- Time

In RINEX files, the time of measurements denotes the time when the signal is received by a receiver. It is considered identical for not only the phase and pseudorange but also all the visible satellites at the epoch.

- Range

  The measured range between the receiver antenna and the satellite antenna is called pseudorange (PR), because it contains biases such as satellite clock offsets, receiver clock offsets, atmospheric delays and ionospheric delays. So the pseudorange can be expressed as:

  $$PR = distance + c * (\delta t - \delta T) + \text{other bias}$$

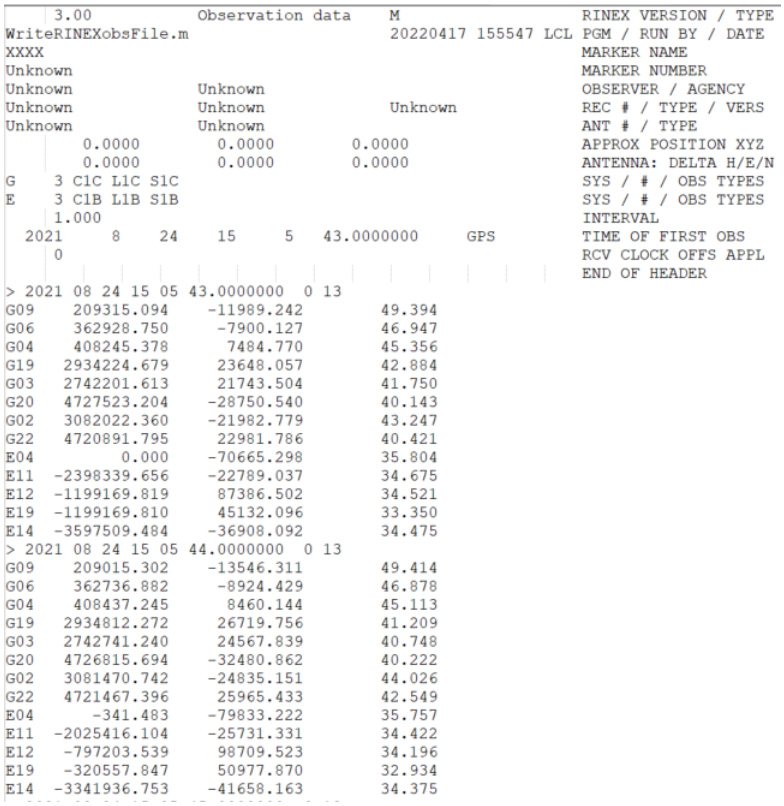
  where δt and δT denote the receiver clock offsets and the satellite clock offsets, respectively. c is the speed of light and *distance* represents the real range between receiver and satellite.

- Phase

  The phase measurements provided by RINEX files are the carrier-phase range between receiver and satellite measured in whole cycles [60]. The estimated distance between the satellite and the can be computed based on phase measurements, carrier frequency and speed of light.

```
     3.03           N: GNSS NAV DATA    G: GPS              RINEX VERSION / TYPE
sbf2rin-13.0.1                         20180807 134243 UTC PGM / RUN BY / DATE
GPSA   4.6566E-09  1.4901E-08 -5.9605E-08 -5.9605E-08       IONOSPHERIC CORR
GPSB   7.7824E+04  4.9152E+04 -6.5536E+04 -3.2768E+05       IONOSPHERIC CORR
GPUT  0.0000000000E+00-3.552713679E-15 319488 2013          TIME SYSTEM CORR
    18                                                      LEAP SECONDS
                                                            END OF HEADER
G08 2018 08 07 13 59 44-1.108469441533E-04-1.364242052659E-12 0.000000000000E+00
     5.600000000000E+01-6.909375000000E+01 4.693766942805E-09 2.658968945529E+00
    -3.445893526077E-06 3.466341877356E-03 2.890825271606E-06 5.153607307434E+03
     2.231840000000E+05-7.078051567078E-08 1.216946629272E+00 1.881271600723E-07
     9.693288258993E-01 3.281562500000E+02-4.019537750338E-01-8.382134863848E-09
    -1.525063525017E-10 1.000000000000E+00 2.013000000000E+03 0.000000000000E+00
     2.000000000000E+00 0.000000000000E+00 5.122274160385E-09 5.600000000000E+01
     2.163660000000E+05 4.000000000000E+00
G10 2018 08 07 14 00 00 1.874673180282E-04-1.023181539495E-12 0.000000000000E+00
     9.400000000000E+01 1.381250000000E+01 4.522688388125E-09-1.897148303659E+00
     7.450580596924E-07 3.671505488455E-03 8.385628461838E-06 5.153660322189E+03
     2.232000000000E+05-6.332993507385E-08-2.961567202624E+00-3.725290298462E-08
     9.617936713441E-01 2.199375000000E+02-2.772568722719E+00-7.915686862988E-09
     4.193031799462E-10 1.000000000000E+00 2.013000000000E+03 0.000000000000E+00
     2.000000000000E+00 0.000000000000E+00 1.862645149231E-09 9.400000000000E+01
     2.164260000000E+05 4.000000000000E+00
G11 2018 08 07 14 00 00-7.261163555086E-04 2.160049916711E-12 0.000000000000E+00
     9.000000000000E+01-1.135625000000E+02 5.868815888310E-09-5.194646198208E-01
    -5.858018994331E-06 1.703533006366E-02 7.892027497292E-06 5.153653854370E+03
     2.232000000000E+05-2.011656761169E-07 1.850773025200E+00-7.450580596924E-09
     9.060442961760E-01 1.972812500000E+02 1.793469270314E+00-9.115736849887E-09
    -8.678932940965E-11 1.000000000000E+00 2.013000000000E+03 0.000000000000E+00
     2.800000000000E+00 0.000000000000E+00-1.210719347000E-08 9.000000000000E+01
     2.188560000000E+05 4.000000000000E+00
G15 2018 08 07 14 00 00-3.490606322885E-04 9.094947017729E-13 0.000000000000E+00
     2.800000000000E+01-1.303125000000E+01 5.615948212499E-09 1.422076576637E+00
    -6.165355443954E-07 1.044976420235E-02 6.215646862984E-06 5.153782745361E+03
     2.232000000000E+05-1.322478055954E-07-1.997357710789E+00 3.911554813385E-08
     9.278903810103E-01 2.464687500000E+02 6.933364770473E-01-8.658932107850E-09
    -3.110843864848E-10 1.000000000000E+00 2.013000000000E+03 0.000000000000E+00
     2.000000000000E+00 0.000000000000E+00-1.071020960808E-08 2.800000000000E+01
     2.176380000000E+05 4.000000000000E+00
```

Figure 2.6: An example of Navigation data file



```
     3.00           Observation data    M                   RINEX VERSION / TYPE
WriteRINEXobsFile.m                     20220417 155547 LCL PGM / RUN BY / DATE
XXXX                                                        MARKER NAME
Unknown                                                     MARKER NUMBER
Unknown             Unknown                                 OBSERVER / AGENCY
Unknown             Unknown             Unknown             REC # / TYPE / VERS
Unknown             Unknown                                 ANT # / TYPE
        0.0000         0.0000         0.0000                APPROX POSITION XYZ
        0.0000         0.0000         0.0000                ANTENNA: DELTA H/E/N
G    3 C1C L1C S1C                                          SYS / # / OBS TYPES
E    3 C1B L1B S1B                                          SYS / # / OBS TYPES
     1.000                                                  INTERVAL
  2021     8    24    15     5   43.0000000     GPS         TIME OF FIRST OBS
     0                                                      RCV CLOCK OFFS APPL
                                                            END OF HEADER
> 2021 08 24 15 05 43.0000000  0 13
G09    209315.094    -11989.242         49.394
G06    362928.750     -7900.127         46.947
G04    408245.378      7484.770         45.356
G19   2934224.679     23648.057         42.884
G03   2742201.613     21743.504         41.750
G20   4727523.204    -28750.540         40.143
G02   3082022.360    -21982.779         43.247
G22   4720891.795     22981.786         40.421
E04         0.000    -70665.298         35.804
E11  -2398339.656    -22789.037         34.675
E12  -1199169.819     87386.502         34.521
E19  -1199169.810     45132.096         33.350
E14  -3597509.484    -36908.092         34.475
> 2021 08 24 15 05 44.0000000  0 13
G09    209015.302    -13546.311         49.414
G06    362736.882     -8924.429         46.878
G04    408437.245      8460.144         45.113
G19   2934812.272     26719.756         41.209
G03   2742741.240     24567.839         40.748
G20   4726815.694    -32480.862         40.222
G02   3081470.742    -24835.151         44.026
G22   4721467.396     25965.433         42.549
E04      -341.483    -79833.222         35.757
E11  -2025416.104    -25731.331         34.422
E12   -797203.539     98709.523         34.196
E19   -320557.847     50977.870         32.934
E14  -3341936.753    -41658.163         34.375
```

Figure 2.7: An example of Observation data file

Figure 2.6 shows an example of a partial Navigation file. The header section contains global information such as the RINEX version, satellite system and leap seconds. The data section of the Navigation file contains details of satellites at epochs. Based on the Navigation file data record, the positions of satellites can be calculated.

An example of the Observation file is presented in Figure 2.7. Besides the time of first observation and antenna-related records, the navigation system and observation type are also presented, which indicate type, band and attribute information. Following the listed system and observation type information, the data section provides observation measurements of visible satellites at each epoch, which includes pesudorange, carrier-phase circle and signal strength. The GPS positioning optimisation algorithm explained in this thesis is based on the raw measurements obtained from RINEX files.

2.4 Frames of Reference and Transformations

2.4.1 Frames of reference

Various frames of reference are utilized by different sensors and navigation systems. It is necessary to transform the measurements into the same reference frame in order to fuse the data or compare positioning differences between them. There are several frames of reference which have been used in this project:

- WGS 84

  WGS84 is also known as world geodetic system 1984, which is one of the most popular coordinate systems around the world. The measurements of GPS are all based on WGS 84 coordinate system [61]. The origin of WGS 84 coordinate is the mass centre of the Earth. The position in WGS 84 is expressed by latitude, longitude and height. As it is shown in Figure 2.8, λ and φ denotes the longitude and latitude, respectively.

- ECEF

  The Earth-centred Earth-fixed coordinate system (ECEF), whici is also named as geocentric coordinate system. Compared with WGS 84, ECEF gets the same origin of coordinate, which is the Earth's mass centre, but ECEF follows Cartesian spatial system. The z axis of ECEF is the line which connects North and South poles of the Earth. $xandy$ axes are in the equator plane. x axis passes through origin and connects 180° longitude and 0° longitude. y axis passes through origin and connects 90°W longitude and 90°E longitude [62]. A demonstration of three axes of ECEF is shown in Figure 2.8

- ENU

  East, North and Up (ENU) coordinate belongs to local reference frame which is defined over a specific small area. With the set origin of local frame, the x, y and z axis passes through origin and points toward to geodesic East, geodesic North and 90° angle to the Earth surface, respectively [63].

- ECI

  Earth-centred inertial (ECI) is also a Cartesian coordinate whose centre is the mass centre of the Earth. z axis is perpendicular to the equatorial plane. The x

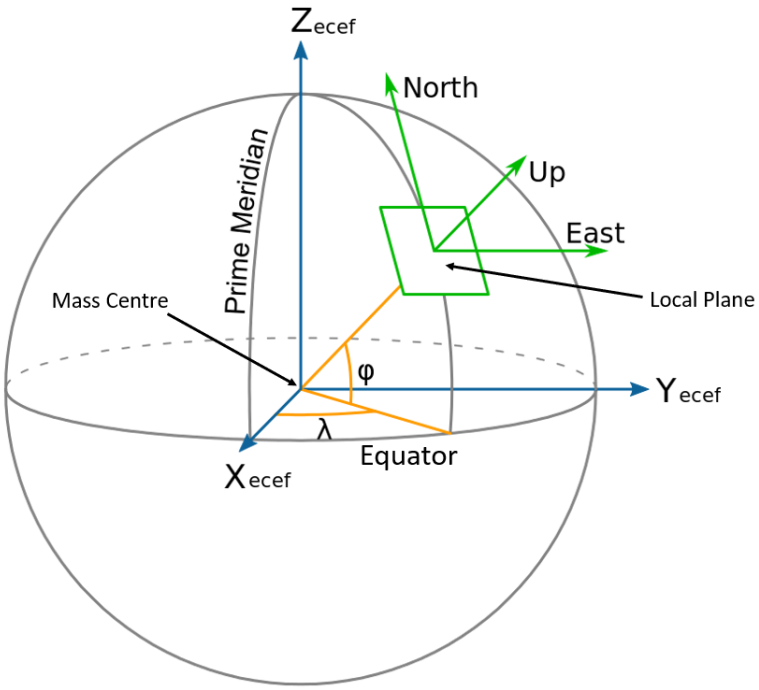


Figure 2.8: Comparison between ECEF, WGS 84 and local frame

axis passes through the origin and points toward the celestial sphere. Celestial sphere is determined as an abstract sphere with arbitrarily large radius and is concentric to the Earth [64]. y axis follows right-hand coordinate system. As a result of these, ECI coordinate does not rotate with the Earth and is usually used to express motion of satellites of GNSS or spacecraft [65].

- Body frame

  Some sensors such as IMU measurement the positioning information based on body frame, which is expressed by yaw, pitch and roll. Figure 2.9 demonstrates the body frame of a moving vehicle. Consider the centre of vehicle or the centre of sensor as the origin of body frame. Yaw, pitch and roll can express the motion attitude of vehicle.

2.4.2 Transformations between Reference Frames

For multisensor navigation systems, different sensors may provide measurements based on different reference frames, so transformations between reference frames are necessary for further processing of sensor measurements such as data fusion.

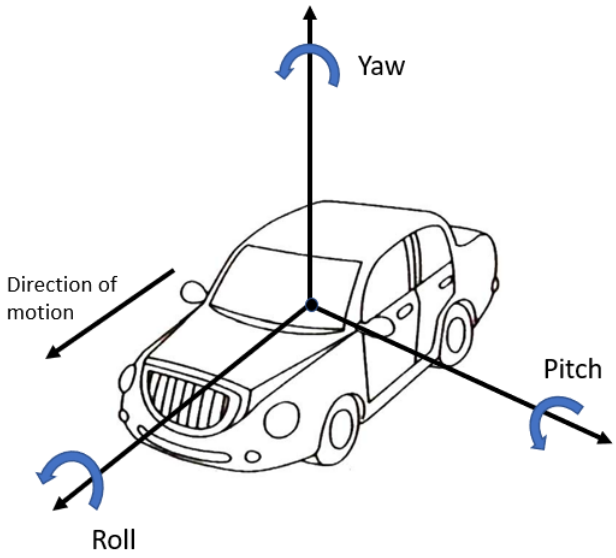


Figure 2.9: Body frame

2.4.2.1 Transform from ECEF to WGS 84

In order to transform positions from ECEF coordinate to WGS 84 coordinate, the matrix in Equation 2.3 should be used.

$$\begin{bmatrix} x \\ y \\ z \end{bmatrix} = \begin{bmatrix} (R_p + h)cos(\varphi)cos(\lambda) \\ (R_p + h)cos(\varphi)sin(\lambda) \\ [R_p(1 - e^2) + h]sin(\varphi) \end{bmatrix} \tag{2.3}$$

where λ, φ and h represents the longitude, latitude and height, respectively. And R_p denotes the prime vertical radius of curvature.

2.4.2.2 Transformation between ENU and ECEF

There are two steps to transform from ENU coordinate to ECEF coordinate [66]:
(1) Rotate $90 - \varphi$ around East axis clockwise, which can be expressed by $Ra[-(\frac{\pi}{2} - \varphi)]$.
(2) Rotate $90 + \lambda$ around z axis clockwise, which can be expressed by $Rc[-(\frac{\pi}{2} + \lambda)]$.
Then the transformation can be described as:

$$\begin{bmatrix} x \\ y \\ z \end{bmatrix} = Rc[-(\frac{\pi}{2} + \lambda)]Ra[-(\frac{\pi}{2} - \varphi)] \begin{bmatrix} E \\ N \\ U \end{bmatrix} \tag{2.4}$$

According to the definition in [67],

$$Ra[\theta] = \begin{bmatrix} 1 & 0 & 0 \\ 0 & cos\theta & sin\theta \\ 0 & -sin\theta & cos\theta \end{bmatrix} \tag{2.5a}$$

$$Rb[\theta] = \begin{bmatrix} cos\theta & 0 & -sin\theta \\ 0 & 1 & 0 \\ sin\theta & 0 & cos\theta \end{bmatrix} \tag{2.5b}$$

$$Rc[\theta] = \begin{bmatrix} cos\theta & sin\theta & 0 \\ -sin\theta & cos\theta & 0 \\ 0 & 0 & 1 \end{bmatrix} \tag{2.5c}$$

Then the transformation matrix can be rewritten as:

$$Rc[-(\frac{\pi}{2}+\lambda)]Ra[-(\frac{\pi}{2}-\varphi)] = \begin{bmatrix} -sin\lambda & -cos\lambda sin\varphi & cos\lambda cos\varphi \\ cos\lambda & -sin\lambda sin\varphi & sin\lambda cos\varphi \\ 0 & cos\varphi & sin\varphi \end{bmatrix} \tag{2.6}$$

Based on this transformation matrix, the position expressed in local frame can be transformed to ECEF coordinate.

The inverse transformation of Equation 2.4 can be described by [66]:

$$\begin{bmatrix} E \\ N \\ U \end{bmatrix} = Ra[\frac{\pi}{2}-\varphi]Rc[\frac{\pi}{2}+\lambda] \begin{bmatrix} x \\ y \\ z \end{bmatrix} \tag{2.7}$$

and the transformation matrix from ECEF to ENU is presented:

$$Ra[\frac{\pi}{2}-\varphi]Rc[\frac{\pi}{2}+\lambda] = \begin{bmatrix} -sin\lambda & cos\lambda & 0 \\ -cos\lambda sin\varphi & -sin\lambda sin\varphi & cos\varphi \\ cos\lambda cos\varphi & sin\lambda cos\varphi & sin\varphi \end{bmatrix} \tag{2.8}$$

2.4.2.3 Transformation between ENU and Body Frame

The transformation procedure from body frame to local frame can be regarded as three times rotations around three axes. Assume ψ, θ and φ denotes the measurements of yaw, pitch and roll, respectively. Then the transformation matrix can be

derived by [62]:

$$
\begin{aligned}
R_{body}^{local} &= \begin{bmatrix} cos\psi & -sin\psi & 0 \\ sin\psi & cos\psi & 0 \\ 0 & 0 & 1 \end{bmatrix} \begin{bmatrix} 1 & 0 & 0 \\ 0 & cos\theta & -sin\theta \\ 0 & sin\theta & cos\theta \end{bmatrix} \begin{bmatrix} cos\varphi & 0 & sin\varphi \\ 0 & 1 & 0 \\ -sin\varphi & 0 & cos\varphi \end{bmatrix} \\
&= \begin{bmatrix} cos\psi cos\varphi - sin\psi sin\theta sin\varphi & -sin\psi cos\theta & cos\psi sin\varphi + sin\psi sin\theta cos\varphi \\ sin\psi cos\varphi + cos\psi sin\theta sin\varphi & cos\psi cos\theta & sin\psi sin\varphi - cos\psi sin\theta cos\varphi \\ -cos\theta sin\varphi & sin\theta & cos\theta cos\varphi \end{bmatrix}
\end{aligned} \tag{2.9}
$$

The transformation from local ENU frame to body frame can be implemented by the inverse matrix of R_{body}^{local}.

2.4.2.4 Transformation between ECEF and ECI

As Figure 2.10 shows, because ECEF coordinate is rotating with respect to stars and ECI is inertial coordinate, the transformation between them can be derived based on angular velocity of Earth rotation and time. Assume ω_R and t represents the Earth rotation angular velocity and reference time, respectively. Then the transformation matrix from ECI to ECEF coordinate can be described as:

$$
R_{ECI}^{ECEF} = \begin{bmatrix} cos\omega_R t & sin\omega_R t & 0 \\ -sin\omega_R t & cos\omega_R t & 0 \\ 0 & 0 & 1 \end{bmatrix} \tag{2.10}
$$

In contrast, the transformation matrix from ECEF to ECI is the inverse of matrix R_{ECI}^{ECEF}.

2.5 LiDAR Mechanization

LiDAR sensor repeatedly emitted pulse of light once it hit a target the sensor determines the range by measuring the transmit and return time between the target and the sensor. In addition to range measurement, LiDAR sensor enable reading multiple points within 360° to generate 2D measurements by using its rotation platform. An advanced LiDAR sensor can provide 3D measurement with a vertical scanning capability. The photo of a LiDAR and interface box is showed in Figure 5.4.

LiDAR positioning consists of feature extraction, feature mapping and relevant

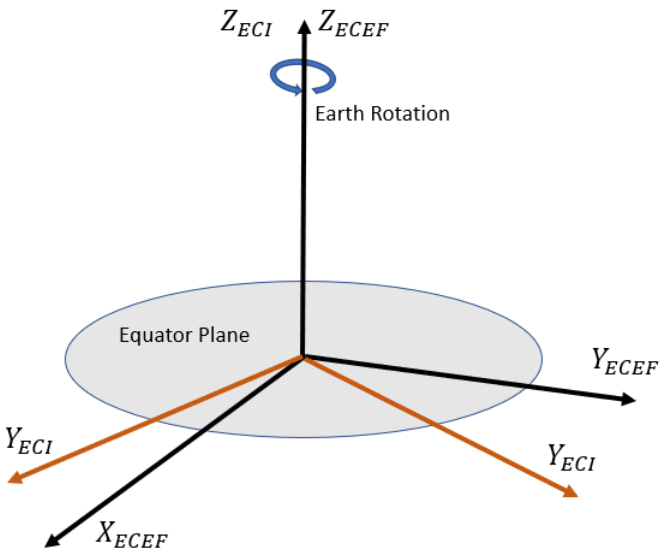


Figure 2.10: Transformation between ECI and ECEF

positioning estimation. The feature extraction is used to provide the reference navigation and the lines are employed for the feature representation. Lines are the most common and repeatable features in the urban environment. Identical line feature from two successive circular scans can be used to provide relative positioning information. Many line extraction algorithms have been proposed using range and angle data from the LiDAR measurement, in this project a Least mean square approach is used to extract the line features. The detail of line feature extraction and mapping are explained in Section 5.2.1.

The LiDAR positioning mechanization is illustrated in Figure 2.11. The doted dash lines are the obstacles or barriers around the LiDAR sensor. At time i LiDAR sensor is denoted as S_i, two line features are extracted denoted as Features F^n and F^{n+1}, at time $i+1$ sensor moves to S_{i+1} with relevant location $[\Delta X, \Delta Y]$ to S_i. Features F^n and F^{n+1} are two identical line features between time i and $i+1$. Once the relevant location $[\Delta X, \Delta Y]$ is identified, velocity in the body frame can be estimated based on the updated time.

To identify the relevant location $[\Delta X, \Delta Y]$, the range between the sensor and the features need to be identified, R_i^n and R_i^{n+1} are the distance between the sensor and the feature F^n and feature F^{n+1} at time i, this distance can be expressed by two perpendicular lines denoted also as R_i^n and R_i^{n+1}. ϕ_i is the angle between the sensor's x axis and the perpendicular line R_i^n and P_i^n is the intersection point between line R_i^n and feature F^n. Two methods are capable to express the coordination of P_i^n, if the location S_i is considered as the original point, in the Cartesian coordinate

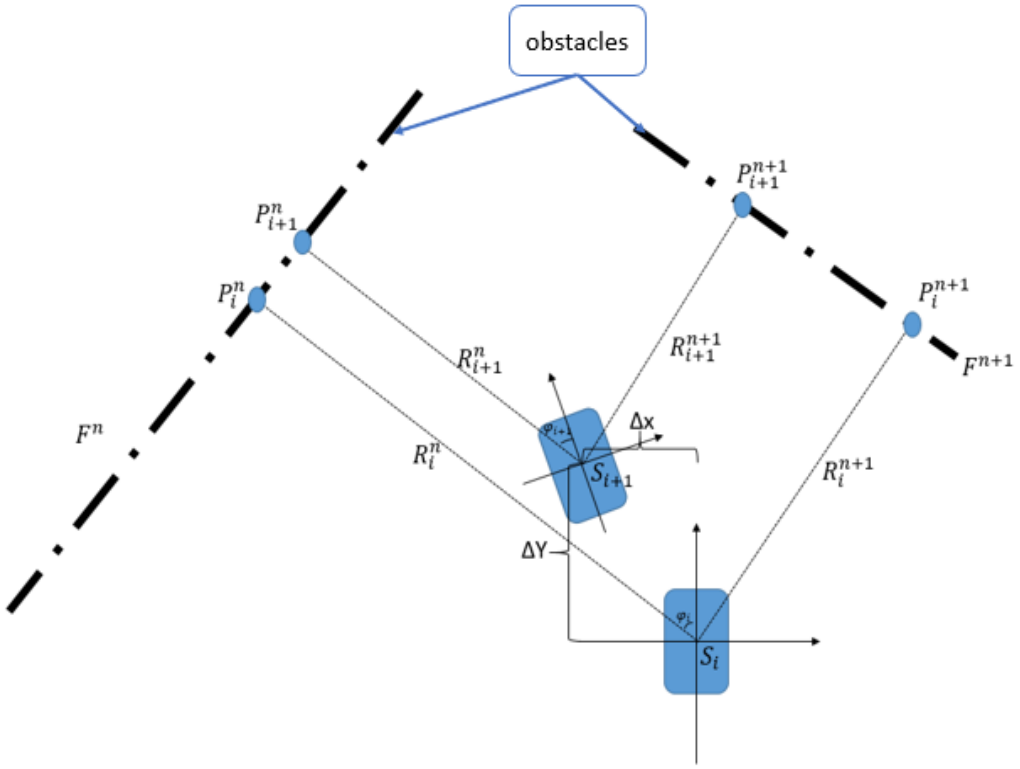


Figure 2.11: LiDAR positioning mechanization

system can be expressed as $[x_i, y_i]$ and in the Polar coordinate system, it can be denoted as $[\rho_i, \phi_i]$.

Meanwhile, P_{i+1}^n is the intersection point between identical feature F_n and perpendicular line R_{i+1}^n with coordination $[x_i + 1, y_i + 1]$ under Cartesian coordinate and $[\rho_{i+1}\phi_{i+1}]$. Since the extracted features are static line R_i^n and R_i^{n+1} are parallel thus the difference between R_i^n and R_i^{n+1} can be expressed as $\Delta\rho = R_{i+1}^n - R_i^n$. As Figure 2.12 presented, the coordinate $[\Delta x, \Delta y]$ can be converted to calculate the length of the two triangle sides.

Finally. the different coordinates $[\Delta x, \Delta y]$

$$\Delta\rho = cos(\phi)\Delta y + sin(\phi)\Delta x \tag{2.11}$$

Therefore, with multiple line features extracted, the positioning equation can be

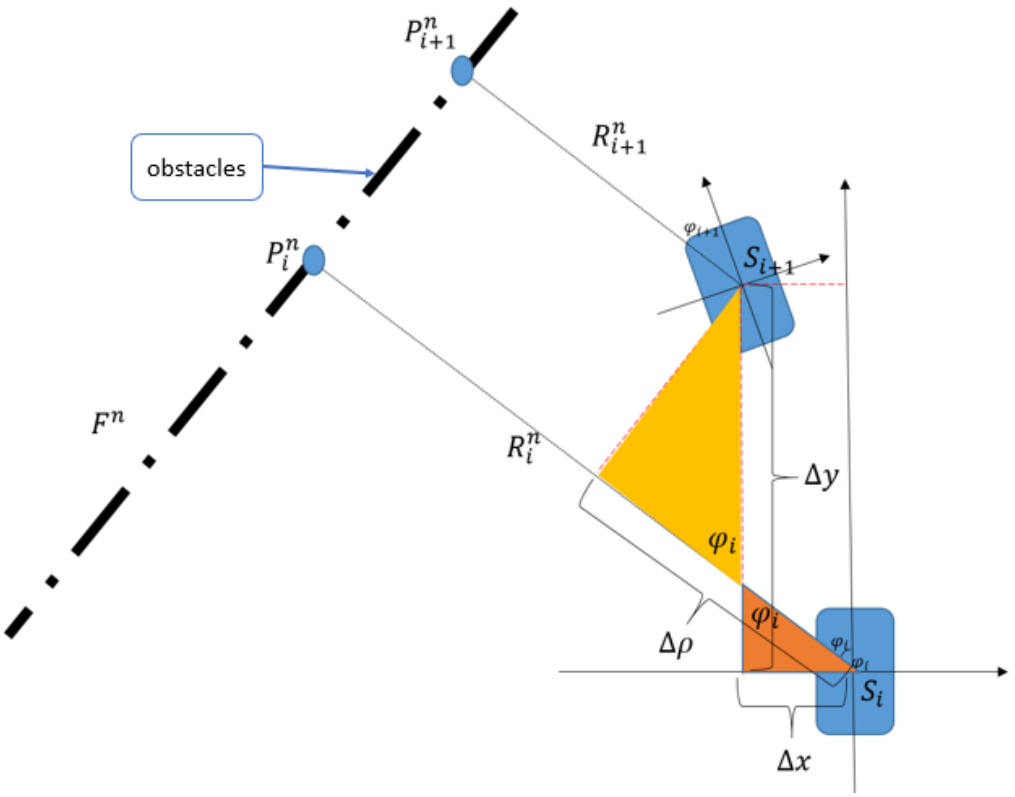


Figure 2.12: Coordination conversion

expressed in matrix form as

$$\begin{bmatrix} \rho_i^1 - \rho_{i+1}^1 \\ \rho_i^2 - \rho_{i+1}^2 \\ \vdots \\ \rho_i^n - \rho_{i+1}^n \end{bmatrix} = \begin{bmatrix} \cos(\phi^1) sin(\phi^1) \\ \cos(\phi^2) sin(\phi^2) \\ \vdots \\ \cos(\phi^n) sin(\phi^n) \end{bmatrix} \begin{bmatrix} \Delta x \\ \Delta y \end{bmatrix} \tag{2.12}$$

The azimuth can be obtained by subtracting the angle ϕ_i and $\phi_i + 1$.

As Equation 2.12 presented, only 2 nonparallel line features are required to obtain the relevant positioning. This allows LiDAR sensor to provide positioning information under urban environments due to the sufficient line features and become a positioning information source when GNSS service is lost under an urban environment.

2.6 Summary

In this chapter, background knowledge for autonomous vehicles are presented including comparison between different automation levels, definition of safety messages within vehicular network and protocol of vehicular networks. The error sources of

satellite positioning are listed and explained. The format of RINEX files and how to extract useful information from them are also included. The definition and transformation between several frames of reference including WGS 84, ECEF, ENU, ECI and body frame are illustrated in detail. The procedure for LiDAR mechanization are explained as well in this chapter.

Chapter 3

Safe and Reliable Spatio-temporal Model for Roundabouts and Road Intersections using Vehicular Communication System

3.1 Motivation and Problem States

Road transport is one of the most critical parts of modern transportation whose safety level and efficiency are top priorities. A lot of research and technologies have been taken and applied in order to implement a more safe and efficient intelligent traffic system. There are several main problems for the development of intelligent transport management:

- Complexity of traffic scenarios

  There are various traffic scenarios such as motorways, crossroads and roundabouts etc., which will contribute to complex combination traffic scenarios such as back-to-back roundabouts and multiple road intersections. In modern traffic system, roundabouts and road intersections are considered a place with a higher possibility of accidents occurring. Based on the data from [68], within the traffic accidents occurring at the roundabout, more than 50% of them happened because of drivers failing to observe or anticipate vehicle positions at entries/exits, or while changing lanes under complex traffic scenarios. A macroscopic level traffic management protocol is necessary which can be

applied on these complex conditions.

- Complexity of accidents causing reasons

  Besides the complexity of the traffic scenario, various factors can contribute to vehicle accidents such as drivers failing to look properly, misjudging the distance or speed, and being careless, reckless or in a hurry [23]. Researches present in [69] shows that approximately 34.6% of crashes are caused by bad weather which could influence the visibility of drivers significantly.

- Complexity of sensors

  In order to implement autonomous vehicles and intelligent traffic systems, different sensors have been applied to collect dynamic information of vehicles and monitor the surrounding environment. However, the accuracy, precision, availability and reliability of sensors improve the usage complexity of sensors.

Researchers from [68] and [69] proved that sharing real-time information of vehicles within 1-2 kilometers via on board unit (OBU) helps avoiding vehicle accidents dramatically. Vehicle to vehicle (V2V) and vehicle to infrastructure (V2I) communication are considered as functional solutions for the problems mentioned above, which can implement information sharing of vehicles. Vehicles within vehicular network can collect information of other users such as position, velocity and trajectory to predict and avoid potential collisions.

In order to collect and share position information of vehicles, a lot of intelligent traffic protocols based on V2X communication utilise GPS to determine position and trajectory for vehicles. For example, research in [34] and [9] present ITS protocols based on reserving positions for vehicles at discrete time nodes, while the positioning information provided by GPS is assumed to be 100% reliable in these two studies. However, the system safety level can be decreased dramatically if there are errors in GPS positioning. There is another transport management protocol which is proposed in [16]. In order to avoid potential collisions, the researchers add fixed size safety buffer to vehicles' position. However, if buffers are not adaptive to different sizes of vehicles with different quality of GPS receivers, the traffic efficiency can be affected.

GPS is one of the most popular sensors for intelligent transport management protocol to provide positions of vehicles. However, there are lots of factors which can influence the quality of GPS signals such as signal fading due to high-rise buildings

and other barriers, multipath effect and insufficient visible satellites etc.. In order to decrease the effect caused by the susceptibility of GPS positioning, it is necessary and significant to compute the real-time reliability of the GPS signal for each vehicle and inject this critical factor into the basic safety messages shared within vehicular network. Vehicles can determine the most reasonable trajectory and acceleration with the support from OBU and road infrastructure after receiving the position information along with the GPS reliability of other users.

A specific example of a complex traffic scenario is picked to provide a more realistic description and to be the simulation scenario. As shown in Figure 3.1, the selected scenario is consist of a four-exit roundabout and a crossroad which locates near Newcastle University. Figure 3.1 shows the locations where real traffic accidents occurred within the scenario during the past 10 years. Most of the accidents occurred at entries/exits of the roundabout and the road intersections, which can be seen on map of Figure 3.1 obviously. According to these, roundabouts and crossroads can slow down the traffic flow, however, they are also the positions where incidents occur usually.



Figure 3.1: The locations of road traffic accidents occurred in chosen scenario near Newcastle University during last 10 years, indicate severity: slight (yellow), serious (red), fatal (black) [8]

The spatio-temporal protocol for roundabouts and road intersection present in

this chapter is designed for semi-autonomous and autonomous vehicles with OBU and V2X communication devices which can implement information sharing within the network. The intelligent traffic protocol is developed based on GPS reliability related basic safety messages which aim to increase safety level and traffic flow efficiency on roundabouts and junctions.

3.2 Application of GPS Reliability on Vehicular Communication

As it was explained, GPS signal can not be trusted 100% all the time when providing accurate position of vehicles, so the reliability of GPS should be applied to vehicular network.

3.2.1 Reliability of GPS Observation

When computing the position information based on pesudorange measurements, some outliers appear, for example, the errors caused by cycle slip of the pseudorange measurements. The reliability of GPS measurements is utilised to estimate the effect caused by outliers, which is also a vital element to evaluate the performance of GPS in accuracy, precision and cost.

The reliability of GPS observation (such as pesudorange and carrier phase) consists of internal reliability and external reliability, which reflect the ability to detect the blunder of the system and the effect caused by undetected blunders, respectively [40]. The internal reliability of GPS observation is defined as marginally detectable blunder (MDB), which is the smallest blunder that can be detected by the system [70]. The external reliability (ER) estimates the effect caused by blunders which are undetected.

The least square method is used to calculate MDB and ER, which starts from the measurement model of GPS positioning:

$$P^k = \rho^k + \varepsilon \tag{3.1}$$

where ε is the pseudorange measurement error, accounting for satellites clock bias, tropospheric errors, ionospheric errors and observation errors. P^k and ρ^k represent

the pseudorange and geometrical range between the satellites and the GPS receiver respectively. ρ^k can be calculated by:

$$\rho^k = \sqrt{(X^k - X)^2 + (Y^k - Y)^2 + (Z^k - Z)^2} + c\delta t \tag{3.2}$$

where (X^k, Y^k, Z^k) and (X, Y, Z) are the positions of the k^{th} satellite and GPS receiver respectively, c is the speed of light and δt is the clock offset value. After linearization, the equation of GPS positioning can be presented by:

$$\delta\rho = H \cdot \delta x + \varepsilon \tag{3.3}$$

where $\delta\rho$ is the misclosure of P^k and ρ^k [40]. H is the Jacobian transition matrix of the measurement model which can be expressed as [71]:

$$H = \begin{bmatrix} a_{x1} & a_{y1} & a_{z1} & 1 \\ a_{x2} & a_{y2} & a_{z2} & 1 \\ \vdots & \vdots & \vdots & 1 \\ a_{xk} & a_{yk} & a_{zk} & 1 \end{bmatrix} \tag{3.4}$$

where k is the number of satellites and:

$$a_{xk} = -\frac{X^k - X}{\rho^k}, a_{yk} = -\frac{Y^k - Y}{\rho^k}, a_{zk} = -\frac{Z^k - Z}{\rho^k} \tag{3.5}$$

δx is the incremental component of the state of the GPS receiver (position coordinate and receiver clock bias), which can be computed using the least square method:

$$\delta x = (H^T C_I^{-1} H)^{-1} H^T C_I^{-1} \delta\rho \tag{3.6}$$

where C_I is the covariance matrix of measurement whose diagonal is the variance of every pseudorange measurement. It is initialised by assuming the variance of pseudorange measurement to 1 as follows:

$$C_I = \begin{bmatrix} 1 & 0 & \cdots & 0 \\ 0 & 1 & \cdots & 0 \\ \vdots & \vdots & \ddots & \vdots \\ 0 & 0 & 0 & 1 \end{bmatrix} \tag{3.7}$$

The value of measurement variance will be updated after every iteration of least square method. And the estimated state of GPS receiver can be updated by:

$$\hat{x} = \vec{x_0} + \delta\vec{x} \tag{3.8}$$

After measuring the state of the GPS receiver, in order to detect the blunders in GPS observation, we need to estimate MDB:

$$MDB_k = \frac{\lambda_0 (C_I)_{kk}}{\sqrt{(C_{\hat{r}})_{kk}}} \tag{3.9}$$

where $C_{\hat{r}}$ can be described as:

$$C_{\hat{r}} = C_I - H(H^T C_I^{-1} H)^{-1} H^T \tag{3.10}$$

And λ_0 is calculated according to the significant level α and missed detection probability β, which is also called the non-centrality parameter [40]. Assuming there is only one blunder to be detected at one time, and the value of non-centrality parameter can be computed by:

$$\lambda_0 = n_{1-\frac{\alpha_0}{2}} + n_{1-\beta_0} \tag{3.11}$$

The value of λ is 17.075, when α and β are set as 10^{-3} and 20% respectively [39]. And as mentioned above, the external reliability of a GPS signal defines the influence caused by undetected blunder, which can be presented as:

$$ER_k = -(H^T C_I^{-1} H)^{-1} H^T C_I^{-1} MDB_k \tag{3.12}$$

where MDB_k is a zeros column except for the k^{th} position that contains the MDB of the k^{th} observation [72]. Internal reliability contributes to errors of the GPS receivers' position which can be expressed by external reliability. The value of MDB and ER represents the quality of GPS signal based positioning measurements. A specific threshold for reliability should be set to evaluate and calibrate the positioning information. After calculating the reliability of GPS observation, measurements with a larger reliability value than the threshold will be deleted to get a more reliable positioning information of vehicles. Usually, the threshold value of MDB and

ER are determined as 0.1 and 2.5 respectively, but they will be changed according to the number of visible satellites.

3.2.2 Accuracy Measurement

Within the vehicular network, the position of vehicles is expressed based on horizontal mapping coordinate which can be transferred from the global coordinate. Easting and northing are the two dimensions of horizontal mapping coordinate which are used to present the position. After getting the reliable positioning information processed based on GPS reliability, easting and northing errors can be computed to derive the distance root mean square (DRMS) which represents the accuracy of positioning under the local frame of reference. DRMS can be calculated by equations following, where σ_E and σ_N are the standard deviations of easting and northing errors respectively:

$$DRMS = \sqrt{\sigma_E^2 + \sigma_N^2} \tag{3.13}$$

σ_E and σ_N can be predicted from the corresponding variance of pseudorange measurement. The probability of DRMS is approximately 65%, which means a circle whose radius equals to DRMS can cover 65% of all the estimated positions. The equation of computing DRMS can be taken further, for instance, around 95% of all estimated positions occur within the circle whose radius is equal to twice DRMS. And the probability can be increased to 97.5% if the radio of circle trends to 3DRMS. As it is discussed, the confidence circle of vehicles can be determined based on differ-

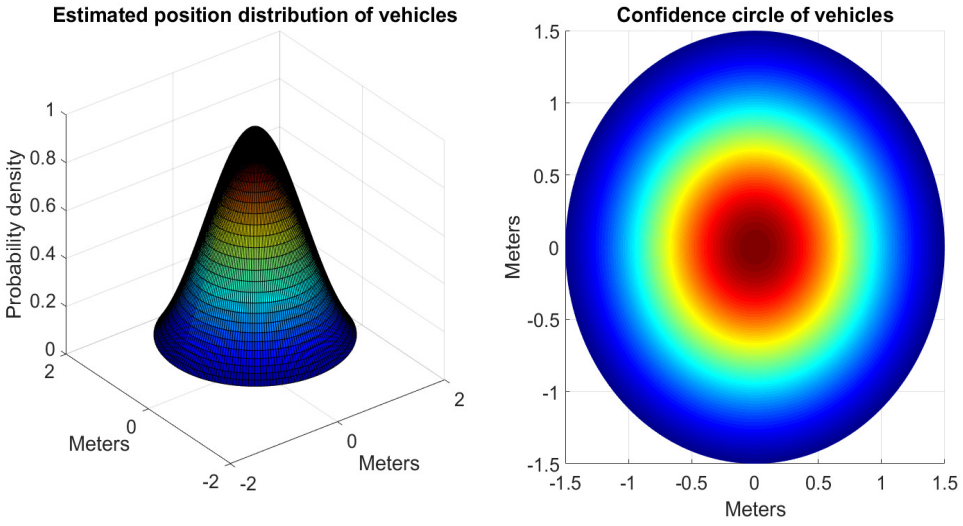


Figure 3.2: Estimated positions and the confidence circle of vehicle

ent value of radius with different probabilities. If the estimated errors are assumed to obey normal distribution, the probability density function of estimated positions can be expressed by the left subfigure of Figure 3.2. S mentioned, with the increase of the multiples of DRMS, the circle will cover larger percentages of all the estimated positions. On the right subfigure of Figure 3.2, the centre of the confidence circle represents the position of the vehicle measured by GPS. Different thresholds will be determined as DRMS, 2DRMS, 3DRMS and 4DRMS which refer to different safety levels, for example, the area covered by the circle with one DRMS radius is labelled as red which means the safety level is low. The red area can only cover 65% of all possible positions of the vehicle which means that if other vehicles drive into the red area of the user, there will be a high probability of a collision. In other words, if vehicles can leave a sufficient safety buffer between each other such as 3DRMS or 4DRMS circle, the safety level of traffic can be increased significantly.

3.3 Intelligent Traffic Management for Roundabout and Road Intersection

The communication protocol of the proposed intelligent traffic management system utilised the alternative space in the basic safety message shared between vehicles which are defied by Society of Automotive Engineers (SAE). The GPS reliability related information which is discussed above is injected in the basic safety message to be shared with vehicles and infrastructures within the network. Each vehicle gets its confidence circles with unique sizes derived from the positioning reliability itself. With the assistance of the proposed communication protocol, spatio-temporal algorithm based intelligent traffic management system is developed to help vehicles dive across the roundabout and road intersection safely and efficiently.

3.3.1 Roundabout and Road Intersection Model

The simulation model of the proposed algorithm is consist of a 4-exit roundabout and a crossroad which is designed based on the real scenario near Newcastle University (shown in Figure 3.1). As it is illustrated in Figure 3.3, the roundabout and crossroad are divided into segments with the same size to represent the trajectory of the vehicle when driving across the scenario. There is a unique number for each segment within

the simulation traffic scenario, which means the trajectory of the vehicle can be expressed by a sequence of numbers, for example, if a vehicle drives from upper entrance of the roundabout to the bottom exit in Figure 3.3, the trajectory of it inside of the roundabout should be numbers from 5 to 13. The determination of size and numbers for segments can be changed based on the size or branches of roundabouts and crossroad intersections.

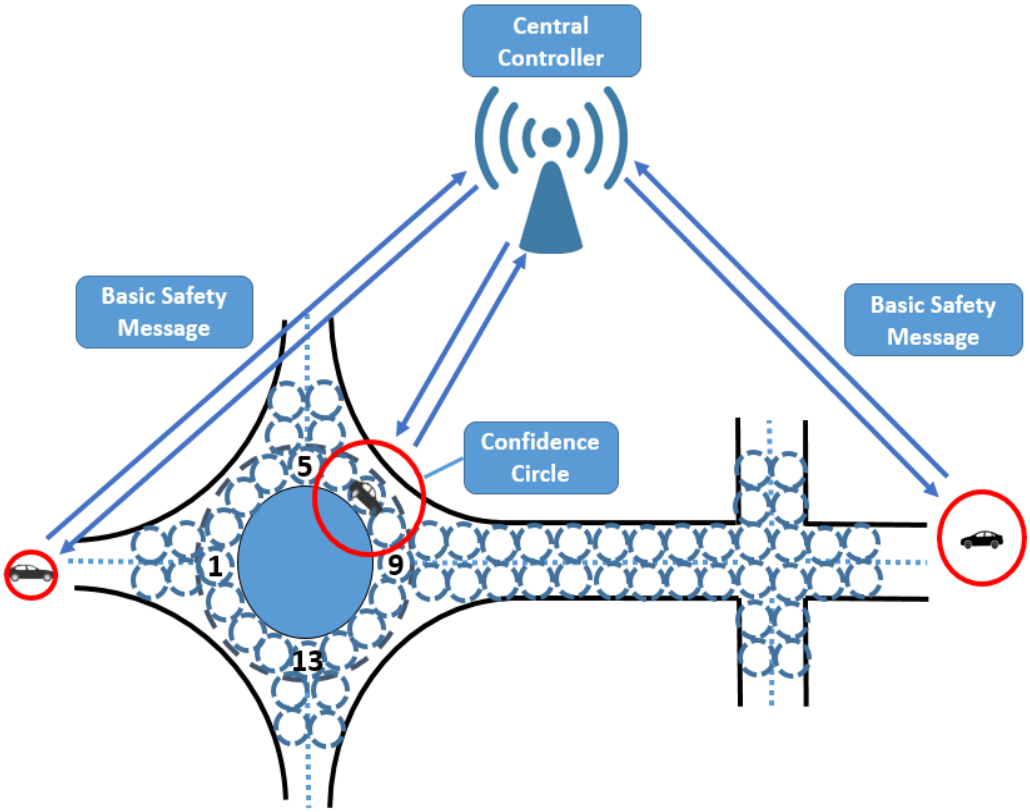


Figure 3.3: An example of divided traffic scenario

3.3.2 Protocol of Basic Safety Message

SAE defines the format and content details of basic safety messages (BSM) shared within the vehicular network based on IEEE 802.11p protocol, where an alternative space for additional useful information is available. In the proposed protocol of basic safety message, the value of DRMS and trajectory segments list are added to provide more information to vehicles within the scenario. The content of BSM in this study is presented in Figure 3.4, which consists of three main categories including header, data message and CRC (cyclic redundancy check) with 8 Bytes, 32 Bytes and 4 Bytes in size, respectively. The header contains the identification information and GPS second. In the data message part, dynamic information (position, motion

and control) for vehicles is included, where the position module provides latitude, longitude and elevation, the motion module includes speed, heading, angle and acceleration, control module contains brake information. The trajectory segment list module provides the start and destination segments of vehicles. The value of DRMS calculated based on the reliability of GPS observation is also injected in BSM. Via this protocol, the position of vehicles is shared with the radius of the confidence circle, which can be utilised to provide effective assistance to avoid collisions. The CRC module is used to correct errors.

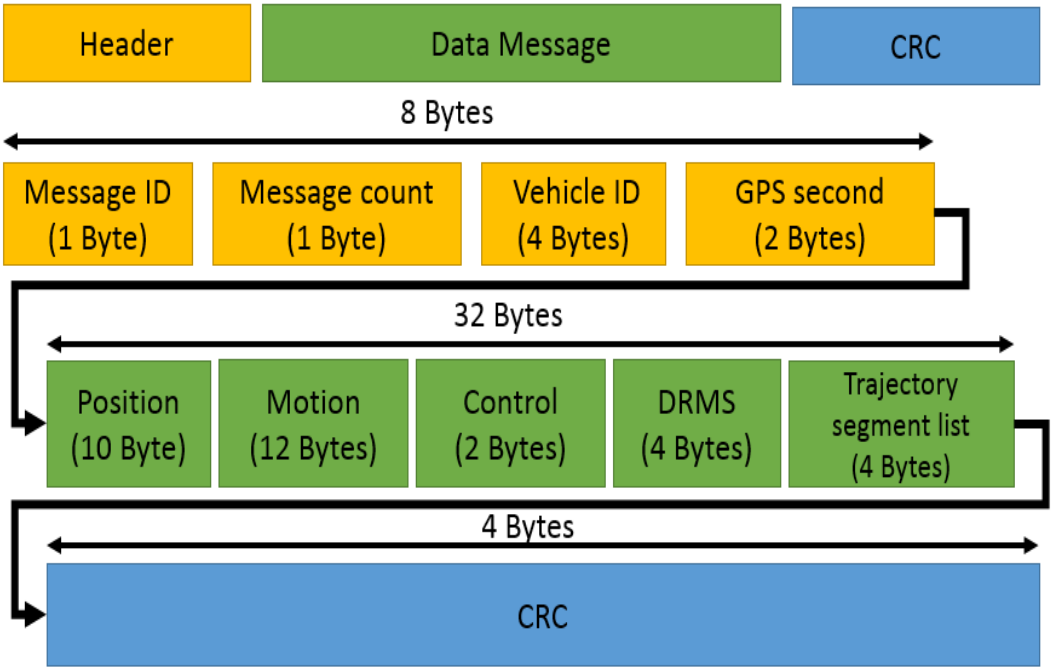


Figure 3.4: Content of basic safety message

As it is shown in Figure 3.3, there is a central controller (CC) to collect the traffic information of vehicles and manage the traffic flow in the scenario. The map of the scenario and segment information is also stored in the database of CC. If the distance between vehicles and CC is less than the specific threshold D_t, the vehicle will be regarded as users within the traffic scenario and will be required to send BSM to CC. D_t is usually determined as 300 meters which is the range of vehicular communication and the value of this threshold can be modified according to the size of the traffic scenario. After receiving the transmitted BSM of the vehicle, the central controller will reserve specific segments for vehicle's trajectory in corresponding discrete time T_t and send back safety message which contains the appropriate driving scheme to vehicles. The driving scheme in feedback BSM will guide the vehicle in which segments it should be in at which discrete times to avoid

collisions with other vehicles.

When the vehicle drives out of the scenario and the distance between it and the central controller is larger than D_t, the vehicle will stop transmitting basic safety messages. Whilst calculating distance and time, the size of the confidence circle will also be considered, for example, the confidence distance from vehicles to the roundabout will be computed as the estimated distance minus 3DRMS.

3.3.3 Spatio-temporal Algorithm

In addition to GPS reliability related information being shared with each other which includes the confidence circle, a spatio-temporal protocol linked with confidence circle is significant to be applied. The main idea for the proposed spatio-temporal algorithm is to avoid more than one vehicle occupying the same segment at one discrete time.

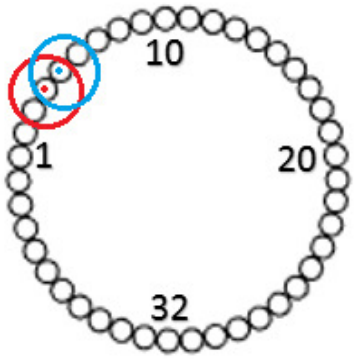


Figure 3.5: An example of occupied segments in each step

After receiving the basic traffic message from the vehicle, the occupation matrix M_v of vehicles based on T_t will be computed by the central controller. Based on the dynamic information (speed, trajectory), reliability related information (radius of confidence circle) and mapping information (size of segments), the segments list which will be occupied at every discrete time can be derived. In Figure 3.5, a vehicle drives from segment 4 to segment 5 (from the red point to the blue point) during t to $t+\Delta t$. The red and blue circles represent the confidence circle of the vehicle at each step respectively. From Figure 3.5, it is easy to see the vehicle occupies segments 3, 4 and 5 at t and segments 4, 5 and 6 at $t+\Delta t$, which means $M_v(t) = [3, 4, 5]$ and $M_v(t+\Delta t) = [4, 5, 6]$. To be noticed, vehicles cannot reserve and occupy the segments outside their legal driving area, even the radius of their confidence circle is larger than the road width.

A global occupation matrix M_{cc} is stored and kept updated in the central controller which contains the occupation information for all the vehicles within the traffic scenario. Each vehicle within the network needs to reserve its occupation in M_{cc}. After a successful reservation, CC will send updated an occupation matrix M_u back to the vehicle which can guide the vehicle on how to drive across the scenario. Each vehicle must adjust its dynamic actions following the information in M_u.

Set $T(m)$ and $T(n)$ to be the time when vehicle arrives and exits the traffic scenario respectively. Assume Δt is the discrete time interval for the occupation matrix. Then the spatio-temporal algorithm applied on the central controller can be explained by the pseudocode in Figure 3.6.

Algorithm 1 Trajectory Reservation, Central Controller

Input: M_v $T(m)$ $T(n)$
Output: M_u

for $t = T(m)$ to $T(n)$
Reserve segments in $M_{cc}(t)$
  if Reservation is successful **then**
    Update M_u
    Skip to $t = T(t + \Delta t)$
  else
    While Reservation is not successful
      Reserve segments in $M_{cc}(t + \Delta t)$
    end
    Update M_u
  end
end

Figure 3.6: Pseudocode of trajectory reservation algorithm applied in the central controller

As the pseudocode describes, after receiving the dynamic information of vehicles, the central controller will try to reserve the segments for vehicles in the corresponding time of M_{cc}. If the required segments are available and can be reserved successfully, central controller will update M_{cc} and M_u to inform vehicles to arrive in these segments at corresponding times. Conversely, if the required segments have been reserved or occupied already by other vehicles, CC will update M_u to inform vehicles

slow down or stop and reserve the latest available time for the required segments. After this procedure, vehicles are aware of where they should be at each discrete time node, which is able to help them drive across the complex traffic scenario safely and efficiently.

Under the circumstance of the central controller breaking down, which means the vehicles entering the scenario cannot receive any driving scheme after sending their information, the on-board unit will be regarded as the controller to receive/analyse data and process the proposed trajectory for vehicles following the spatio-temporal algorithm. All vehicles are required to transmit/receive messages with higher frequency. The intelligent traffic system will not crash until the central controller is fixed, although the accuracy and efficiency of processing/analysing are lower in this odd situation.

3.4 Simulation Setup and Results Analysis

The ITS model proposed in this chapter is tested based on an open-source simulator named ISR Traffic Simulator (ISR-TFS) which is able to simulate traffic scenarios within V2V/V2I communication environment [9]. The simulation environment is presented in Figure 3.7. Similar to the picked road scenario presented in Figure 3.1, the simulation scenario is consist of a 4-exit roundabout and a road intersection. Each entrance and exit gets two lanes. The vehicles with different radius of confidence circles are generated following the preset traffic influx of each entering lane. The trajectories of vehicles are created randomly by the simulator. The size of vehicles is not concerned in the simulation and not accounted for segments reservation.

In order to compare the safety level and traffic efficiency of different traffic managements, three types of traffic management are simulated upon different traffic influx. The intelligent transport management with confidence circle (ITMCC) explained in this chapter is compared with conventional transport management (transport controlled by traffic lights) and non-reliable transport management (the same algorithm with ITMCC but does not concern positioning reliability related information). The radius of the confidence circle around vehicles in ITMCC equals to 3DRMS.

The traffic influx at each entering lane of the scenario is determined as 100

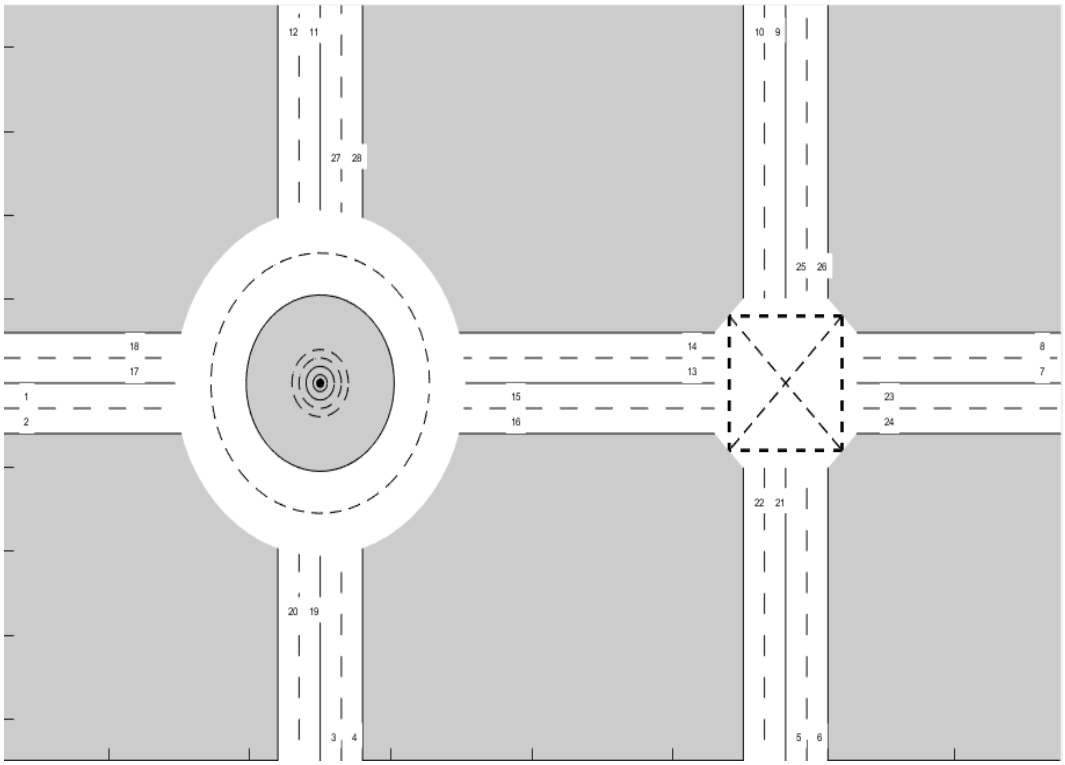


Figure 3.7: Simulation scenario for proposed ITM scheme [9]

cars/hour, 150 cars/hour and 200 cars/hour respectively. Within the roundabout and crossroad combination scenario, there are 12 entering lanes (two lanes for each entrance), so the total number of cars driving inside the simulation scenario will be 1800 per hour if the setup influx is 150 cars/hour.

The number of cars processed in each transport management system during 10 minutes are illustrated in Figure 3.8. It is obvious that the number of processed cars in intelligent transport management with confidence circle (ITMCC) and non-reliable intelligent transport management (ITM) is larger than that of conventional transport management (CTM), especially when traffic influx is high (200 cars/hour per entering lane), there are about 200 more cars processed in ITM/ITMCC than CTM during 10 minutes period. This means that the proposed spatio-temporal algorithm based transport management can support higher throughout than traffic lights controlled management, especially during rush hour. The processed car number difference between ITMCC and ITM is negligible. Figure 3.9 and Figure 3.10 show the total stop time and the average velocity of all processed vehicles during the simulation period. Obviously, CTM gets a much longer stop time and lower average velocity than those of ITMCC and ITM, which represents far lower transport efficiency than ITM and ITMCC. With the increase of traffic volume, the

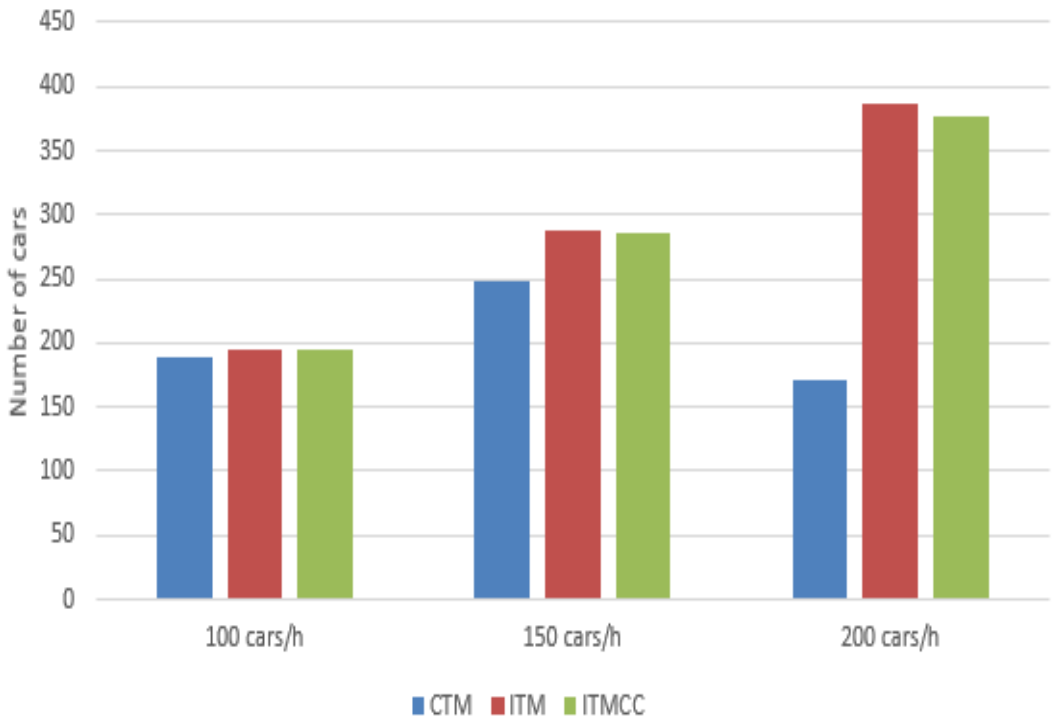


Figure 3.8: Number of cars processed during simulation period

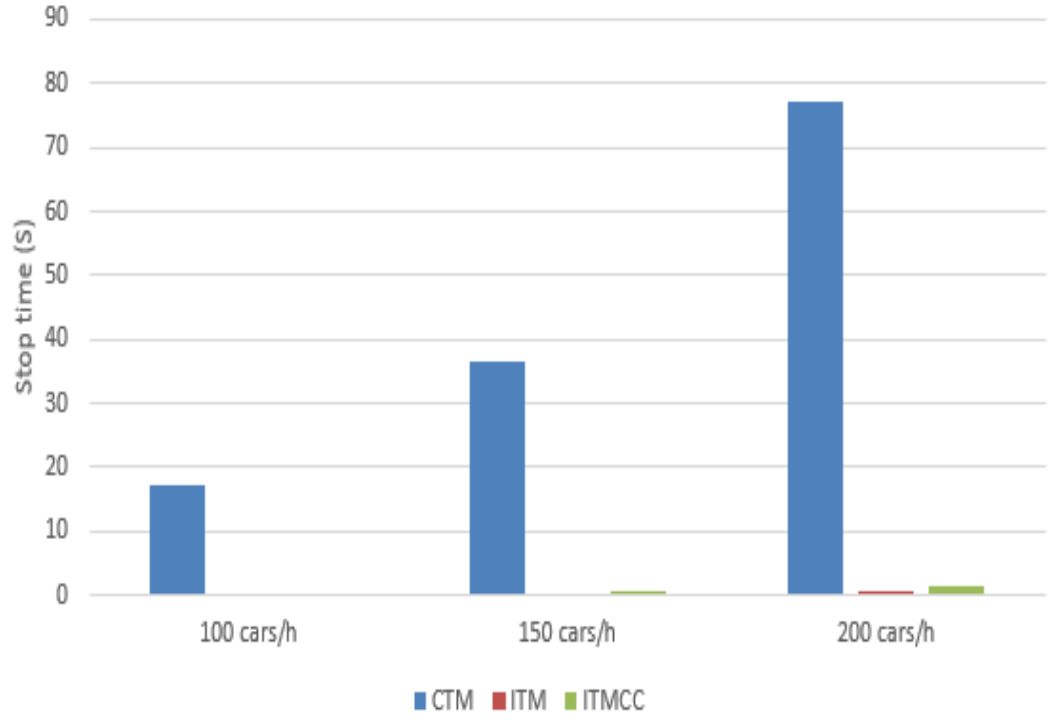


Figure 3.9: Total stop time of cars when driving across the simulation scenario

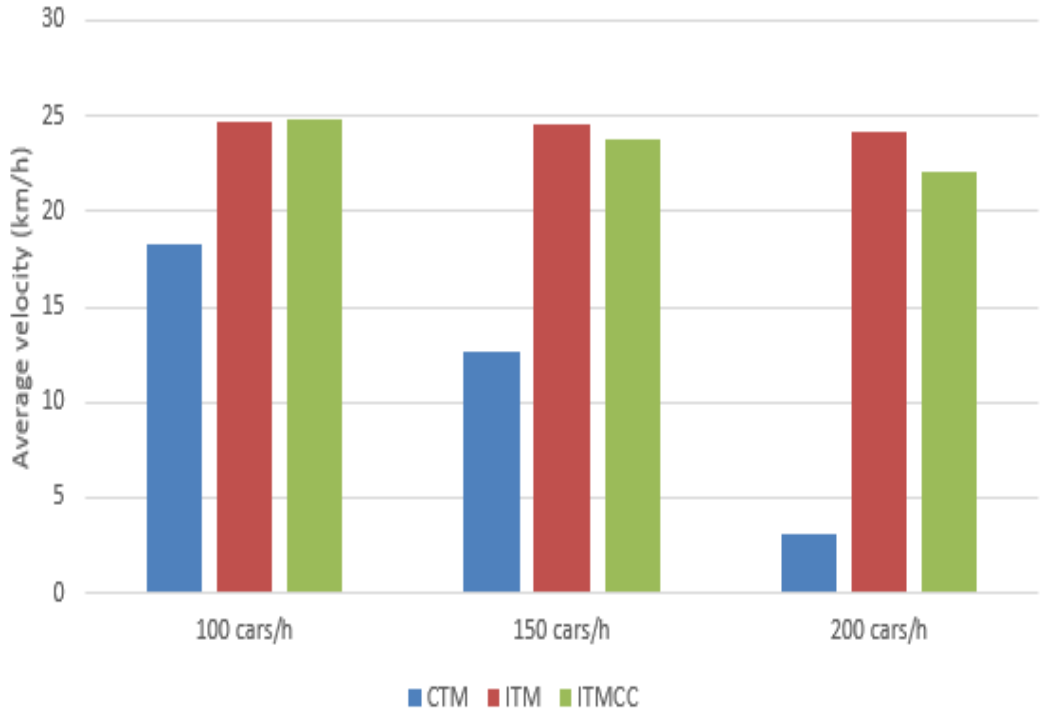


Figure 3.10: Average velocity of cars when driving across the simulation scenario

CTM traffic efficiency decreases dramatically, while that of ITM and ITMCC is not affected significantly. For the ITMCC, although the efficiency is marginally lower than ITM because of the application of the confidence circle, it is still vastly more efficient than CTM.

Further simulation has been done to test the safety level for ITMCC and ITM. For ITM, which manages transport without concerning the GPS reliability information, positioning information provided by GPS is trusted completely and the trajectories and velocities of vehicles are decided based on the positioning with errors. The errors follow the distribution which has been discussed in this chapter. For ITMCC, same errors of GPS positioning are applied upon the decision of vehicles' trajectories, while a confidence circle derived from reliability related information is added around vehicle to provide a safety buffer. In the safety tests, trajectory segments are reserved based on positioning with errors, the real position of vehicles is also provided, then the number of collisions can be counted according to the number of one segment occupied by more than one vehicles (real positions) at the same discrete time node. For example, if there are intersections between the real positions of vehicles when they drives following the trajectories decided based on positioning information with errors, that means collisions occur.

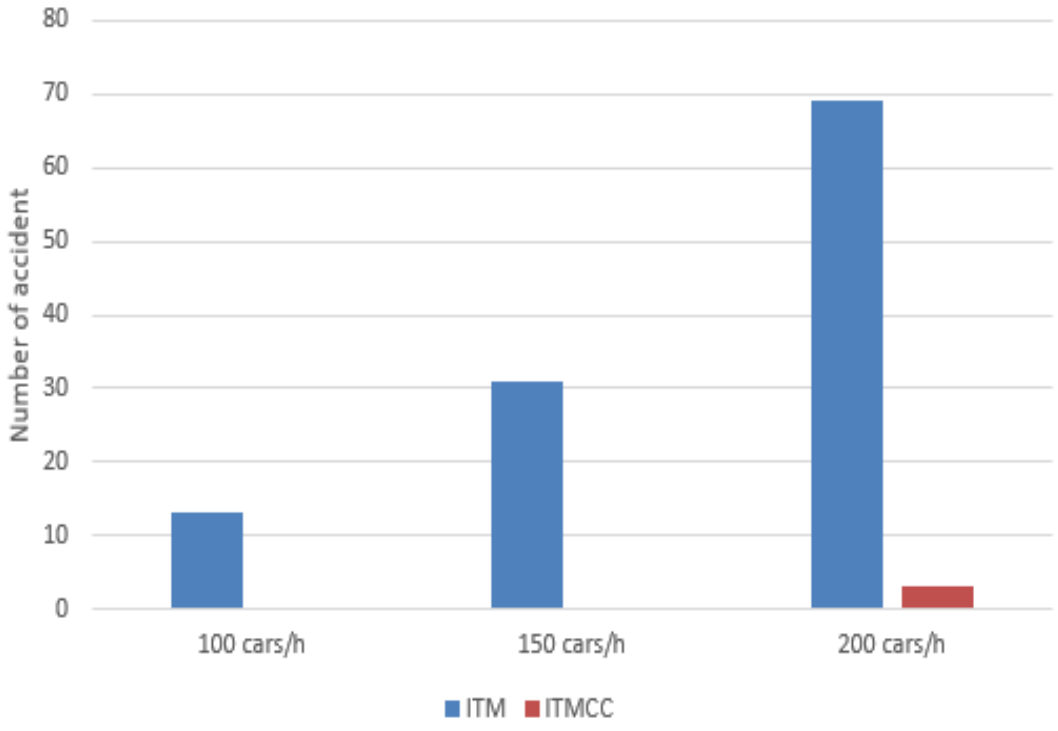


Figure 3.11: Number of vehicle accidents during simulation

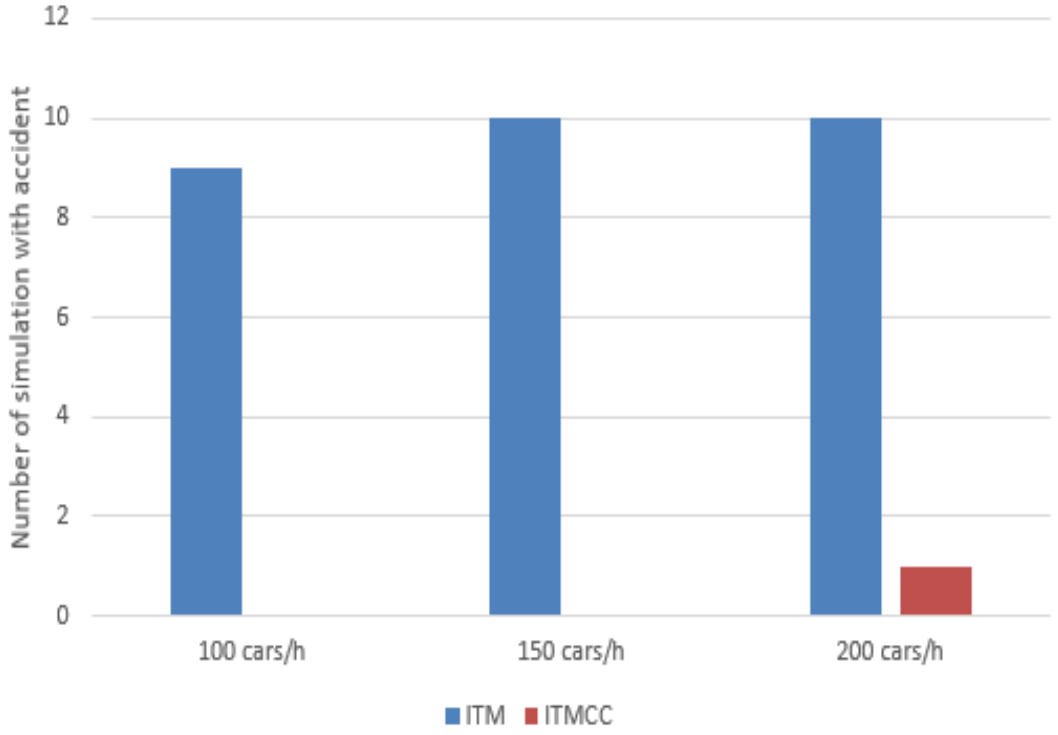


Figure 3.12: Number of simulations with accidents (out of 10)

Figure 3.11 and Figure 3.12 present the average number of vehicle collisions during the testing and the number of simulations with accident (out of 10 times testing), respectively. It is distinct that the average number of accidents and simulation with collisions drop dramatically by concerning confidence circle. With the increase of vehicles entering each lane, the average accidents number of ITM rises markedly and almost all tests based on ITM come with accidents. After applying confidence circle as safety buffer according to vehicles' different positioning reliability, the probability of vehicle accidents is much lower. The car accident rate for ITM is high because ITM decides the trajectories of vehicles based on GPS positioning measurements without evaluating reliability of them in advance. Significant difference between real positions and GPS estimated positions can easily contribute to car collisions, if the GPS measurements are trusted 100% by traffic management algorithm.

Overall, by sacrificing a minimal amount of traffic efficiency, the proposed ITMCC can gain a large amount of additional safety through the incorporation of GPS reliability related confidence circle. The throughput of ITMCC is remarkably improved comparing with the conventional transport management system.

3.5 Summary

Safety should always get the first priority no matter in which traffic scenario. There is no significance to improve the traffic efficiency only without concerning to guarantee the safety of users. Some ITMs ignore the reliability of GPS observation which may contribute to absolute wrong positioning for vehicles and lead to collisions. From the results and analysis in last section, it is easy to see the proposed intelligent transport management performs much better than traffic lights controlled conventional transport management. The key point of this work is the application of GPS measurement reliability which is the confidence circle derived from. It helps vehicles within the vehicular network to collect more reliable positioning information of themselves and other users, which can improve the safety level of the whole system significantly, although the application of confidence circles decreases the traffic efficiency marginally. The proposed model is able to work not only on full autonomous vehicles driving within roundabouts and crossroads, but also for semi-autonomous vehicles.

Ordinary vehicles without on-board units or vehicular communication equipment

are not involved in this proposed ITM, which will be left for future work. Secondly, size of vehicles is not concerned in current reservation algorithm. How to determine the shape and size of confidence buffer for different types of vehicles could be one of the future works. Additionally, besides GPS, more sensors are expected to be used for more accurate and precise positioning of vehicles, which can also be the extending work for this study.

Chapter 4

GPS Positioning Optimisation and Multisensor Fusion for Autonomous Vehicle in Urban Environment

The PNT (position, navigation and timing) information shared within a vehicular network is critical for collision avoidance and intelligent traffic management. Various methods and algorithms have been developed for more accurate PNT solutions.

Multisensor data fusion is an significant approach to increase the accuracy and precision of vehicle PNT solution. Multiple sensors are placed on-board in order to collect more useful information of vehicles during driving. However, the reliability and consistency of sensors can be affected dramatically by numerous elements especially when vehicles are driving under challenging environmental conditions and circumstances. For example, GPS signal can be influenced significantly in urban environments with high-rise buildings, tree canopies, tunnels etc.. Fusing unreliable sensor data could contribute to worse positioning results. As a result of this, it is critical to evaluate the reliability and consistency of sensors before fusing data to compute a PNT solution.

ICC (Intraclass Correlation Coefficient) is the coefficient to evaluate the reliability and consistency of measurements taken by different methods or observers measuring the same targets [73]. In the algorithm proposed in this chapter, GPS and IMU (Inertial Measurement Unit) are utilised for collecting the vehicle's kinetic

information and data fusion. ICC is used to evaluate the reliability of measurements taken by GNSS and IMU and decide which measurements are reliable and reasonable to be fused for vehicle positioning.

4.1 Intraclass Correlation Coefficient application

4.1.1 Conceptions and Computation of ICC

The reliability of all the measurements or assessments needs to be estimated before they are applied. Reliability is the key factor which reflects not only the degree but also the agreement between measurements [74]. Reliability can be described as the ratio of true variance over true variance plus error variance [75].

The intraclass correlation coefficient is widely used to evaluate test-retest, intrarater and interrater reliability analyses [10]. The definitions of different types of reliability are listed in Table 4.1. According to the definitions of reliability, interrater reliability can be applied to multisensor measurements model, for example, multiple sensors have been used to measure the positions of one vehicle. Intrarater reliability is more suitable to be used when evaluating one sensor's measurements across several trials such as positioning data on different seconds provided by GPS.

Table 4.1: Definitions of different types of reliability [10]

Reliability Types	**Definitions**
Interrater	It reflects the variation between 2 or more raters who measure the same group of subjects
Intrarater	It reflects the variation between 2 or more trials measured by one rater
Test-retest	It reflects the variation for measurements taken by one instrument on the same subject under the same conditions

P. E. Shrout and J. L. Fleiss determined six forms of ICC in [73] where ICC types are presented via two numbers in parenthesis. The first number represents models (1: one-way random effect model, 2: two-way random effects model, 3: two-way mixed effects model), and the second number represents types (1: single rater/measurements, k: the mean of k raters/measurements). K. O. McGraw and S. P. Wong determined a 10-form definition for ICC in [76] which is widely used in data processing software such as SPSS. Besides the 'model' and 'type' which have been explained by Shrout and Fleiss earlier, the ten forms are also classified according

to 'definition' of a relationship considered to be important (consistency or absolute agreement).

Combining the definitions presented by those two research, the formulas to compute ICC of different types can be determined as Table 4.2 lists [73] [76].

Table 4.2: Formulas for different types of ICC

ICC	Model	Type	Definition	Formulas
ICC(1,1)	one-way random	single	absolute agreement	$\frac{MS_R - MS_W}{MS_R + (K+1)MS_W}$
ICC(1,k)	one-way random	multiple	absolute agreement	$\frac{MS_R - MS_W}{MS_R}$
ICC(2,1)	two-way random/mixed	single	absolute agreement	$\frac{MS_R - MS_E}{MS_R + (k-1)MS_E + \frac{k}{n}(MS_C - MS_E)}$
ICC(2,k)	two-way random/mixed	multiple	absolute agreement	$\frac{MS_R - MS_E}{MS_R + \frac{MS_C - MS_E}{n}}$
ICC(3,1)	two-way random/mixed	single	consistency	$\frac{MS_R - MS_E}{MS_R + (k-1)MS_E}$
ICC(3,k)	two-way random/mixed	multiple	consistency	$\frac{MS_R - MS_E}{MS_R}$

where MS_R, MS_C, MS_W and MS_E represent mean square for rows, mean square for columns, mean square for residual sources of variance and mean square for error, respectively. n is the number of subjects and k is the number of raters/measurements.

An example is shown in Table 4.3 in order to explain how to compute ICC value for different forms.

Table 4.3: An example for ICC application

Subjects	**Judge1**	**Judge2**	**Judge3**	**Judge4**
1	9	2	5	8
2	6	1	3	2
3	8	4	6	8
4	7	1	2	6
5	10	5	6	9
6	6	2	4	7

There are 4 raters who are rating 6 subjects, which means the value of k and n equal to 4 and 6, respectively. Assuming $MeanS$, $MeanJ$ and $MeanT$ represent mean of subjects (means of each row), mean of judges (mean of each column) and mean of total measurements respectively, then the equations for MS_R, MS_C, MS_W and MS_E can be described as:

$$MS_R = \frac{k\sum_{i=1}^{n}(MeanS_i - MeanT)^2}{n-1} \tag{4.1}$$

$$MS_C = \frac{n\sum_{i=1}^{k}(MeanJ_i - MeanT)^2}{k-1} \tag{4.2}$$

$$MS_W = \frac{\sum(X_{i,j} - MeanS)^2}{n(k-1)} \tag{4.3}$$

$$MS_E = \frac{\sum(X_{i,j} - MeanS)^2 - n\sum_{i=1}^{k}(MeanJ_i - MeanT)^2}{(n-1)(k-1)} \tag{4.4}$$

$X_{i,j}$ is the measurements that judges take, where i and j represent the row and column of Table 4.3 respectively. Based on equations 4.1-4.4, the MS_R, MS_C, MS_W and MS_E of example in Table 4.3 can be computed, which is 11.2417, 32.4861, 6.2639 and 1.0194, respectively. The ICC value for different types can be calculated then via formulas in Table 4.2.

4.1.2 Selection of ICC forms for GPS positioning

As it is explained, there are different forms of ICC referring to different application conditions. The formula of ICC computation varies from form to form, which means even with the same input data, different form selections could lead to different ICC values. As a result of this, it is critical to select ICC forms properly and correctly. The flow chart shown in Figure 4.1 illustrates the flow of how to select ICC form [10].

It is obvious that there are 3 key processes in ICC form selection which are 'model' selection, 'type' selection and 'definition' selection.

- 'Model' selection

  There are four types in 'Model' including one-way random effects, two-way mixed effects and two-way random effects.

  The difference between 'one-way' and 'two-way' effects is if each subject/target are rated by the same set of raters/judges. If different sets of raters are involved for each subject, one-way effects should be chosen. And we will choose two-way effects for the situation that all subjects are rated by the same group of raters.

  As for 'random' and 'mixed' effects, the key point is if the raters are selected randomly from a large population of possible raters or if they are specific sets

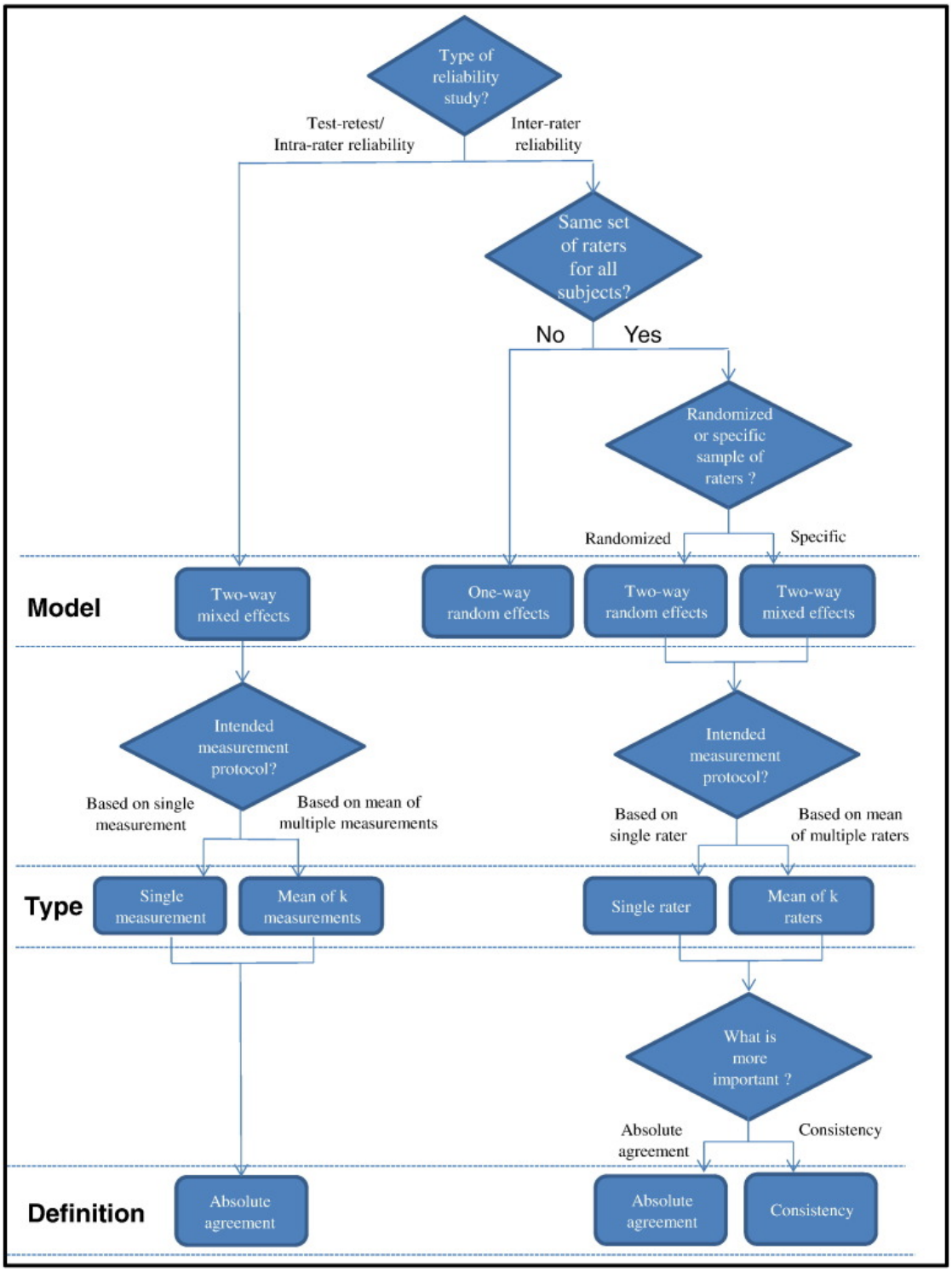


Figure 4.1: The flow chart of ICC form selection [10]

of raters [10]. If the reliability is for test-retest or intrarater, then choose two-way mixed model for this part directly.

- 'Type' selection

  'Single' or 'multiple' should be selected for the 'Type' selection. If only one rater/measurement is considered in reliability computation, the 'single' type

is applicable. If the mean of more than 3 raters/measurements is considered to be the basis of reliability computation, the 'multiple' type should be used.

- 'Definition' selection

  'Definition' means the definition of a relationship considered to be critical which includes 'consistency' and 'absolute agreement'.

  'Absolute agreement' considers if the measurements between raters for the same subjects are equal to each other, however, 'consistency' considers whether the measurements taken by different raters are additive manner. For example, for the same group of subjects, if rater X and rater Y give (2, 4, 6) and (4, 6, 8) respectively (i.e. Y=X+2). The ICC value using 'absolute agreement' is low while it is high using 'consistency' because 'absolute agreement' does not include systematic errors as part of true measurements.

In the proposed algorithm explained in this chapter, ICC is applied for GPS positioning optimisation. The positioning accuracy and precision will be affected significantly when GPS receiver is within challenging environments such as tunnels, archways in a bridge and areas with skyscrapers. ICC is utilized to derive reliability factors for outliers detection and reliable measurements selection.

As is explained in this section, 3 steps need to be decided before ICC form selection. In the proposed positioning optimisation algorithm, three subjects will be measured including differences between the pseudorange and carrier phase of two adjacent epochs and carrier-to-noise ratio (CNR). These three subjects are measured by GPS only at each epoch, which means the ICC value of a specific time slot reflects the variation of measurements taken by GPS across 2 or more trials (intrarater reliability). Based on this, 'two-way mixed effects' and 'absolute agreement' should be selected for 'model' and 'definition' according to Figure 4.1. And because the mean of multiple measurements within epochs is considered, 'multiple' is picked for 'type' selection. As a result of these, the equation of ICC computation for the application in the proposed algorithm should be:

$$ICC = \frac{MS_R - MS_E}{MS_R + \frac{MS_C - MS_E}{n}} \tag{4.5}$$

where n is the number of subjects which equals to 3. MS_C and MS_R represent the mean square for epochs within a specific time slots and the mean square for

measured subjects, respectively. MS_E is the mean square for error which can be calculated by using equation 4.4.

4.2 Reliability Factor Applied Positioning Optimisation of Multisensor system for Autonomous vehicle

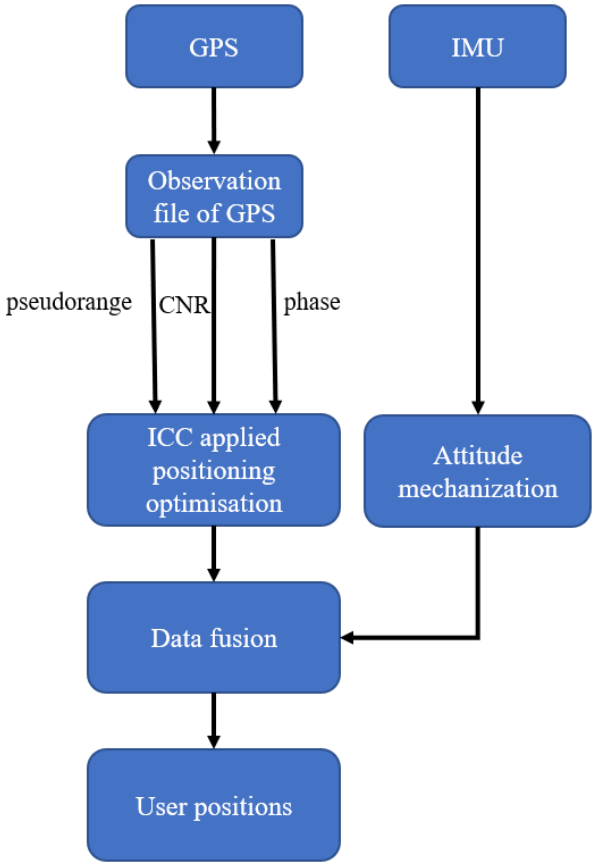


Figure 4.2: Data processing diagram for the ICC applied positioning optimisation System

Figure 4.2 shows the diagram of data processing for ICC applied multisensor positioning optimisation. Two sensors are utilized including Global Positioning System (GPS) and Inertial Measurement Unit (IMU) for vehicle positioning. ICC is applied as a reliability factor which optimises GPS measurements based on raw data showed by the RENIX Observation file.

The differences between pseudorange measurements or carrier phase for every two adjacent epochs are supposed to be constant within a short period. Dramatic variation for them may indicate an affected GPS signal and contribute to lower re-

liability of GPS measurement. CNR denotes the ratios of received carrier power to noise density. Low CNR can contribute to a higher bit error rate (BER), higher carrier and code tracking loop jitter and thus low precision and accuracy of positioning. The variation for carrier-to-noise ratio should also be stable if there are no negative effects for GPS signals. So the differences between pseudorange & carrier phase for two adjacent epochs and CNR provided by GPS Observation file are considered to be the subjects for ICC computation. The measurements of these three subjects taken by GPS at each epoch are considered as trials of a single rater.

In order to avoid relying on one single sensor and get more accurate and precise positions of the vehicle, also to improve the consistency and availability of the system, IMU is used to support GPS for data fusion. Positioning information for a vehicle can be derived from original measurements of IMU via attitude mechanization. The GPS measurements processed via ICC based optimisation algorithm will be fused with positioning data obtained by IMU to derive the vehicle positions. Loosely coupled Kalman filter is used for data fusion.

4.2.1 Algorithm for ICC Applied positioning Optimisation

ICC is applied in GPS positioning optimisation. The measurements are taken by GPS are processed based on ICC applied algorithm before being fused with the positioning measurements taken by IMU.

Assume K is the preset threshold value of ICC selection, Δt is the time interval for ICC computation, RF is the value of the reliability factor (ICC). $CNR(T)$ is the CNR at t. $PR(T)$ and $CP(T)$ represent the difference between pseudorange and carrier phase for T and (T-1), respectively. $PRN(i)$ is the code for each visible satellite and s is the number of visible satellites. $T(m)$ and $T(n)$ are the starting time and end time of vehicle driving. PE represents the final estimated position got from the proposed optimised GPS positioning algorithm. The ICC applied GPS positioning optimisation algorithm can be described by the pseudocode in Figure 4.3.

As the algorithm block explains, for each visible satellite, the reliability factor (RF) for each preset time interval will be computed first. After calculating the mean of RFs, each RF will be compared with the mean value. If the difference between RF and the mean value is larger than the preset threshold, the measurement for

Algorithm 1 RF detection and optimisation

Input: K, Δt, $PR(T)$, $CNR(T)$, $CP(T)$
Output: PE

for $PRN(i)$, $i = 1$ to s
  for $t = T(m)$ to $T(n)$
    Compute every RF for $t = T(m) + j * \Delta t$ of $PR(T)$, $CNR(T)$ and $CR(T)$, $j = 0, 1, 2...$
  end
  Compute the mean μ of RFs
  if $RF(t)$ - $\mu > K$ **then**
    Delete measurements of $PRN(i)$ within t
  else
    skip to $PRN(i + 1)$
end
Compute PE for each epoch

Figure 4.3: Algorithm for ICC based GPS positioning optimisation

these epochs will be labelled as low-reliability points and be deleted, which means the unreliable measurements of satellites at a specific time will not be counted in the process of deriving the receiver's positions.

This process is applied upon every time interval for every satellite seen by the receiver during the experiment. Because the unreliable measurements are detected and deleted, the errors in positioning are smaller than the conditions involving measurements with low reliability, in other words, the accuracy and precision could be increased by applying the reliability factor based optimisation algorithm.

4.2.2 Data Fusion for Optimised GPS Measurements and IMU Measurements

Another sensor used for more precise positioning in our proposed scheme is IMU. The estimated positions of the vehicle got based on the IMU measurements will be fused with ICC selected GPS positioning information to derive the final positions of the vehicle. IMU consists of an accelerator and a gyroscope which returns the acceleration and rotation angle for x, y, and z axis. In order to get the positioning of the vehicle, attitude mechanization and IMU mechanization are necessary.

4.2.2.1 Euler Angle Attitude Mechanization

The measurement provided by IMU is based on body-frame which should be transformed to the navigation frame. Before the measurements of IMU can be used, the attitude mechanization is necessary whose key component is the transformation of the reference frame. There are three transformation methods including Euler angles, Direct Cosine Matrix (DCM) and quaternion [77].

Euler angle is the most common way for attitude mechanization of IMU. In this system, we used Euler angle because it is easy to use and understand.

The attitude measurements from IMU are consist of three elements including yaw. pitch and roll, which can be denoted by ψ, θ and ϕ, respectively. A vector (x,y,z) rotate can be divided into three steps rotation around three axes. Firstly, it rotate ψ angle around the z-axis, the rotation matrix $C_n^b(\psi)$ can be written as:

$$C_n^b(\psi) = \begin{bmatrix} cos\psi & sin\psi & 0 \\ -sin\psi & cos\psi & 0 \\ 0 & 0 & 1 \end{bmatrix} \tag{4.6}$$

Secondly, rotate θ angle around the y-axis, the rotation matrix $C_n^b(\theta)$ is presented as:

$$C_n^b(\theta) = \begin{bmatrix} cos\theta & 1 & -sin\theta \\ 0 & 1 & 0 \\ sin\theta & 0 & cos\theta \end{bmatrix} \tag{4.7}$$

Thirdly, rotate ϕ angle around x-axis, the rotation matrix $C_n^b(\phi)$ should be expressed as:

$$C_n^b(\phi) = \begin{bmatrix} 1 & 0 & 0 \\ 0 & cos\phi & sin\phi \\ 0 & -sin\phi & cos\phi \end{bmatrix} \tag{4.8}$$

The integrated rotation matrix $C_n^b(\phi, \theta, \psi) = C_n^b(\phi) \cdot C_n^b(\theta) \cdot C_n^b(\psi)$ can be formed as:

$$C_n^b(\phi, \theta, \psi) = \begin{bmatrix} cos\psi cos\theta & cos\theta sin\psi & -sin\theta \\ cos\psi sin\phi sin\theta - cos\phi sin\phi & cos\phi cos\psi + sin\phi sin\psi sin\theta & cos\theta sin\phi \\ sin\phi sin\psi + cos\phi cos\psi sin\theta & cos\phi sin\psi sin\theta - cos\psi sin\phi & cos\phi cos\theta \end{bmatrix} \tag{4.9}$$

After taking attitude mechanization, the IMU measurements can be transformed to

navigation frame based on the attitude of last time step.

4.2.2.2 Loosely Coupled Integration of GPS and IMU

Kalman filter is used for data fusion in the proposed algorithm presented in this chapter. Kalman filter uses prior information to obtain the optimal estimate value in a linear model which has been widely used in navigation and data fusion applications [78].

There are two stages of Kalman filter including 'prediction'(or 'estimation') and 'correction' (or 'propagation') [79]. The equations of Kalman filter are listed in table 4.4.

Table 4.4: Summary of the Kalman filter algorithm

Prediction	
Project the state ahead	$\hat{x}_k^- = F\hat{x}_{k-1}^+ + Bu_{k-1} + w_{k-1}$
Project the error covariance ahead	$P_k^- = FP_{k-1}^+F^T + Q$
Correction	
Measurement residual	$\widetilde{y}_k = z_k - H\hat{x}_k^-$
Kalman gain	$K_k = P_k^-H^T(HP_k^-H^T + R)^{-1}$
Updated state estimate	$\hat{x}_k^+ = \hat{x}_k^- + K_k\widetilde{y}$
Updated error covariance	$P_k^+ = (I - K_kH)P_k^-$

The characters with ' ˆ ', '-' and '+' denote the estimated value of the variable, prior and posterior estimates, respectively. [80]. k represents the time step of variables. Within the prediction stage, F and B are the state transition matrix and input-control matrix, respectively. w is the process noise which is assumed to follow Normal distribution with zero mean and covariance Q. Within the correction stage, z_k represents the measurement vector and H is the measurement matrix. The measurement noise is zero-mean Gaussian with covariance R. P and K are two key elements in the Kalman filter algorithm which represent the error covariance of the system and Kalman gain, respectively.

As for the fusion procedure used in the proposed positioning optimisation algorithm, measurements from IMU and GPS are utilized. After attitude mechanization, IMU is able to provide 3-D acceleration of vehicle which will be utilized in the 'prediction' part and GPS measurements for position and velocity are used in 'correction' part of Kalman filter. The state matrix of Kalman filter in this algorithm consists

of the 3-D position and velocity of vehicle equipment:

$$x = [p, v]^T \tag{4.10}$$

where

$$\begin{aligned} p &= [p_x, p_y, p_z] \\ v &= [v_x, v_y, v_z] \end{aligned} \tag{4.11}$$

The elements in p and v are defined in axes x, y and z. According to the kinematic equations, the state at time k can be derived based on the state at time $k-1$:

$$x_k = \begin{bmatrix} p_k \\ v_k \end{bmatrix} = \begin{bmatrix} p_{k-1} + v_{k-1}\Delta t + \frac{1}{2}\widetilde{a}_{k-1}\Delta t^2 \\ v_{k-1} + \widetilde{a}_{k-1}\Delta t \end{bmatrix} \tag{4.12}$$

where $\widetilde{a}_{k-1}$ represents the acceleration of the vehicle at time step $k-1$. Equation 4.12 can be rewritten as:

$$x_k = \begin{bmatrix} I_{3\times3} & I_{3\times3}\Delta t \\ 0_{3\times3} & I_{3\times3} \end{bmatrix} x_{k-1} + \begin{bmatrix} \frac{1}{2}I_{3\times3}\Delta t^2 \\ I_{3\times3}\Delta t \end{bmatrix} \widetilde{a}_{k-1} \tag{4.13}$$

where $I_{3\times3}$ and $0_{3\times3}$ denote 3×3 identities and zero matrices, respectively. The acceleration measurements come from IMU are the input parameter of the state transmission equation which also contributes to process noise [80]. Assuming e_{k-1} is the noise of IMU accelerator output which follows the normal distribution with zero mean and $I_{3\times3}\sigma_e^2$ variance. According to the covariance formula, $Cov(Ax) = ACov(x)A^T$, the process noise covariance matrix Q can be computed by:

$$Q = \begin{bmatrix} \frac{1}{2}I_{3\times3}\Delta t^2 \\ I_{3\times3}\Delta t \end{bmatrix} I_{3\times3}\sigma_e^2 \begin{bmatrix} \frac{1}{2}I_{3\times3}\Delta t^2 \\ I_{3\times3}\Delta t \end{bmatrix}^T = \begin{bmatrix} \frac{1}{4}I_{3\times3}\Delta t^4 & 0_{3\times3} \\ 0_{3\times3} & I_{3\times3}\Delta t^2 \end{bmatrix} \sigma_e^2 \tag{4.14}$$

Following the process part equation of Kalman filter:

In our fusion system, F, B and w are determined as:

$$F = \begin{bmatrix} I_{3\times3} & I_{3\times3}\Delta t^2 \\ 0_{3\times3} & I_{3\times3} \end{bmatrix} \tag{4.15}$$

$$B = \begin{bmatrix} \frac{1}{2} I_{3\times 3} \Delta t \\ I_{3\times 3} \Delta t \end{bmatrix} \tag{4.16}$$

$$w_{k-1} \sim N(0, Q) \tag{4.17}$$

The position and velocity of the vehicle provided by GPS are defined as the input measurements of this Kalman filter:

$$z_k = \begin{bmatrix} p_k \\ v_k \end{bmatrix} + \Upsilon_k \tag{4.18}$$

where the observation model matrix H and measurement Υ are presented by:

$$H = I_{6\times 6} \tag{4.19}$$

$$\Upsilon_k \sim N(0, R) \tag{4.20}$$

Following the procedure and parameter determinations explained above, the ICC selected GPS measurements are fused with IMU measurements for more precise and accurate positions of vehicles. The measurements taken by IMU and GPS are processed via MATLAB to obtain 3-dimension acceleration, position and velocity for each epoch. The fusion procedure is implemented based on MATLAB, which is a post processing for the experiments data.

4.3 Experiment Scenario and Equipment Setup

4.3.1 Experimental Equipment Setup

In order to test the proposed positioning optimisation algorithm explained in this chapter, hardware experiments have been taken based on a trolley. Universal software radio peripheral (USRP), IMU, receiver antenna, and laptop for data storage and processing are equipped on the trolley.

Figure 4.4 shows the details of the USRP X310 used in the trolley test which is applied as GPS radio frequency front end. The RENIX file for experiment period including the Navigation file and Observation file will be generated and saved in USRP. The ICC applied GPS optimisation algorithms are used based on raw data collected during the trolley test.



Figure 4.4: USRP X310, showing the front and rear panels of USRP [11]



Figure 4.5: MTi-G [12]

The IMU used in this trolley test as Figure 4.5 shows is MTi-G produced by XSENS. MTi-G is a low-cost IMU which could provide 3D orientation and 3D acceleration with a high update rate.

4.3.2 Experiment Scenario

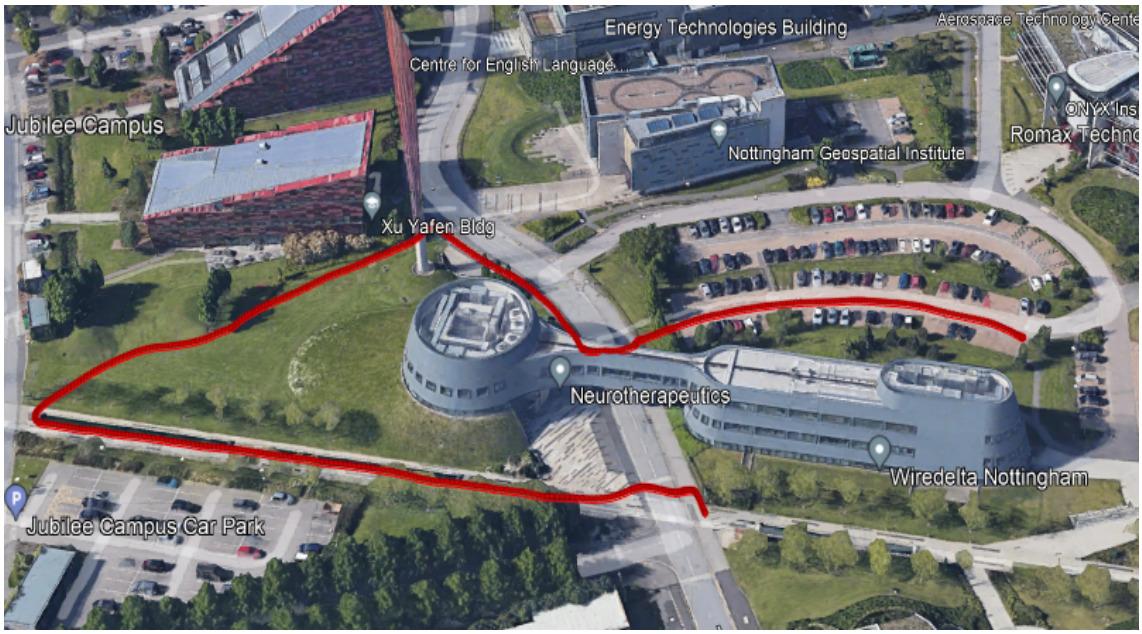


Figure 4.6: The experiment scenario for electronic trolley, reference trajectory of trolley (red)

The complexity of traffic scenarios is one of the main reasons for traffic accidents. It can also affect the performance of sensors, for example, the GPS signals could be too weak to provide accurate positioning information when vehicles are driving through tunnels. In order to test the proposed algorithm, a specific scenario consisting of a complex traffic environment should be picked.

The selected experiment scenario for the trolley test is in the Jubilee campus of the University of Nottingham. This complex scenario includes environment where massive multipath effects expected (tall sculptures, various buildings, high-rise trees) and open areas.

The red line in Figure 4.6 illustrates the trajectory of the trolley in the experiment. The trolley moved across various scenarios which could bring different effects on the GPS signal. The trolley started from the intersection at the lower middle part and ended at the car park area on the right side of the map.

4.4 Results Analysis

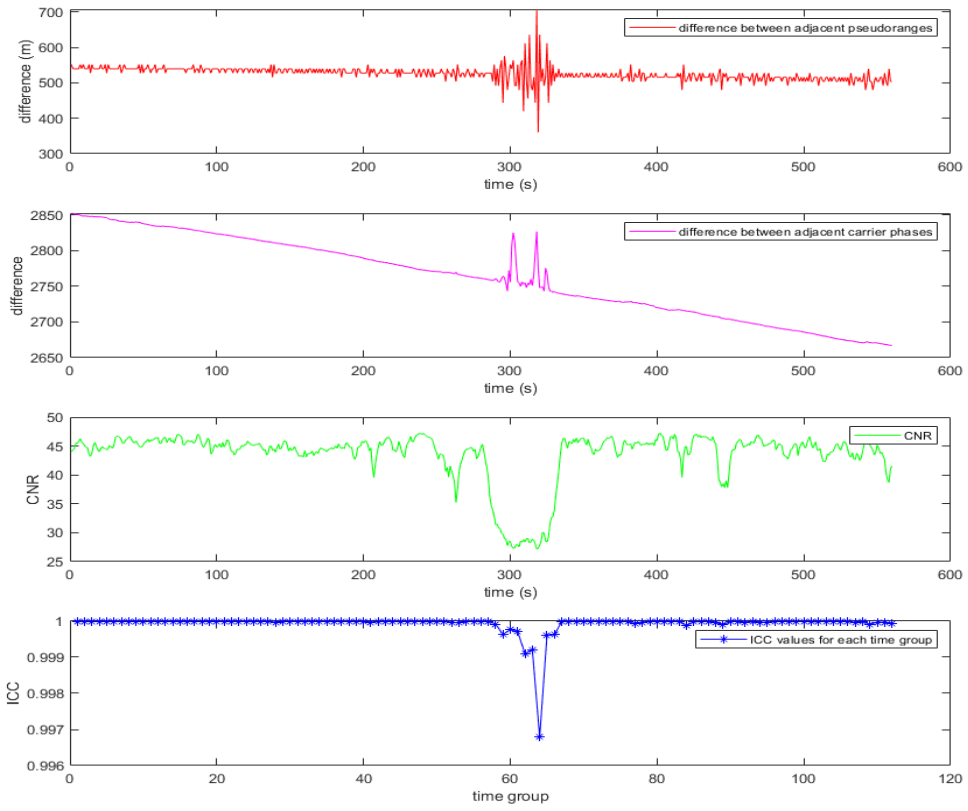


Figure 4.7: ICC detection of odd measurements for G02

It is shown in Figure 4.7 that the ICC detection of odd measurements for GPS satellite G02. The first three subfigures in Figure 4.7 show the difference of pseudorange and carrier phase between two adjacent epochs, the value of carrier-to-noise ratio (CNR) against time, respectively. The differences of peudorange and carrier phase between adjacent epochs are supposed to be stable and no dramatic fluctuation should occur during a short period, which means the measurement of GPS may be unreliable if odd fluctuation occurs. As it is shown in figure, the red line (differences between adjacent pseudorange) and the violet line (differences between adjacent carrier phases) fluctuate dramatically during the period from around 280s to 330s, which indicates the signal of GPS may be affected significantly and the measurements taken by G02 for these epochs are not reliable enough for satellite positioning. As the green line (CNR) shows, measurements with abnormal low CNR occur at 260s and 280-320s approximately. The subfigure at bottom of Figure 4.7 illustrates the value of ICC for each group of epochs. The computation of ICC is divided into groups with 5 seconds interval, which means 60 in the X-axis denotes 300s of the experiment time. It is obvious that the values of ICC equal to 1 approximately except several odd points such as group 57 to group 66 (285s to 330s), which matches the main period where odd measurements occur in the first three subfigures.

Figure 4.8 shows the error comparison between the original positioning and ICC selected positioning. The errors are compared based on local East, North and Up coordinates. It is easy to see that compared with the original positioning, ICC selection algorithm optimised most measurements with large errors in East, North and Up, especially during the first 20 seconds of the experiment and the period between around 280s and 350s. As for the period when the original positioning gets smaller errors such as the 50s-270s, the ICC selected positioning performs better which can be seen from the smoother error line than the original.

In order to compare the errors statistically, the mean and standard deviation of original positioning and ICC selected positioning on East, North, Up and Horizontal are presented in Figure 4.9. Obviously, by applying the ICC selection algorithm, the mean and standard deviation on all axes are reduced significantly, which means the accuracy and precision of GPS positioning have been improved.

Figure 4.10 presents the trajectories of the trolley processed by different algorithms on Google Earth. The red dots, blue dots and green dots represents the

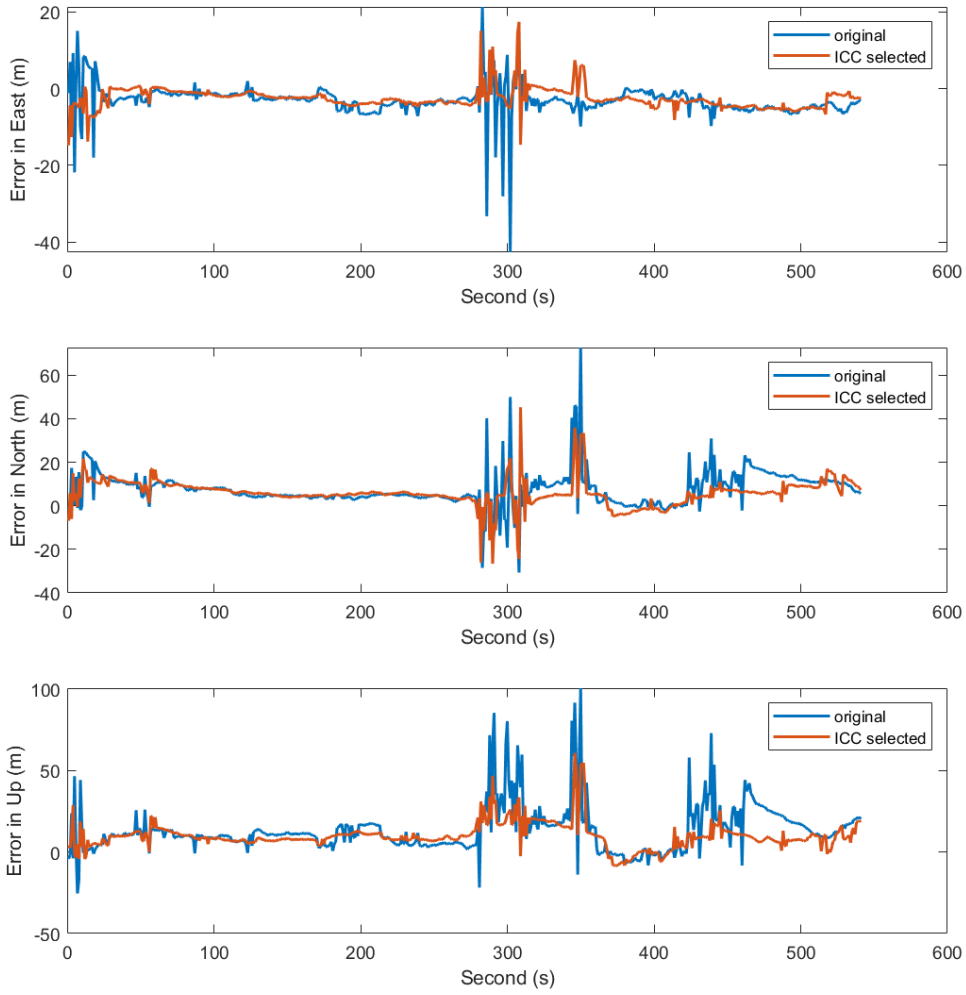


Figure 4.8: Error comparison between original positioning and ICC selected positioning

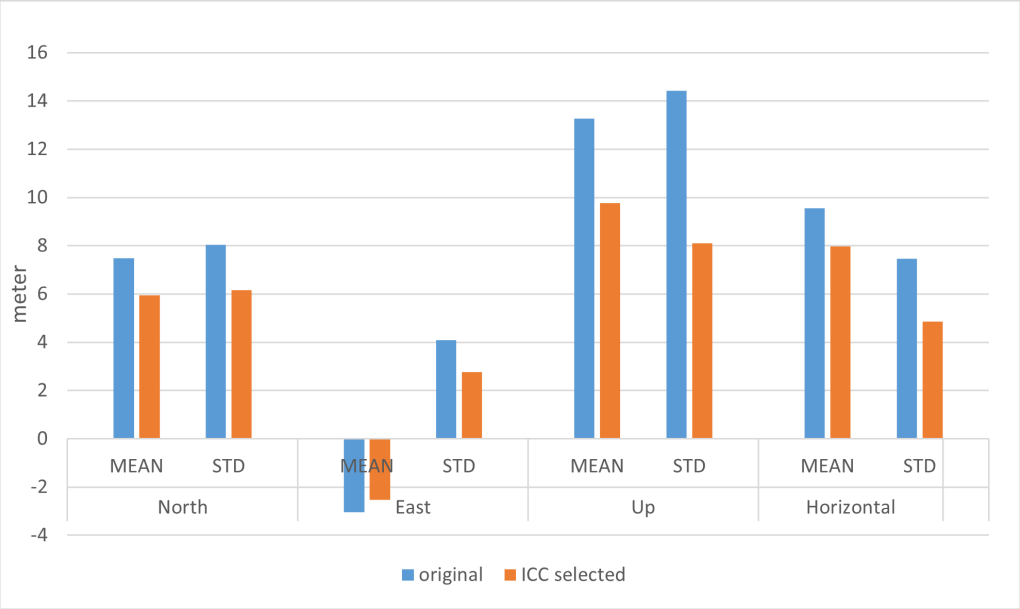


Figure 4.9: Comparison of Mean and standard derivation of errors

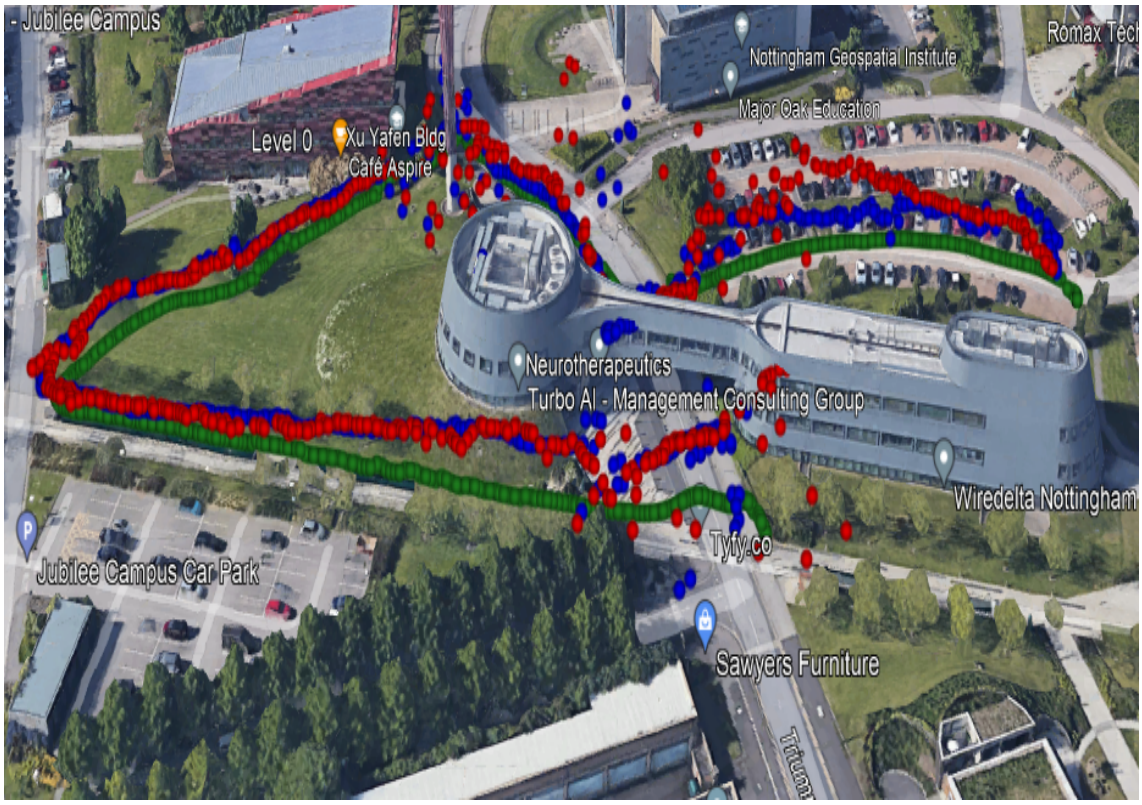


Figure 4.10: Trolley trajectories comparison between original positioning (red), ICC selected positioning (blue) and reference (green)

trajectory of the original GPS positioning, ICC selected GPS positioning and reference (true trajectory). It is obvious that the trajectory consisting of positions processed by the ICC selection algorithm is smoother and closed to the reference trajectory. A lot of odd positioning dots which locates far away from reference dots have been modified and corrected, especially when the trolley went around the building and the high sculpture. The positioning for trajectory near the car park area on the top right of the map is also improved significantly. However, there are still estimated positions with big errors which need further processing procedure.

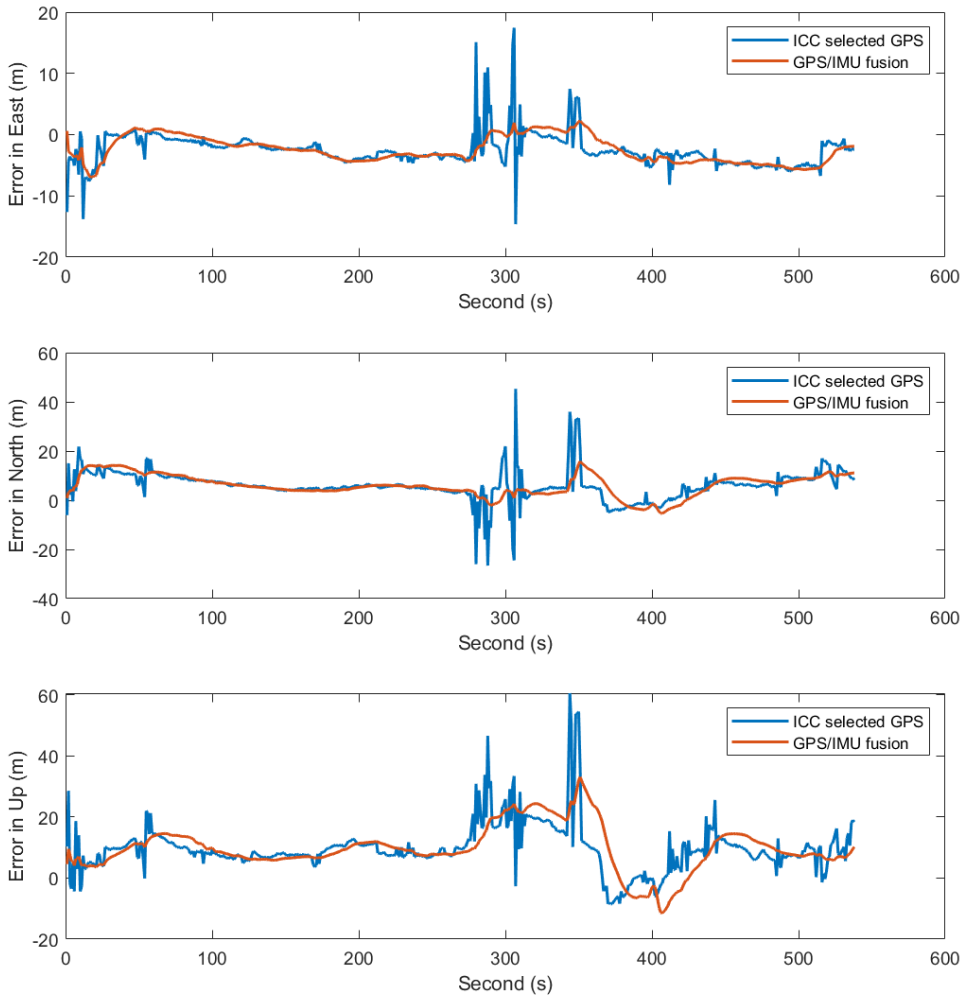


Figure 4.11: Error comparison between GPS only positioning and GPS/IMU fusion positioning

The errors in East, North and Up for local geodetic coordinates are compared on Figure 4.11, where the blue line and orange line denote the errors for ICC selected GPS positioning and GPS/IMU fusion positioning, respectively. As it is shown in

figure, Kalman filter based GPS/IMU fusion provides a further improvement in the positioning. After fusion, the errors are reduced dramatically, particularly where measurements with maximum errors occurring.

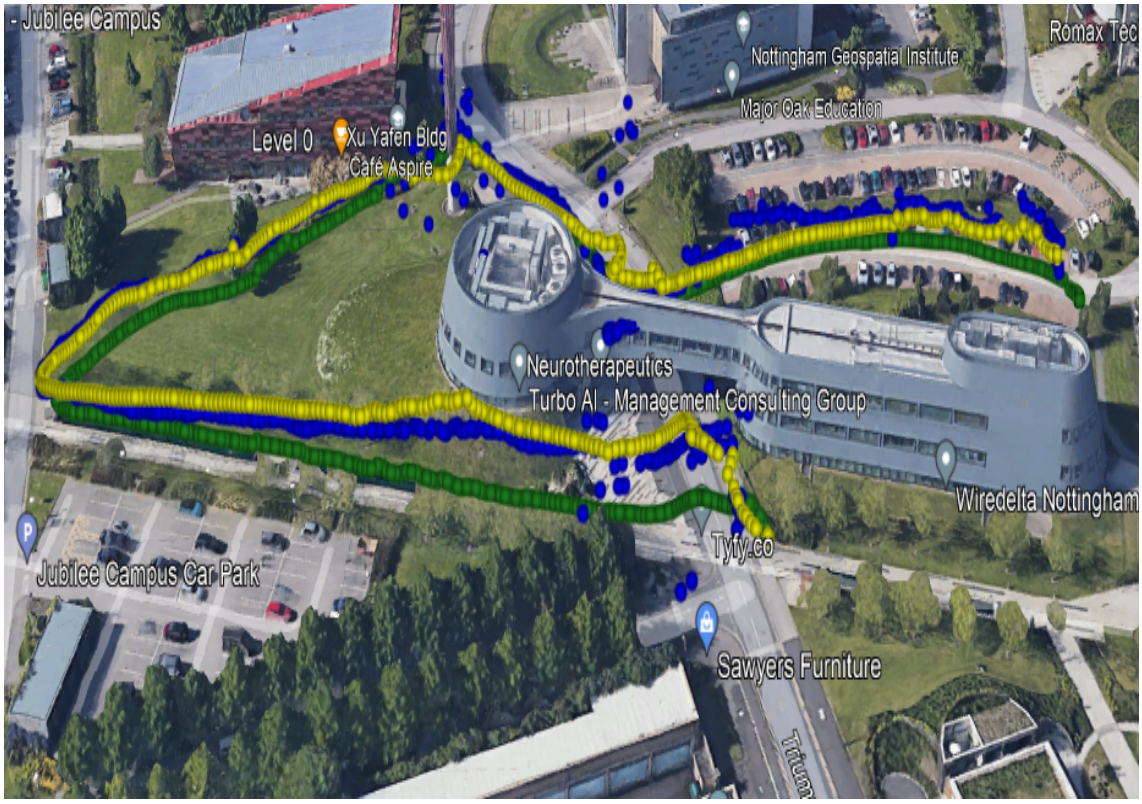


Figure 4.12: Trolley trajectories comparison between GPS only positioning (blue), GPS/IMU fusion positioning (yellow) and reference (green)

As shown in Figure 4.12, blue dots and yellow dots represent the trajectories that got from ICC selected GPS positioning and GPS/IMU fusion positioning, respectively. The green dots line denotes the true trajectory of the trolley in the experiment. With the support of IMU, most measurements with large errors taken by GPS are corrected. Multisensor fusion leads to more accurate and smoother trajectories rather than GPS only positioning. At the beginning of the trolley test, fused data got higher errors than average because of the feature of the Kalman filter. After rounds of iteration for error covariance and Kalman gain, the estimation converges, which contributes to a more accurate and precise trajectory.

4.5 Summary

In this chapter, an ICC applied multisensor positioning optimisation algorithm is explained. An intraclass correlation coefficient is applied on GPS positioning to

detect unreliable satellite measurements. The measurements with low reliability are filtered before positioning. Then inertial measurement unit is utilised for further improvement of positioning accuracy. ICC processed GPS data is fused with IMU data by using the Kalman filter. A trolley test containing low-cost IMU and USRP-based GPS receiver has been done within a scenario including open areas, sculptures and buildings. From the results shown in this chapter, the reliability factor (ICC) related optimisation algorithm is able to increase the accuracy and precision of GPS positioning. The fusion of GPS and IMU contributes to further reduction of positioning errors and avoiding system relying on only one sensor.

The noise from IMU can be accumulated continuously if GPS loses signal for a long time. In order to increase the reliability and availability of the system under more complex challenging driving environments, more sensors are necessary. Furthermore, the velocity of the trolley is limited, real vehicle based field trial is expected.

Chapter 5

Multisensor Selection and Fusion for Autonomous Vehicle in Sensor-degraded Environment

In order to improve the performance of GPS, the intraclass correlation coefficient (ICC) is applied to GPS measurements in Chapter 4. And IMU is used for data fusion to mitigate positioning errors. However, GPS signal is not available all the time, for example, when the number of visible satellites is lower than 4. Without correction from GPS, the drift that come from IMU will accumulate after providing positioning information alone for a long time. As a result of these, GPS and IMU are not sufficient enough for a multisensor integration system with high availability, other sensors are necessary. Researchers in [46] and [45] developed multisensor integration navigation aided by a digital compass and odometer, which can provide the direction and velocity of vehicles as aiding information. However, digital compass and odometer are not independent positioning sensors, which means they can only provide assistance aiding information. A sensor can work as the alternative positioning option when GPS signal losses are required. LiDAR (light detection and ranging) is a sensor which uses a laser to scan obstacles around and returns the measured ranges between LiDAR and obstacles. In the proposed multisensor positioning algorithm, LiDAR is utilized to provide useful positioning information for the vehicle, especially in the situation when GPS signal is lost.

When multiple sensors are included in integrate navigation system, the availability and performance of each sensor should be concerned. The reliability and

availability of different sensors can be affected by different environments, for instance, GNSS (global navigation satellite system) is one of the most reliable sensors in open areas, while may lose signal tracking when the receiver is in garage or indoor environment. Therefore, how to choose the fusion combination of sensors and when to switch between different navigation algorithms are one of the most critical and difficult parts of the multisensor navigation system. [47] and [48] apply multiple sensors in the navigation system, however, both of the algorithms integrate all sensors without evaluating the reliability of each sensor first. The robustness and performance of these two systems can be affected negatively if one of the sensors are unreliable. At least three sensors are utilized in [49] and [3]. Switching algorithms are developed to detect the environment (indoor or outdoor) and switch between fusion modes (GNSS/IMU navigation or dead reckoning navigation). Nevertheless, the algorithms are applied only in scenarios with angular ramp garages and specific sizes of the gate, which is not applicable to other scenarios. ICC is applied to the measurements of GPS as a reliability factor in Chapter 4, which contributes to more accurate and precise positioning for GPS only. Within a system including several sensors, ICC can not only be used upon sensors separately but also be utilized to select the most reliable fusion combination of sensors. In the proposed multisensor fusion algorithm presented in this chapter, GNSS, IMU and LiDAR are utilized for vehicle positioning. ICC is used as the evaluation factor for different modes of navigation and decides when to switch between different navigation modes.

In order to improve the reliability and continuity of providing positioning information, GNSS, IMU and LiDAR are integrated based on the Kalman filter for vehicle navigation. Furthermore, an ICC based switching and selecting algorithm is developed for navigation mode switch and decision. The system algorithm is tested by field trial based on a van which is equipped with the devices mentioned above. The results of the experiment indicate the performance of the proposed system is superior under challenging driving environments.

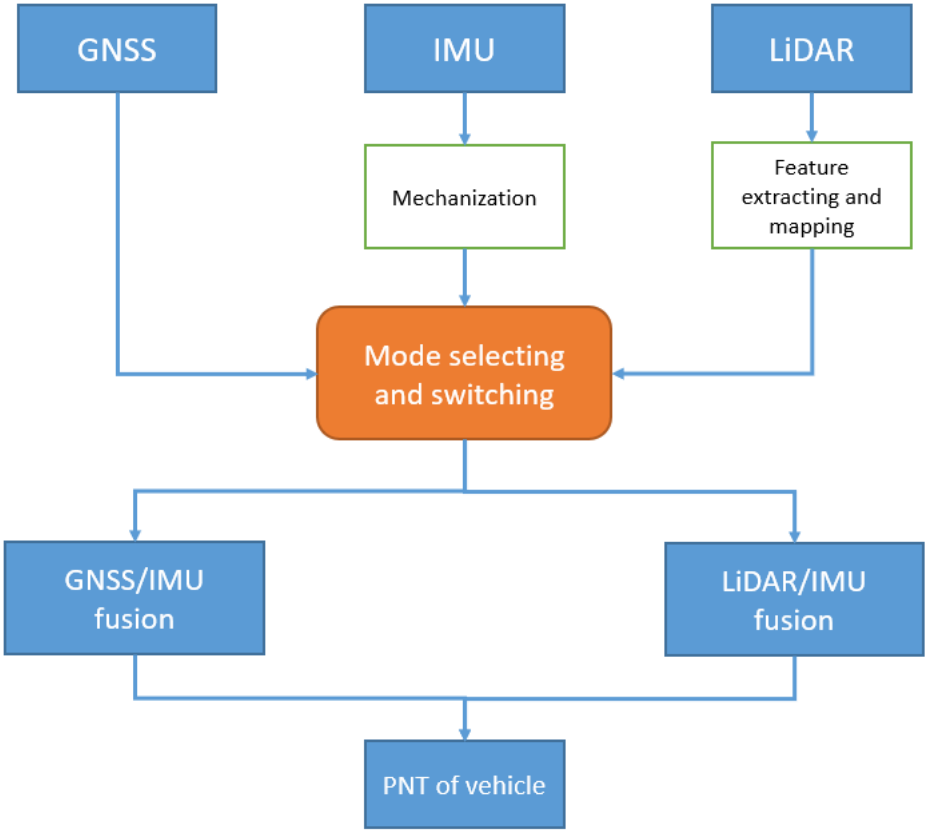


Figure 5.1: The block diagram of data processing

5.1 Challenging Environment Navigation Switching Algorithm for Autonomous Vehicles

Figure 5.1 shows the data processing block diagram of the proposed algorithm. The data collected by IMU, LiDAR and GNSS will be preprocessed first to derive the same level positioning information respectively, for example, feature extraction and mapping scheme is used for LiDAR positioning. The positioning measurements will be input into the mode selecting and switching block before fusion. GNSS and LiDAR can work properly during each others' poor performance period, for example, GNSS can provide PNT information with high accuracy in open areas, while LiDAR can barely return data because of not sufficient obstacles around. And IMU is able to collect dynamic data constantly, so there are two fusion modes including GNSS/IMU fusion and LiDAR/IMU fusion in the proposed system. Mode selecting and switching block judges and selects fusion mode with higher reliability at each discrete time, then the PNT information of the vehicle will be estimated by fusion mode which is selected.

Within the mode selecting and switching algorithm, ICC value is regarded as

selection factor. Based on the ICC concepts which have been explained in last chapter, the positions of the vehicle in different dimensions (x/y/z or E/N/U) are the three 'subjects' and different sensors are 'judges'. 'Two-way mixed' model, 'multiple' type and 'absolute agreement' are picked for the ICC models applied in this algorithm, whose value can be computed by Equation 4.5.

5.1.1 Algorithm for mode selecting and switching

Assume K is the preset threshold value of ICC selection, SF is the value of the selection factor (ICC). $PG(t)$, $PL(t)$ and $PI(t)$ are the preprocessed positioning measurements of GNSS, LiDAR and IMU at t, respectively. $T(m)$ and $T(n)$ are the starting time and end time of vehicle driving. PE represents the final estimated position got from the proposed optimised multisensor fusion algorithm. The fusion data selection algorithm based on the selection factor can be described by the pseudocode in Figure 5.2.

As it describes in the algorithm, The ICCs for both fusion modes (GNSS/IMU or LiDAR/IMU) are computed and compared to get which fusion combination is most reliable at each time. The fusion mode with a higher ICC value will be selected to reduce the negative effects caused by unreliable data. If both fusion modes are not reliable enough (the ICC of both modes are lower than the preset threshold), the positioning information will be derived based on IMU data only. The fusion results are used as the initial data for positioning of the next second.

5.2 Data Preprocess for LiDAR and IMU

5.2.1 Line Tracking and Mapping for LiDAR

In order to derive positions of the vehicle based on LiDAR measurements, feature extraction and mapping should be done first. Lines are the most frequently used feature for LiDAR feature extracting because they are common and repeatable in various scenarios such as urban and suburban areas. By identifying the same line from two adjacent successive scans of LiDAR, reference positioning information can be derived for vehicle positions. Compared with the conventional line extraction schemes including split and merge, line tracking and random sampling consensus, a LS based line tracking approach with higher efficiency and lower implementation

Algorithm 1 Mode selecting and switching

Input: K $PG(t)$ $PL(t)$ $PI(t)$

Output: $PE(t)$

for $t = T(m)$ to $T(n)$

Compute RF for t of every fusion mode

$RF_1 = ICC(PG(t)/PI(t))$, $RF_2 = ICC(PL(t)/PI(t))$

  if $RF_1 < K$ & $RF_2 < K$ **then**

    Compute $PE(t)$ based on IMU data only

    skip to $t = t + 1$

  else

    Pick the fusion mode with higher SF

    Compute PE via selected fusion mode

    skip to $t = t + 1$

  end

end

Figure 5.2: Mode selecting and switching algorithm

difficulty is used in this project. As it is explained, the measurements obtained by LiDAR are the angle and range between LiDAR and obstacles, which can be represented by α and ρ, respectively. Assume x and y are the coordinates of the scanned obstacle point in Cartesian coordinates, N is the number of scanned points in a line. The translation between Polar coordinate and Cartesian coordinate can

be taken by Equations:

$$\rho = \bar{x}cos(\alpha) + \bar{y}sin(\alpha) \tag{5.1a}$$

$$\alpha = \frac{1}{2}tan^{-1}(\frac{2 \cdot \sum_{i=1}^{N}(\bar{x} - x_i) \cdot (\bar{y} - y_i)}{\sum_{i=1}^{N}(\bar{y} - y_i)^2 - \sum_{i=1}^{N}(\bar{x} - x_i)^2}) \tag{5.1b}$$

$$\bar{x} = \frac{1}{N}\sum_{i=1}^{N} x_i \tag{5.1c}$$

$$\bar{y} = \frac{1}{N}\sum_{i=1}^{N} y_i \tag{5.1d}$$

To find the break point of each line, the first two points of scanning clouds are used to create the original line. The equations of the extracted line can be calculated based on LS [81]. Then the successive scanned points will join the line except when the Euclidean distance D_e between the new point and the line or the standard deviation σ_l distance between the scanned point and the line is larger than preset threshold [82]. The D_e and σ_l can be computed by:

$$D_e = \rho - x_i cos(\alpha) - y_i sin(\alpha) \tag{5.2}$$

$$\sigma_l = \sqrt{\frac{\sum_{i=1}^{N}[\rho - x_i cos(\alpha) - y_i sin(\alpha)]^2}{N-1}} \tag{5.3}$$

Where x_i and y_i is the Cartesian coordinate of the new point. The point which is not allowed to join will be the break point or the first point of next line.

After extracting line features of each scan, mapping is necessary to identify which lines are corresponded to each other in adjacent scans. By implementing mapping, the relative positions and attitudes of LiDAR can be estimated. The extracted line can be described by a linear equation:

$$a_n^j x_i + b_n^j y_i + c = 0 \tag{5.4}$$

where n and i denote the number of scanning circle and the number of point joined the J_{th} line. The distance between one points to the extracted line is computed by:

$$d_{i,j}^n = \frac{a_j x_i + b_j y_i + c}{\sqrt{a^2 + b^2}} \tag{5.5}$$

The total distance for a line with S points can be calculated by:

$$D_j^n = \sum_{i=1}^{S} \frac{a_j x_i + b_j y_i + c}{\sqrt{a_j^2 + b_j^2}} \tag{5.6}$$

Because the line extraction is based on the least mean square, the total distance between points to line should be the same within the two scans. If the difference between two total distances are less than or equal to the preset threshold ($|D_j^{n+1} - D_j^n| \leq D_{threshold}$), these two lines will be considered as the same line in two scans [83]. After mapping the line features, the positions of the vehicle based on LiDAR measurements can be got via the LiDAR mechanization procedure.

5.2.2 IMU Mechanization

In order to transform the measurements of IMU from angular velocity and specific force to position, velocity, IMU mechanization is needed [84]. The measurement of IMU from gyroscope and accelerator can be expressed as:

$$\tilde{\omega} = \omega_{ib}^b + \Delta\omega_{ib}^b \tag{5.7a}$$

$$\tilde{f}^b = f^b + \Delta f^b \tag{5.7b}$$

where Δf^b and $\Delta\omega_{ib}^b$ denote the error of specific force and the error of angular velocity, respectively. Regarding the local frame as a reference, the relation between position and velocity can be described as:

$$\dot{r}^n = D^{-1} v^n \tag{5.8}$$

where r^n represents the 3-D (Latitude ϕ, longitude λ, and height h) states of position and D^{-1} is computed by:

$$D^{-1} = \begin{bmatrix} \frac{1}{R_M + h} & 0 & 0 \\ 0 & \frac{1}{(R_N + h)cos\alpha} & 0 \\ 0 & 0 & -1 \end{bmatrix} \tag{5.9}$$

where R_M and R_N denote the radius of curvature for meridian and prime vertical, which can be calculated by Equation 5.10.

$$\begin{aligned} R_M &= \frac{a(1-e^2)}{(1-e^2 \cdot sin^2\varphi)^{3/2}} \\ R_N &= \frac{a}{(1-e^2 \cdot sin^2\varphi)^{1/2}} \end{aligned} \tag{5.10}$$

where a is the semi-major axis length which equals to 378317.0m and e is the eccentricity of the WGS-84 ellipsoid which equals to 0.0818 [85]. The velocity state can be computed via:

$$\dot{v}^n = R_b^{ENC}(f^b - b_a) - (2\omega_{ie}^n + \omega_{en}^n)v^n + g^n \tag{5.11}$$

where R_b^{ENC} is the transformation matrix from body-frame to local level frame (North, East and Down). f^b is the specific force measured by the accelerator of IMU. ω_{ie}^n represents the Earth's turn rate in a local level frame and ω_{en}^n represents the turn rate of local level frame relatives to Earth. Both of the parameters can be obtained from Equation 5.12.

$$\omega_{ie}^n = \begin{bmatrix} 0 & \sigma cos\phi & \sigma sin(\phi) \end{bmatrix}^T \tag{5.12a}$$

$$\omega_{en}^n = \begin{bmatrix} \frac{-v_n}{R_M+h} & \frac{v_E}{R_N+h} & \frac{v_E tan\phi}{R_N+h} \end{bmatrix} \tag{5.12b}$$

where g and b_a denote the gravity vector and accelerator drift, respectively. Set ω_{ib}^b to be the angular velocity measured by gyroscopes based on the body frame and b_g is the gyroscope drift, the attitude mechanization can be derived by:

$$\omega_{nb}^b = \omega_{ib}^b - R_{ENC}^b(\omega_{ie}^n + \omega_{en}^n)b_g \tag{5.13}$$

where R_{ENC}^b denotes the transformation matrix from the local level frame to the body frame.

5.2.3 INS error models

Within the measurements of IMU and the mechanisation process, certain and random errors occur and accumulate. It is necessary to analyse and estimate the errors based on the error models. The INS error models are also utilized in IMU-based

data fusion such as the Kalman filter and particle filter.

5.2.3.1 Position Error Model

Assume ϕ, λ and h denote the differential position in latitude, longitude and height above the Earth surface, respectively. V_n, V_e and V_d represent the velocity base on North, East, Up frame. Then the position differential coefficient in geodetic coordinates can be computed by Equation 5.14 [86].

$$\begin{bmatrix} \dot{\phi} \\ \dot{\lambda} \\ \dot{h} \end{bmatrix} = \begin{bmatrix} \frac{V_n}{R_M+h} \\ \frac{V_e}{cos(\phi)(R_N+h)} \\ -V_d \end{bmatrix} \tag{5.14}$$

Equation 5.14 can be expressed in a nonlinear model as:

$$\begin{aligned} \dot{P} &= f_p(P, v) \\ \dot{\hat{P}} &= f_p(\hat{\dot{P}}, \hat{\dot{v}}) \end{aligned} \tag{5.15}$$

Use the Taylor series to linearize $\dot{P}$ around $\hat{\dot{P}}$ and neglect the higher order. $\dot{P}$ can be expressed as:

$$\dot{P} = f_p(\hat{P}, \hat{v}) + F_{rr}\delta P + F_{rv}\delta v + F_{r\varepsilon}\varepsilon \tag{5.16}$$

The position error can be further modelled as Equation 5.17 presents.

$$\Delta P = F_{rr}\delta P + F_{rv}\delta v + F_{r\varepsilon} + \delta\varepsilon \tag{5.17}$$

Where F_{rr}, F_{rv} and $F_{r\varepsilon}$ are presented as:

$$F_{rr} = \begin{bmatrix} 0 & 0 & \frac{-\hat{v}_n}{(R_M+h)^2} \\ \frac{\hat{v}_e sin(\hat{\varphi})}{(R_N+\hat{h})cos(\hat{\varphi})^2} & 0 & \frac{-\hat{v}_e}{(R_N+\hat{h})^2 cos(\hat{\varphi})} \\ 0 & 0 & 0 \end{bmatrix} \tag{5.18a}$$

$$F_{rv} = \begin{bmatrix} \frac{1}{(R_M+\hat{h})} & 0 & 0 \\ 0 & \frac{1}{(R_N+\hat{h})cos(\hat{\varphi})} & 0 \\ 0 & 0 & -1 \end{bmatrix} \tag{5.18b}$$

$$F_{r\varepsilon} = \begin{bmatrix} 0 & 0 & 0 \\ 0 & 0 & 0 \\ 0 & 0 & 0 \end{bmatrix} \tag{5.18c}$$

5.2.3.2 Velocity Error Model

As for velocity error, it can be described by Equation 5.19 [86].

$$\dot{\hat{V}}_e^n = f^n - Pf^n + \hat{R}_b^n \Delta f^b + g^n - \delta g^n - (\hat{\omega}_{en}^n + 2\hat{\omega}_{ie}^n)\hat{V}^n \tag{5.19}$$

Subtract Equation 5.19 from Equation 5.11, and linearize the result by Taylor series, the velocity error can be expressed as:

$$\delta\dot{V} = F_{vr}\delta P + F_{vv}\delta V + F_{v\varepsilon}\varepsilon - R_b^n \delta f^b \tag{5.20}$$

where $P = \varepsilon(\times)$, and the F_{vr}, F_{vv} and $F_{v\varepsilon}$ are:

$$F_{vr} = \begin{bmatrix} 2\sigma(V_u sin\varphi + V_N cos\varphi) + \frac{V_E V_N}{(R_N+h)cos^2\varphi} & 0 & \frac{V_E V_U}{(R_N+h)^2} - \frac{V_E V_N tan\varphi}{(R_N+h)^2} \\ -2\sigma V_E cos\varphi - \frac{V_E^2}{(R_N+h)cos^2\varphi} & 0 & \frac{V_{R_N} V_U}{(R_M+h)^2} + \frac{V_E^2 tan\varphi}{(R_N+h)^2} \\ -2\sigma V_E sin\varphi & 0 & -\frac{V_E^2}{(R_N+h)^2} - \frac{V_{R_N}^2}{(R_M+h)^2} + \frac{2g}{R+h} \end{bmatrix} \tag{5.21a}$$

$$F_{vv} = \begin{bmatrix} \frac{V_N tan\varphi}{R_N+h} - \frac{V_U}{R_N+h} & 2\sigma sin\varphi + \frac{V_E tan\varphi}{R_N+h} & -2\sigma cos\varphi - \frac{V_E}{R_N+h} \\ -2\sigma sin\varphi - \frac{2V_E tan\varphi}{R_N+h} & -\frac{V_U}{R_M+h} & -\frac{V_N}{M+h} \\ 2\sigma cos\varphi + \frac{2V_E}{R_N+h} & \frac{V_N}{R_M+h} & 0 \end{bmatrix} \tag{5.21b}$$

$$F_{v\varepsilon} = \begin{bmatrix} 0 & f_U & -f_N \\ -f_U & 0 & f_E \\ f_N & -f_E & 0 \end{bmatrix} \tag{5.21c}$$

5.2.3.3 Attitude Error Model

According to Equation 5.13, the attitude error model can be expressed as [86]:

$$\dot{\varepsilon} = \hat{R}_b^n(\delta\omega_{ib}^b - \delta\omega_{in}^b) \tag{5.22}$$

And $\delta\omega_{in}^n$ can be computed by:

$$\delta\omega_{in}^b = \hat{R}_n^b(\delta\omega_{in}^n - P\hat{\omega}_{in}^n) \tag{5.23}$$

Substitute $\delta\omega_{in}^n$, then

$$\dot{\varepsilon} + \hat{\omega}_{in}^n\varepsilon = -\delta\omega_{in}^n + R_b^n\delta\omega_{ib}^b \tag{5.24}$$

Set $\delta\omega_{in}^n = \omega_{in}^n - \hat{\omega}_{in}^n$ and linearize it by Taylor series

$$\delta\omega_{in}^n = [\frac{\partial\hat{\omega}_{in}}{\partial\hat{\varepsilon}}, \frac{\partial\hat{\omega}_{in}}{\partial\hat{V}}] \begin{bmatrix} \delta\varepsilon \\ \delta V \end{bmatrix} \tag{5.25}$$

So the attitude error can be modeled as:

$$\dot{\varepsilon} = F_{\varepsilon P}\delta P + F_{\varepsilon V}\delta V + F_{\varepsilon\varepsilon}\delta\varepsilon + \hat{R}_b^n\delta\omega_{ib}^b \tag{5.26}$$

Where

$$F_{\varepsilon r} = \begin{bmatrix} 0 & 0 & -\frac{V_N}{(R_M+h)^2} \\ \sigma sin\varphi & 0 & \frac{V_E}{(R_N+h)^2} \\ -\sigma cos\varphi - \frac{V_E}{(R_N+h)cos^2\varphi} & 0 & \frac{V_E tan\varphi}{(R_N+h)^2} \end{bmatrix} \tag{5.27a}$$

$$F_{\varepsilon v} = \begin{bmatrix} 0 & \frac{1}{R_M+h} & 0 \\ -\frac{1}{R_N+h} & 0 & 0 \\ -\frac{tan\varphi}{R_N+h} & 0 & 0 \end{bmatrix} \tag{5.27b}$$

$$F_{\varepsilon\varepsilon} = \begin{bmatrix} 0 & \sigma sin\varphi + \frac{V_E tan\varphi}{R_N+h} & -\sigma cos\varphi - \frac{V_E}{R_N+h} \\ \sigma sin\varphi - \frac{V_E tan\varphi}{R_N+h} & 0 & \frac{V_N}{R_M+h} \\ \sigma cos\varphi + \frac{V_E}{R_N+h} & \frac{V_N}{R_M+h} & 0 \end{bmatrix} \tag{5.27c}$$

5.3 Data Fusion for GNSS/IMU and LiDAR/IMU

Kalman filter is used in this project for loose multisensor integration. Compared with classic Kalman filter, a 15 states vector of errors is used as the estimation of the Kalman filter. [87]. The state equation for Kalman filter estimation is presented as Equation 5.28

$$x = [\delta r_{xyz}\ \delta v_{xyz}\ \delta \varepsilon_{xyz}\ \delta b_a\ \delta b_g] \tag{5.28}$$

where, δr is the position error in three dimensions, δv is the velocity error in three dimensions and $\delta \varepsilon$ is the attitude error in three dimensions, δb_a and δb_g are the bias of accelerator and gyroscope in three dimensions respectively. According to the basic equations of each part for the Kalman filter in Table 4.4, the state prediction equation is:

$$x_t = F_t x_{t-1} \tag{5.29}$$

where F denotes the state transition matrix. Based on the INS error models explained in last subsection, Equation 5.29 can be rewritten as:

$$\begin{bmatrix} \delta\dot{r} \\ \delta\dot{v} \\ \delta\dot{\varepsilon} \\ \dot{\delta b_a} \\ \dot{\delta b_g} \end{bmatrix}_t = \begin{bmatrix} F_{rr} & F_{rv} & F_{r\varepsilon} & 0_3 & 0_3 \\ F_{vr} & F_{vv} & F_{v\varepsilon} & C_b^n & 0_3 \\ F_{\varepsilon r} & F_{\varepsilon v} & F_{\varepsilon\varepsilon} & 0_3 & C_b^n \\ 0_3 & 0_3 & 0_3 & \beta_{ba} & 0_3 \\ 0_3 & 0_3 & 0_3 & 0_3 & \beta_{bg} \end{bmatrix} \cdot \begin{bmatrix} \delta r \\ \delta v \\ \delta\varepsilon \\ \delta b_a \\ \delta b_g \end{bmatrix}_{t-1} + \omega_{t-1} \tag{5.30}$$

The error covariance can be computed by:

$$P_{t|t-1} = [E(x_t - \hat{x}_{t|t-1})(x_t - \hat{x}_{t|t-1})^T] \tag{5.31a}$$

$$P_{t|t-1} = F_t P_{t-1|t-1} F_t^T + Q_t \tag{5.31b}$$

where Q represents the process noise covariance which comes from the bias of gyroscope and accelerator.

There are two different modes for the 'measurement' part including GNSS/IMU and LiDAR/IMU, which is picked by an ICC-based selecting algorithm. The difference in position, velocity and attitude in 3-D between GNSS, LiDAR and IMU is used as the input measurements for the system. Assume z to be the measurement,

then the measurements for two modes are:

$$z_{GNSS/IMU} = \begin{bmatrix} r_{GNSS} - r_{IMU} \\ v_{GNSS} - v_{IMU} \end{bmatrix} \tag{5.32}$$

$$z_{LiDAR/IMU} = \begin{bmatrix} r_{LiDAR} - r_{IMU} \\ v_{LiDAR} - v_{IMU} \\ \varepsilon_{LiDAR} - \varepsilon_{IMU} \end{bmatrix} \tag{5.33}$$

The input measurements will be decided after the selection based on ICC, which means z is selected according to the reliability of GNSS and LiDAR. If neither modes are selected which means both GNSS and LiDAR cannot provide reliable or available positioning information, there is no data fusion, and the positioning of the vehicle will rely on IMU only after one or both GNSS and LiDAR can collect reliable enough data.

To derive Kalman gain and update estimate error state and error covariance, the observation matrix is dynamic as well. For GNSS/IMU fusion mode, observation matrix can be presented as:

$$H_t^{GNSS/IMU} = \begin{bmatrix} I_{3\times3} & 0_{3\times3} & 0_{3\times3} & 0_{3\times3} & 0_{3\times3} \\ 0_{3\times3} & I_{3\times3} & 0_{3\times3} & 0_{3\times3} & 0_{3\times3} \end{bmatrix} \tag{5.34}$$

and the LiDAR/IMU mode observation matrix is:

$$H_t^{LiDAR/IMU} = \begin{bmatrix} I_{3\times3} & 0_{3\times3} & 0_{3\times3} & 0_{3\times3} & 0_{3\times3} \\ 0_{3\times3} & I_{3\times3} & 0_{3\times3} & 0_{3\times3} & 0_{3\times3} \\ 0_{3\times3} & 0_{3\times3} & I_{3\times3} & 0_{3\times3} & 0_{3\times3} \end{bmatrix} \tag{5.35}$$

Set Kalman gain is K, then the estimate state and error covariance can be updated as:

$$\hat{x}_{t|t} = \hat{x}_{t|t-1} + K(z - H_t\hat{x}_{t|t-1}) \tag{5.36}$$

$$P_{t|t} = P_{t|t-1} - K_t H_t P_{t|t-1} \tag{5.37}$$

The integration system is dynamic because two subsystems are involved and data fusion content switches between these two subsystems following the decision made by the selection algorithm. The integrated PNT results for the vehicle will be the initial set of data fusion in the next time step.

5.4 Field Trial Setup and Testing Scenario

An equipped van based field trial has been implemented to test the proposed algorithm. Compared with trolley test, real van test provides experimental scenario with higher reality such as faster testing velocity and more complex roadside environment.

5.4.1 Experiment Equipment

The GNSS (global navigation satellite system) receiver used in the field trial is Septentrio PolaRx 5S which is shown in Figure 5.3. PolaRX 5S is able to support following constellations and frequency:

- GPS: L1CA, L1P, L2P, L5
- GALILEO: E1, E5a, b, AltBoc E6
- SBAS: L1, L5

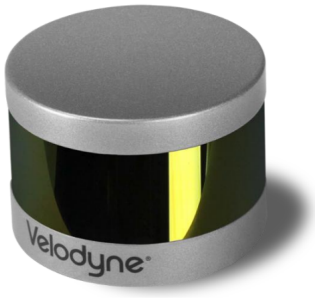
Only L1, L5 of GPS and E1, E5 of GALILEO are utilized for positioning in this project. The front and rear panel of PolaRx 5S is whown in Figure [13]. On the front panel, 'PWR' is connected with power supply. And 'COMS3-4/USB' port is connected with on-board unit via pin7-USB cable for data storage. On the rear panel, antenna (main) is connected with GNSS antenna for RF signal.



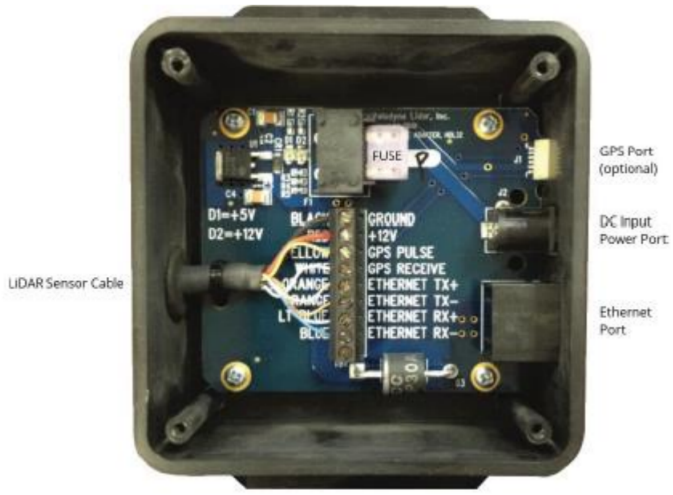
Figure 5.3: PolaRX 5S front and rear panel [13]

The upper figure in Figure 5.4 shows the LiDAR used in this field trial which is Velodyne VLP-16. VLP-16 uses 16 infra-red lasers to detect the obstacles within

surrounding environment and measure the distance between obstacle points to LiDAR. Sub-figure (b) in Figure 5.4 illustrates the interface box of VLP-16. The power supply and synchronization cable are both integrated with interface box. An Ethernet cable with RJ45 Ethernet connector is connected between LiDAR and on-board unit for data recording.



(a) Photo of LiDAR sensor [88]



(b) VLP-16 interface box [89]

Figure 5.4: Velodyne VLP-16 LiDAR

The NovAtel SPAN UIMU-LCI is used to provide reference trajectory of vehicle which is shown in Figure 5.5. The SPAN can provide 3-D inertial measurements and derive reference trajectory via using NovAtel's licensed software. It will be compared with other results in field trial for error computation.

MTi-G IMU is used for GNSS/IMU data fusion which has been introduced in last chapter. All the non-GNSS sensors and on-board unit are time synchronized with GNSS receiver via GNSS supplied pulse per second (PPS) clock signal.



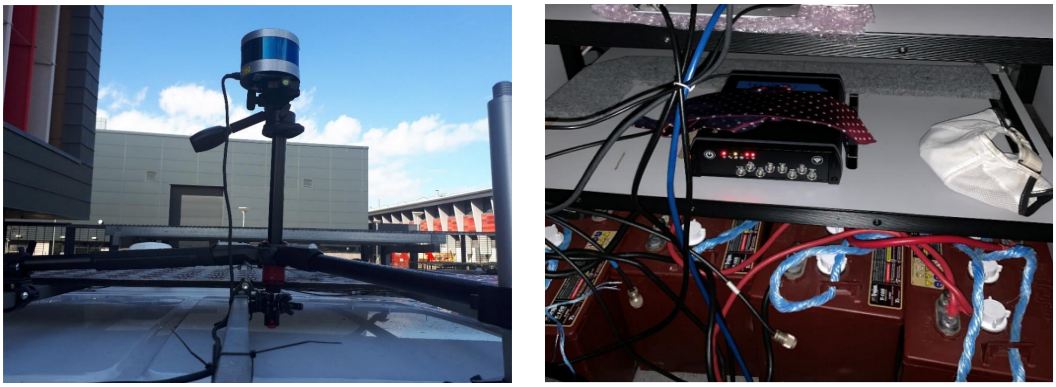
Figure 5.5: NovAtel SPAN UIMU-LCI [14]



Figure 5.6: The equipped testing van

5.4.2 Field Trial Equipment Setup

Figure 5.6 shows the front site of equipment arrangement on testing van. Three sensors including GNSS, IMU and LiDAR are set up. The on-board unit is utilized for data storage and preliminary data processing. LiDAR and GNSS antenna are set on the roof of the van. IMU, GNSS receiver and on-board unit are equipped inside the van. As figure 5.7(a) shows, in order to reduce scanning shadows such as shadows caused by racks and roof of the van, LiDAR is mounted on the centre of the van roof and is raised up 40 cm from the surface of the roof. The PolaRx 5S receiver is secured to a fixed mounting plate inside the van as shown in Figure 5.7(b). The accumulators which provides power supply for all equipment are settled on the floor and tied to avoid them from moving around.



(a) LiDAR roof mounting

(b) GNSS receiver and accumulators mounting

Figure 5.7: Experiment equipment mounting

5.4.3 Field Trial scenario



Figure 5.8: Scenario of field trial

The testing scenario is located in Coventry which is shown in Figure 5.8. Two motorways M6 and M69 intersect within the picked field trial scenario. Following the red arrow shown in Figure 5.8, the quipped testing van drove from East to West on M69 and drove through the tunnel covered by the bridge of M69. Within the area covered by a green square, the trajectory of testing van can be divided into three parts including open area before the tunnel, tunnel and open area after the tunnel. As it is explained, the tunnel can block or affect the signal of GNSS, which means

satellite positioning under the tunnel comes with lower accuracy and precision when compared with open area. In contrast, the LiDAR sensor can collect more data on obstacles under the tunnel, which is able to provide more relative positioning information rather than open areas. When testing van drives through the scenario with high velocity for the motorway, the surrounding environment switches fast as well. Multisensor selecting and switching algorithms should be able to detect the reliability and availability of sensors to choose a more reasonable fusion mode for the testing van. The picked field trial scenario provides a complex environment consisting of different challenging environments for different sensors to evaluate the performance of the proposed multisensor navigation system.

5.5 Results, Analysis and Discussion

Figure 5.9 presents the positioning errors in East, North and horizontal for each sensor used in the field trial. It is easy to see the errors for each sensor are stable except for GNSS during 4.6s to 4.9s. The positioning errors of GNSS increase dramatically between 4.6s and 4.9s, which means the measurements of GNSS are affected by challenging environments or other factors significantly. There is no data for LiDAR from start to 2.6s, which is caused by not sufficient obstacles within the surrounding environment. From Figure 5.8, we can observe that the testing van started from an open area where LiDAR can not collect sufficient measurements from. The average positioning error of available LiDAR measurements is slightly greater than that of GNSS measurements and IMU measurements.

The ICC values for both fusion modes (GNSS/IMU and LiDAR/IMU) are shown in Figure 5.10. They are computed based on the proposed algorithm which is explained in this chapter. Obviously, when the measurements of LiDAR are unavailable within the open area, the ICC values for LiDAR/IMU mode are equal to 0. Because the proper range of ICC value is between 0 to 1, it means LiDAR/IMU mode is absolutely unreliable (unavailable) when the value of ICC equals 0. After getting available measurements from LiDAR, the ICC for LiDAR/IMU is much larger. However, the ICC values for LiDAR/IMU mode are still smaller than those of GNSS/IMU mode except for odd period between 4.6s and 4.9s. That represents GNSS/IMU mode gets higher reliability and it will be selected as fusion mode except for the odd period. By comparing the ICC values with positioning errors of

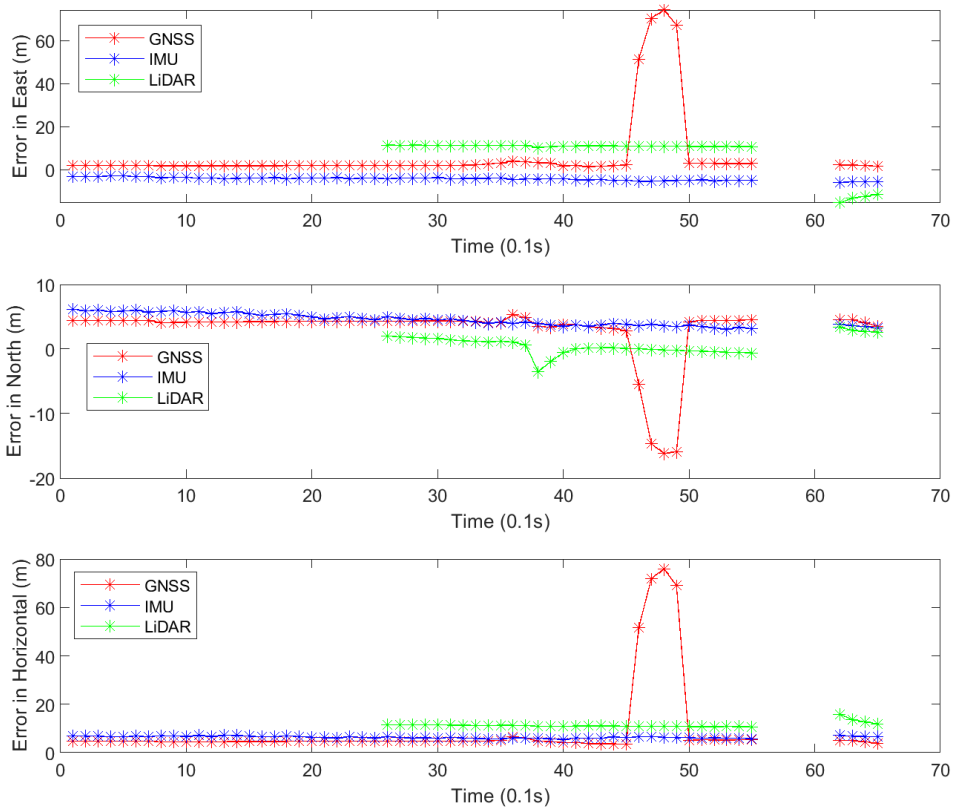


Figure 5.9: Positioning errors comparison between sensors

sensors, the odd period with high errors for LiDAR and GNSS are matched to the detection of ICC values for both modes. In other words, the ICC is able to detect the reliability of sensors and select the better fusion mode with lower errors.

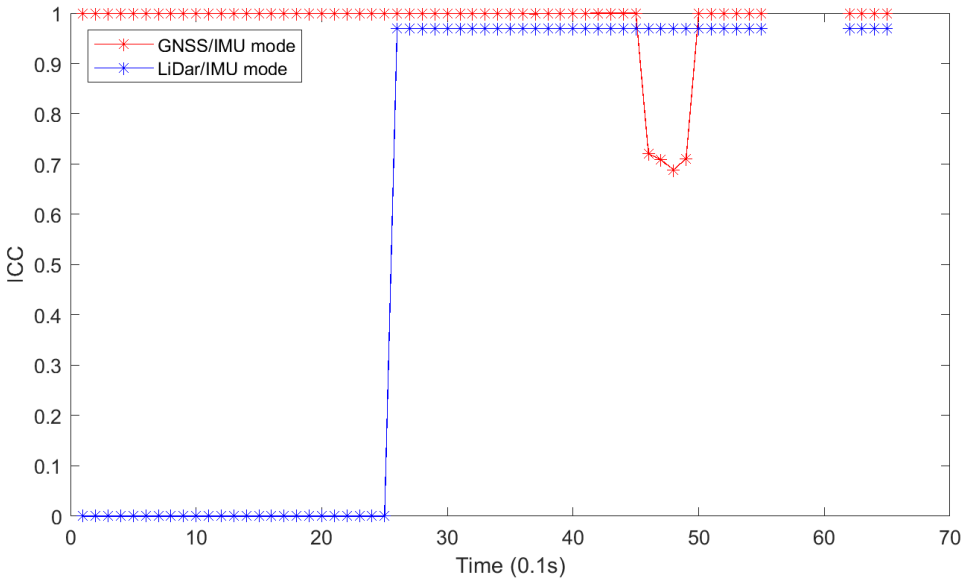


Figure 5.10: ICC comparison between different modes

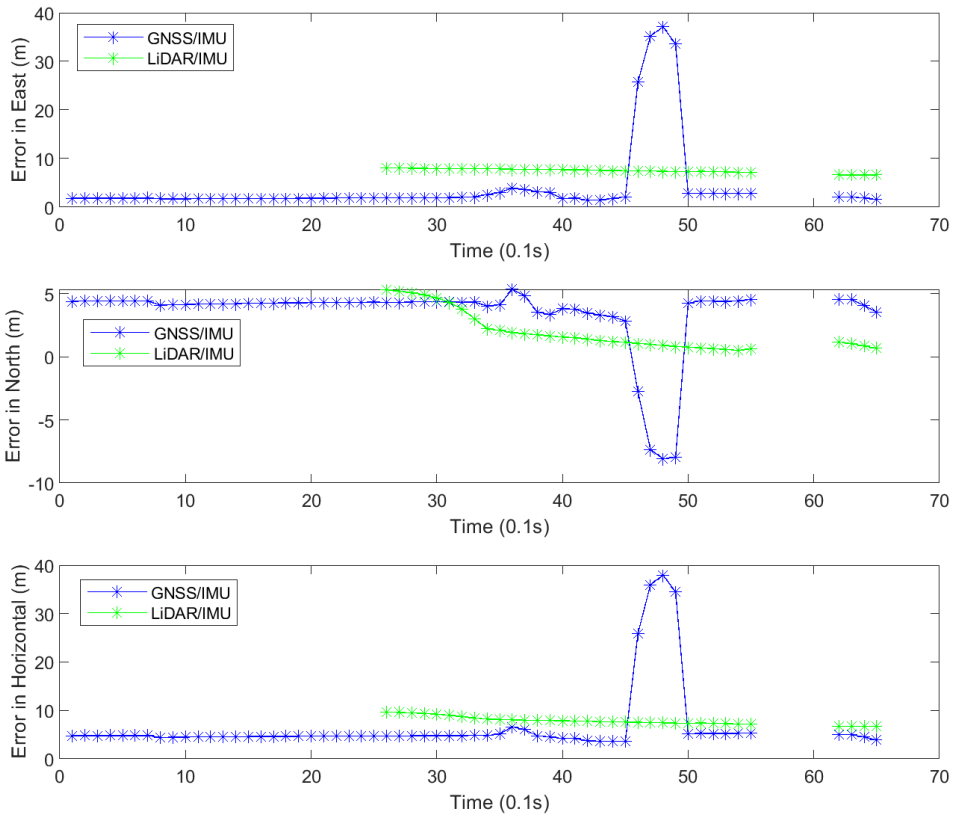


Figure 5.11: Positioning errors comparison between fusion modes

It is shown in Figure 5.11 that the positioning error comparison between fusion modes. The errors in EAST, North and horizontal of both modes are calculated by fusion results of GNSS/IMU and LiDAR/IMU, respectively. From the amplitude of peak errors for odd points, data fusion has reduced the positioning errors for GNSS measurements. However, the errors of GNSS/IMU fusion during 4.6s to 4.9s are still significant. LiDAR/IMU mode gets larger errors than GNSS/IMU mode for most testing periods except the odd duration of GNSS. Matching with ICC values of both modes, fusion mode with lower errors for each time step can be detected and will be selected as estimated positions of the vehicle at the movement.

Figure 5.12 presents the reference trajectory of the testing van and the trajectory estimated by the algorithm proposed in this chapter. The green dots and yellow dots represent the trajectory from the proposed algorithm estimation and SPAN sensor, respectively. The red dots are the positions estimated by GNSS/IMU fusion mode during the odd period, which have been substituted by LiDAR/IMU fusion mode estimation. Following the ICC selection results shown in Figure 5.10, the fusion mode will be switched from GNSS/IMU to LiDAR/IMU during 4.6s to 4.9s



Figure 5.12: Trajectory comparison between proposed algorithm (green), reference (yellow) and odd estimation (red) on Google Earth

(the period when GNSS measurements are not reliable enough). As the result of this, according to the trajectories in Figure 5.12, the positioning errors are reduced significantly by applying the proposed selection and switching algorithm.

It is obvious to find from Figure 5.9 - Figure 5.12 that an unexpected break period occurs before the end of the field trial. All sensors including GNSS, LiDAR, Xsense IMU and SPAN IMU lost data during this period. And the measurements of three sensors are affected after the gap period. All IMU sensors get local clock individually, so this situation is not caused by GNSS losing timing signals from satellites then cannot support time synchronization. Because there is no data collected, the ICC computation is not able to return any value or to make any selection. The reason that caused this abnormal situation requires further investigations. Inspired by these, in order to deal with the situation such as power off of all sensors, an emergency block should be added alongside the selection and switching block in the diagram in Figure 5.1.

A primary algorithm for the emergency situation is presented in Figure 5.13. After getting no data from all sensors, an alert message should be sent to the user immediately for emergency actions such as switching to manual driving. The posi-

Algorithm 2 Emergency aiding

```
for No sensor data epochs
    1. Sending emergency alert to user
    2. Estimate next position and velocities based on
    last available fusion results
      if At least one sensor works properly
        break
      end
end
Back to proper estimation algorithm
```

Figure 5.13: Algorithm for emergency aiding

tions for the next epoch will be computed based on the last available fusion results including position, velocity and acceleration. Constant acceleration dynamic equation will be used until at least one sensor can work properly. However, the emergency aiding algorithm can only be applied for short seconds because of uncertainties. Further research and experiments should be done to update and implement the primary version of emergency aiding algorithm.

5.6 Summary

In this chapter, a mode-switching algorithm applied multisensor positioning system is described. Three sensors are utilized including GNSS receiver, IMU and LiDAR. A selection and switching algorithm for GNSS/IMU and LiDAR/IMU fusion modes under different environments is developed. By computing ICC values of both fusion modes, a more reliable fusion combination is selected for position estimation. Error state based Kalman filter is used for data fusion. A field trial based on the equipped testing van has been designed and made in the scenario consisting of open area and tunnel. The measurements of GNSS and LiDAR can be affected under tunnel and open area, respectively. According to the results presented in this chapter, the proposed multisensor positioning system is able to switch fusion modes according to different challenging environments and fuse data from more reliable sensors to get more accurate estimations.

An unexpected break off of all sensors occurred during the field trial. Even though the proposed system can be evaluated by the rest data of sensor, the break-off period needs further investigation such as the reasons to contribute to the situation and solutions for them. A primary stage of emergency aiding algorithm is designed

which requests further modification and evaluation to be implemented in the future. Other testing vehicles are expected in future field trials for V2V (vehicle to vehicle) communication and building of the vehicular network. Additionally, more complex scenarios such as intersection with multiple entrances and dense urban area should be involved for field trial, which could provide more completed analysis results for the proposed multisensor selection and fusion system.

Chapter 6

Conclusion and Future Research

In modern traffic systems, traffic safety and traffic congestion have been the most critical problems. According to the data listed in this thesis, serious losses have been caused by vehicle accidents and traffic jams during past years, such as road traffic collision deaths, economic damages and extra time consumption. Vehicular communication which could share driving information of vehicles with each other is one of the effective solutions for these problems. GPS is a major and common navigation system which can provide positioning information for vehicles within the vehicular network. However, the positioning accuracy and precision of GPS can be affected by numerous factors such as multipath effects, time-varying ionospheric irregularities and signal attenuation caused by tunnels or skyscrapers in the urban area. As for multisensor system which is supposed to be more robust and accurate when estimating PNT information of vehicles, various challenging traffic environment can also bring influence on different sensors.

In order to deal with the mentioned problems, several innovative schemes and algorithms are proposed in this thesis. A reliable spatio-temporal model using vehicular communication system is developed to reduce vehicle accidents and increase traffic throughput within roundabout and crossroad scenarios. An ICC based GPS positioning optimisation algorithm is applied in a GPS/IMU multisensor navigation system. The experiment results illustrate that the positioning errors caused by unreliable measurements can be decreased after using the proposed algorithm. Moreover, a three-sensor navigation system is designed, which contains reliability detecting and selecting model. By applying the proposed algorithm, vehicles can detect the reliability of sensors and select more reliable fusion modes under complex

challenging environment.

6.1 Conclusion

The thesis explained a spatio-temporal model for roundabouts and road intersections using vehicular communication system firstly. The traffic scenario is divided into segments with unique numbers, which means the trajectories of vehicles can be expressed by a string of numbers. The reliability of GPS observation is used to evaluate the measurements and to derive the confidence circle. Trajectories and sizes of confidence circle of vehicles are processed by a central controller. In this way, vehicles can go through the scenario following the received basic safety messages from central controller. The conventional traffic management (traffic controlled by traffic lights), proposed ITM without confidence circle (ITM) and ITM with confidence circle (ITMCC) are simulated based on different traffic influx levels. In order to evaluate the traffic efficiency, three aspects are concerned, which include the number of cars processed, the total stop time of cars and the average velocity of cars. As for the evaluation of safety levels, number of vehicle accidents and number of simulations with accidents are compared. The simulation results show that compared with conventional traffic management, the proposed ITM with/without confidence circle can increase the traffic efficiency dramatically. After adding a confidence circle around vehicles, the efficiency of traffic is affected because each vehicle occupied more segments during driving. Although the traffic efficiency of ITMCC is marginally lower than that of ITM by applying a safety buffer, it is still vastly more efficient than conventional management. The safety level simulation results denote that the number of collisions and possibility of vehicle accidents drops dramatically due to the application of confidence circle. Overall, by sacrificing the traffic efficiency minimally, ITMCC can gain additional safety remarkably. And the throughput of ITMCC is significantly improved comparing with the conventional traffic light management.

In order to improve the GPS positioning under challenging environments, intra-class correlation coefficient is applied to evaluate the reliability of GPS measurements before data fusion. The difference of pseudorange and carrier phase between two adjacent epochs, as well as the carrier-to-noise ratio are used as 'subject' for ICC evaluation. The measurements with lower ICC values than the preset threshold

will be filtered. And measurements from IMU are fused with pre-processed GPS measurements by loosely coupled integration for further improvement of positioning performance. A trolley test has been done under a specific scenario within university campus, multipath environment. A low-cost IMU and a USRP-based GPS receiver are equipped on the trolley. The experiment results denote that computing ICC is able to detect the GPS measurements which are not reliable enough. By filtering the measurements with low reliability, the positioning errors of GPS are decreased in East, North and Up of local frame. Especially for positions with large errors which are caused by challenging environments. Furthermore, fusing with IMU measurements contributes to further lower positioning errors in all three axes of local frame. Trajectories comparison on Google Earth shows that the proposed positioning optimisation algorithm can provide a smoother trajectory with much fewer outliers in the positioning of trolley.

A three-sensor-based multisensor navigation system has been developed to provide positioning information of vehicles under various challenging traffic environment. GNSS, LiDAR and IMU are included in this system. For LiDAR navigation, a LMS-based line extraction and mapping scheme are used. In order to improve the robustness, reliability and availability of the navigation system, a mode selecting and switching algorithm is designed. Two fusion modes including GNSS/IMU and LiDAR/IMU are switched between each other for utilizing data from different sensors. The selecting and switching algorithm computes the reliability of both modes at each time step and decide which fusion mode should be used. After the selection and switching have been implemented, an error-state-based Kalman filter is utilised for data fusion to estimate the positions of the vehicle. A field trial has been done to evaluate the proposed navigation system. The testing van is equipped with GNSS receiver, IMU, LiDAR, NovAtel SPAN, laptop, antenna and accumulator. A real traffic scenario consist of open area and under bridge tunnel is picked as the testing scenario. The results of field trial proved that the performance of GNSS and LIDAR could be affected by environment significantly, and the proposed selecting algorithm can detect the unreliable measurements correctly and switch the fusion mode to the combination with higher reliability. By applying the proposed multisensor navigation system on-board, the van can be adjusted using selection of fusion modes according to environment introduced noise, which means more reliable estimation can be taken to derive more accurate and precise PNT information for vehicles.

6.2 Future Work

There are some research and work expected to be implemented based on the achievements in this thesis.

Manual vehicles without on-board units, sensors and vehicular communication equipment are not concerned in the proposed ITM protocol. It is necessary to be focused on, particularly the hybrid situation which includes both autonomous vehicles and ordinary vehicles. Furthermore, the ITM protocol does not involve the size of vehicles driving in the scenario. How to merge the different vehicle size and confidence circle should be one of the works in the future.

More sensors such as high-resolution camera could be included in multisensor navigation system for optical sensor based navigation in GNSS-denied environment. With the increasing size of information transmitted within the network, the dedicated frequency band for vehicular communication at 5.9 GHz may be insufficient in the future. Cognitive radio could be used to sense and use unoccupied licensed channels at other frequencies, which is a potential approach to release the pressure of frequency band usage and to improve the utilisation efficiency of channels.

References

[1] World Health Organization, "World health organization global status report on road safety 2018," 2018.

[2] S. Akaraci, M. A. Usman, M. R. Usman, and D. J. Ahn, "From smart to smarter cities: Bridging the dimensions of technology and urban planning," in *2016 International Conference on Smart Green Technology in Electrical and Information Systems (ICSGTEIS)*. IEEE, 2016, pp. 74–78.

[3] N. Li, L. Guan, Y. Gao, S. Du, M. Wu, X. Guang, and X. Cong, "Indoor and outdoor low-cost seamless integrated navigation system based on the integration of ins/gnss/lidar system," *Remote Sensing*, vol. 12, no. 19, p. 3271, 2020.

[4] R. Tiwari, T. Stacey, and F. Toran, "Integrity monitoring and prediction concept and prototype for fully autonomous vehicle resilience and safety," in *Proceedings of the 2020 International Technical Meeting of The Institute of Navigation*, 2020, pp. 538–556.

[5] G. S. Kumar, G. S. B. Rao, and M. Kumar, "Gps signal short-term propagation characteristics modeling in urban areas for precise navigation applications," 2013.

[6] M. Tahsin, S. Sultana, T. Reza, and M. Hossam-E-Haider, "Analysis of dop and its preciseness in gnss position estimation," in *2015 International conference on electrical engineering and information communication technology (ICEEICT)*. IEEE, 2015, pp. 1–6.

[7] M. Atiq, "Historical review of ionosphere in perspective of sources of ionization and radio waves propagation," *Research & Reviews: Journal of Space Science & Technology*, vol. 7, no. 2, pp. 28–39, 2018.

[8] Insightwarehouse. (2018, February) Crashmap. [Online]. Available: http://www.crashmap.co.uk

[9] L. C. Bento, R. Parafita, and U. Nunes, "Intelligent traffic management at intersections supported by V2V and V2I communications," in *IEEE 15th International Conference on Intelligent Transportation Systems (ITSC)*, 2012, pp. 1495–1502.

[10] T. K. Koo and M. Y. Li, "A guideline of selecting and reporting intraclass correlation coefficients for reliability research," *Journal of chiropractic medicine*, vol. 15, no. 2, pp. 155–163, 2016.

[11] R. Research. (2022, May) Usrp x310. [Online]. Available: https://www.ettus.com/all-products/x310-kit/

[12] XSENS, "Miniature ahrs with integrated gps," 2011.

[13] Septentrio, "Septentrio pola5s gnss receiver user manual v 1.2," 2018.

[14] NovAtel Inc., "Uimu-lci product sheet," 2014.

[15] INRIX, "Inrix 2017 global traffic scorecard," 2018.

[16] R. Azimi, G. Bhatia, R. R. Rajkumar, and P. Mudalige, "STIP: Spatio-temporal intersection protocols for autonomous vehicles," in *ICCPS'14: ACM/IEEE 5th International Conference on Cyber-Physical Systems (with CPS Week 2014)*. IEEE Computer Society, 2014, pp. 1–12.

[17] Society of Autonomous Engineers, "Taxonomy and definitions for terms related to driving automation systems for onroad motor vehicles," 2018.

[18] Department for Transport, "Reported road casualties in great britain: 2019 annual report," 2020.

[19] Local Government Association, "A country in a jam: tackling congestion in our towns and cities," 2017.

[20] Sky New, "Congestion crisis warning as vehicle numbers soar by 2.5 million," Saturday 28 July 2018, last accessed 13 September 2020. [Online]. Available: https://news.sky.com/story/congestion-crisis-warning-as-vehicle-numbers-soar-by-25-million-11451965

[21] Minnesota Department of Transportation, "2019 congestion report," 2020.

[22] International Road Transport Union, "A scientific study into european truck accident causation," 2007.

[23] Department for Transport. Road Accident Statistics Branch. (2015, July) Road accident data, 2014. [Online]. Available: http://doi.org/10.5255/UKDA-SN-7752-1

[24] H. Li, I. Gulati, S. Stainton, S. A. Ali, V. Pickert, and S. Dlay, "Sliding mode control for vehicular platoon based on v2v communication," in *Proceedings of the 32nd International Technical Meeting of the Satellite Division of The Institute of Navigation (ION GNSS+ 2019)*, 2019, pp. 2078–2089.

[25] H. Li, H. Wu, I. Gulati, S. A. Ali, V. Pickert, and S. Dlay, "An improved sliding mode control (smc) approach for enhancement of communication delay in vehicle platoon system," *IET Intelligent Transport Systems*, vol. 16, no. 7, pp. 958–970, 2022.

[26] A. El-Rabbany, *Introduction to GPS: the global positioning system.* Artech house, 2002.

[27] P. J. Teunissen and A. Kleusberg, "Gps observation equations and positioning concepts," in *GPS for Geodesy.* Springer, 1998, pp. 187–229.

[28] S. M. Deshpande, *Study of interference effects on GPS signal acquisition.* University of Calgary, Department of Geomatics Engineering, 2004.

[29] R. B. Langley, P. J. Teunissen, and O. Montenbruck, "Introduction to gnss," in *Springer handbook of global navigation satellite systems.* Springer, 2017, pp. 3–23.

[30] N. Ahmad, R. A. R. Ghazilla, N. M. Khairi, and V. Kasi, "Reviews on various inertial measurement unit (imu) sensor applications," *International Journal of Signal Processing Systems*, vol. 1, no. 2, pp. 256–262, 2013.

[31] F. Caron, E. Duflos, D. Pomorski, and P. Vanheeghe, "Gps/imu data fusion using multisensor kalman filtering: introduction of contextual aspects," *Information fusion*, vol. 7, no. 2, pp. 221–230, 2006.

[32] U. Wandinger, "Introduction to lidar," in *Lidar*. Springer, 2005, pp. 1–18.

[33] S. Azimi, G. Bhatia, R. Rajkumar, and P. Mudalige, "Reliable intersection protocols using vehicular networks," in *Proceedings of the ACM/IEEE 4th International Conference on Cyber-Physical Systems*, 2013, pp. 1–10.

[34] C. Wuthishuwong, A. Traechtler, and T. Bruns, "Safe trajectory planning for autonomous intersection management by using vehicle to infrastructure communication," *EURASIP Journal on Wireless Communications and Networking*, vol. 2015, no. 1, p. 33, 2015.

[35] T. Osman, S. S. Psyche, J. S. Ferdous, and H. U. Zaman, "Intelligent traffic management system for cross section of roads using computer vision," in *2017 IEEE 7th Annual Computing and Communication Workshop and Conference (CCWC)*. IEEE, 2017, pp. 1–7.

[36] L. C. Bento, R. Parafita, S. Santos, and U. Nunes, "Intelligent traffic management at intersections: Legacy mode for vehicles not equipped with V2V and V2I communications," in *IEEE 16th International Conference on Intelligent Transportation Systems-(ITSC)*, 2013, pp. 726–731.

[37] H.-S. Seo, D.-G. Noh, C.-J. Lee, and S.-S. Lee, "Design and implementation of intersection movement assistant applications using v2v communications," in *2013 Fifth International Conference on Ubiquitous and Future Networks (ICUFN)*. IEEE, 2013, pp. 49–50.

[38] S.-C. Pyo, J.-H. Yoon, J.-W. Lee, and S.-S. Lee, "Intersection safety service model using vehicle-to-vehicle communication," in *2014 International Conference on Information and Communication Technology Convergence (ICTC)*. IEEE, 2014, pp. 605–606.

[39] P. Teunissen and C. de Jong, "Reliability of gps cycle slip and outlier detection," in *Proceeding of INSMAP98*, 1998, pp. 78–86.

[40] H. Kuusniemi and G. Lachapelle, "GNSS signal reliability testing in urban and indoor environments," in *Proceedings of the NTM Conference*, 2004.

[41] I. Mohamad, M. A. M. Ali, and M. Ismail, "Availability, reliability and accuracy of gps signal in bandar baru bangi for the determination of vehicle position

and speed," in *2009 International Conference on Space Science and Communication*. IEEE, 2009, pp. 224–229.

[42] G. Chang, "Loosely coupled ins/gps integration with constant lever arm using marginal unscented kalman filter," *The Journal of Navigation*, vol. 67, no. 3, pp. 419–436, 2014.

[43] K. Saadeddin, M. F. Abdel-Hafez, and M. A. Jarrah, "Estimating vehicle state by gps/imu fusion with vehicle dynamics," *Journal of Intelligent & Robotic Systems*, vol. 74, no. 1, pp. 147–172, 2014.

[44] W. Fu-Mei and Y. Yuan-xi, "An extended adaptive kalman filtering in tight coupled gps/ins integration," *Survey Review*, vol. 42, no. 316, pp. 146–154, 2010.

[45] M. Ilyas, Y. Yang, Q. S. Qian, and R. Zhang, "Low-cost imu/odometer/gps integrated navigation aided with two antennae heading measurement for land vehicle application," in *2013 25th Chinese Control and Decision Conference (CCDC)*. IEEE, 2013, pp. 4521–4526.

[46] P. Zhang, J. Gu, E. E. Milios, and P. Huynh, "Navigation with imu/gps/digital compass with unscented kalman filter," in *IEEE International Conference Mechatronics and Automation, 2005*, vol. 3. IEEE, 2005, pp. 1497–1502.

[47] J. Tang, Y. Chen, X. Niu, L. Wang, L. Chen, J. Liu, C. Shi, and J. Hyyppä, "Lidar scan matching aided inertial navigation system in gnss-denied environments," *Sensors*, vol. 15, no. 7, pp. 16 710–16 728, 2015.

[48] Y. Gao, S. Liu, M. M. Atia, and A. Noureldin, "Ins/gps/lidar integrated navigation system for urban and indoor environments using hybrid scan matching algorithm," *Sensors*, vol. 15, no. 9, pp. 23 286–23 302, 2015.

[49] N. Li, Y. Gao, Y. Wang, Z. Liu, L. Guan, and X. Liu, "A low-cost underground garage navigation switching algorithm based on kalman filtering," *Sensors*, vol. 19, no. 8, p. 1861, 2019.

[50] E. Stayton and J. Stilgoe, "It's time to rethink levels of automation for self-driving vehicles [opinion]," *IEEE Technology and Society Magazine*, vol. 39, no. 3, pp. 13–19, 2020.

[51] Society of Autonomous Engineers, "Dsrc implementation guide a guide to users of sae j2735 message sets over dsrc," 2010.

[52] J. Liu and A. J. Khattak, "Delivering improved alerts, warnings, and control assistance using basic safety messages transmitted between connected vehicles," *Transportation research part C: emerging technologies*, vol. 68, pp. 83–100, 2016.

[53] N. Vivek, P. Sowjanya, B. Sunny, and S. Srikanth, "Implementation of ieee 1609 wave/dsrc stack in linux," in *2017 IEEE Region 10 Symposium (TENSYMP)*. IEEE, 2017, pp. 1–5.

[54] E. D. Kaplan and C. Hegarty, *Understanding GPS/GNSS: Principles and applications*. Artech house, 2017.

[55] B. Parkinson, "Gps error analysis,"global positioning system: Theory and application volume 1: Volume 163, american institute of aeronautics and astronautics," *Inc., Washington, DC*, 1994.

[56] K. Borre, D. M. Akos, N. Bertelsen, P. Rinder, and S. H. Jensen, "Carrier and code tracking," *A software-defined GPS and GALILEO receiver: a single-frequency approach*, pp. 87–108, 2007.

[57] A. Ahmed, "Scintillation on global navigation satellite signals and its mitigation," Ph.D. dissertation, Newcastle University, 2015.

[58] J. Spilker Jr, "Tropospheric effects on gps," *Global Posiotioning System: Theory and Applications*, vol. 1, pp. 517–546, 1996.

[59] J. A. Klobuchar, "Ionospheric effects on gps," *Chapter 12 of Global Positioning System: Theory and Applications*, vol. 1, p. 30, 1996.

[60] I. R. W. Group *et al.*, "The receiver independent exchange format, version 4.00. 1 december 2021," 2021.

[61] R. A. Snay and T. Soler, "Modern terrestrial reference systems part 3: Wgs 84 and itrs," *Prof. Surv*, vol. 3, pp. 1–3, 2000.

[62] G. Cai, B. M. Chen, and T. H. Lee, "Coordinate systems and transformations," in *Unmanned Rotorcraft Systems*. Springer, 2011, pp. 23–34.

[63] ——, *Unmanned rotorcraft systems*. Springer Science & Business Media, 2011.

[64] G. Rizzi and M. L. Ruggiero, *Relativity in rotating frames: relativistic physics in rotating reference frames*. Springer, 2004.

[65] I. G. Petrovski, *GPS, GLONASS, Galileo, and BeiDou for mobile devices: from instant to precise positioning*. Cambridge University Press, 2014.

[66] J. S. Subirana, J. J. Zornoza, and M. Hernández-Pajares, "Transformations between ecef and enu coordinates," *URL: https://gssc. esa. int/navipedia/index. php/Transformations_between_ECEF_and_ENU_coordinates (visited on October 2022). Technical University of Catalonia, Spain*, 2011.

[67] ——, "Transformation between terrestrial frames," *URL: https://gssc. esa. int/navipedia/index. php/Transformation_between_Terrestrial_Frames. (visited on October 2022). Technical University of Catalonia, Spain*, 2011.

[68] T. Hels and I. Orozova-Bekkevold, "The effect of roundabout design features on cyclist accident rate," *Accident Analysis & Prevention*, vol. 39, no. 2, pp. 300–307, 2007.

[69] B. Burdett, A. R. Bill, and D. A. Noyce, "Evaluation of roundabout-related single-vehicle crashes," *Transportation Research Record: Journal of the Transportation Research Board*, no. 2637, pp. 17–26, 2017.

[70] W. Baarda, "A testing procedure for use in geodetic networks," *Geodesy*, vol. 2, no. 5, 1968.

[71] Y. He and A. Bilgic, "Iterative least squares method for global positioning system," *Advances in Radio Science: ARS*, vol. 9, p. 203, 2011.

[72] S. Ryan and G. Lachapelle, "Impact of GPS/Galileo integration on marine navigation," in *IAIN World Congress/ION Annual Meeting*, 2000, pp. 721–731.

[73] P. E. Shrout and J. L. Fleiss, "Intraclass correlations: uses in assessing rater reliability." *Psychological bulletin*, vol. 86, no. 2, p. 420, 1979.

[74] A. Bruton, J. H. Conway, and S. T. Holgate, "Reliability: what is it, and how is it measured?" *Physiotherapy*, vol. 86, no. 2, pp. 94–99, 2000.

[75] R. L. Ebel, "Estimation of the reliability of ratings," *Psychometrika*, vol. 16, no. 4, pp. 407–424, 1951.

[76] K. O. McGraw and S. P. Wong, "Forming inferences about some intraclass correlation coefficients." *Psychological methods*, vol. 1, no. 1, p. 30, 1996.

[77] M. Kok, J. D. Hol, and T. B. Schön, "Using inertial sensors for position and orientation estimation," *arXiv preprint arXiv:1704.06053*, 2017.

[78] R. E. Kalman, "A new approach to linear filtering and prediction problems," 1960.

[79] P. S. Maybeck, "The kalman filter: An introduction to concepts," in *Autonomous robot vehicles*. Springer, 1990, pp. 194–204.

[80] Y. Kim and H. Bang, "Introduction to kalman filter and its applications," *Introduction and Implementations of the Kalman Filter*, vol. 1, pp. 1–16, 2018.

[81] J. Yin, "Gps precise positioning using multisensor data fusion for vehicular communication," Ph.D. dissertation, Newcastle University, 2019.

[82] G. A. Borges and M.-J. Aldon, "Line extraction in 2d range images for mobile robotics," *Journal of intelligent and Robotic Systems*, vol. 40, no. 3, pp. 267–297, 2004.

[83] A. Soloviev, D. Bates, and F. Van Graas, "Tight coupling of laser scanner and inertial measurements for a fully autonomous relative navigation solution," *Navigation*, vol. 54, no. 3, pp. 189–205, 2007.

[84] O. J. Woodman, "An introduction to inertial navigation," University of Cambridge, Computer Laboratory, Tech. Rep., 2007.

[85] I. Definition, "Relationships with local geodetic systems," *National Imagery and Mapping Agency, Department of Defense World Geodetic System*, 1984.

[86] J. Farrell, *'Ins error state dynamic equations' in Aided navigation: GPS with high rate sensors*. McGraw-Hill, Inc., 2008.

[87] R. Li, J. Liu, L. Zhang, and Y. Hang, "Lidar/mems imu integrated navigation (slam) method for a small uav in indoor environments," in *2014 DGON inertial sensors and systems (ISS)*. IEEE, 2014, pp. 1–15.

[88] CADDEN. (2015) Velodyne lidar puck. [Online]. Available: https://www.cadden.fr/en/technologies/lidar-laser/

[89] Velodyne, "Vlp-16 user manual," 2019.